Interactive comment on "Capturing optically important constituents and properties in a marine biogeochemical and ecosystem model"

by S. Dutkiewicz et al.

Interactive comment on Biogeosciences Discuss., 12, 2607-2695.

Response to Reviewer 1 (Emmanuel Boss):

Reviewer's comments are in black, our replies are in blue. In some of the quoted text, some latex symbols are included (apologies as this makes them a bit more difficult to read).

This paper focus on the modification of the MIT-gcm model to explicitly include optics. The authors show the output of global simulation showing the ability of the model to provide qualitatively realistic results. They then do a series of sensitivity runs where specific optically important components are varied and observe their impact on the global fields.

The paper is well written and concise. I am in favor of publishing this paper as it describes an important modification of the model which will open a variety of avenues for research with this model in future studies.

We thank the reviewer for the positive comments, and we do feel that this manuscript will provide an important foundation for future studies.

I have some significant comments that I feel, if addressed, could improve this paper. Significant comments:

1. The global runs with the explicit model were not compared to run when optics was not explicit? Why not? The community needs to know if adding optics is important in general (e.g. to obtain the appropriate biogeography, nutrient fields etc') or not? Is it worth the increased computation costs? Does it help to better constrain the model's parameters by having more data to compare to (e.g. Fujii et al).? W/o that I don't see the use of the initial run. Until now you have published papers on BGC and species distribution where the optical model used was even simpler. Were their results (distribution, timing etc') systematically wrong in ways that the optics has now fixed?

Previous models (ours or others) are not necessarily "worse", but are designed and used to ask different questions. Our intent in adding the complexity was to have a tool to explore questions on links between ecosystems and optics that required these further refinements. We also did

not initially include analysis on this because we felt that many studies, including Fujii et al (2007), already set out the value of adding optics to biogeochemical models (a point that we now make in the introduction of the revised version of the text, see below). However, we appreciate the suggestion that such analysis would be informative in the current paper, and have consequently added a new section just after the model validation (new section 4) to the revised version with a series of experiments, specifically asking the question of how important this new level of complexity is to the results and compares results to an older version of the model without the explicit spectral radiative transfer component. It is instructive to see that non-radiative transfer, non-optical models can get many of the features similar and some not. The results were interesting and we have made much of them in the abstract, discussion and conclusion; and thank the reviewer for the suggestion of including this topic.

We do, however, maintain that the main purpose of the model development was not to create a 'better' model per se, but to address questions of phytoplankton assemblages that required consideration of spectral optical properties as well as a closer connection to satellite products, such as reflectance, than was previously resolved. We make this point clear in both the abstract, introduction and discussion.

Abstract (old pg 2609, replacing line 24-28): "*This new model that captures bio-optical feedbacks will be important for improving our understanding of the role of light and optical constituents on ocean biogeochemistry, especially in a~changing environment. Resolving surface upwelling irradiance will make is easier to connect to satellite derived products in the future.*"

We also add an extra sentence to the abstract specifically acknowledging what the new model capture relative to old model:
"*We find that incorporating the different optically important constituents and spectral irradiance was crucial to capture the regionally varying depth of the subsurface Chl-a maximum.*"

Introduction (pg 2611, after lines 4): "*Fujii et al. (2007) suggested that including explicit optics in an ecosystem model allowed a more accurate subsurface light field and allowed additional constraints on model parameters. Several additional studies have demonstrated the value of adding optics to biogeochemical models (e.g. Babin et al, 1993; Sathyendranath and Platt, 2007; Kettle and Merchant, 2008).*"

Discussion (near old pg 2634, line 26): "*The model developments presented were necessary for capturing the regional variability in depth of the subsurface chlorophyll maximum, in particular, by resolving the deep penetration of blue-green wavelengths in the subtropical gyres. Not including any of the constituents leads to an unrealistically regionally uniform depth of the deep chlorophyll maximum.*"

Conclusions (old text, pg 2636, line 1):

2

"Capturing each of the optically important constituents explicitly, and including a spectrum of light was important for obtaining realistic variability in depth of the subsurface chlorophyll maximum, and in resolving the deep penetration of blue-green wavelengths in the subtropical gyres important for phytoplankton community structure."

New section 4 is as follows and includes an additional figure (new Fig 14):
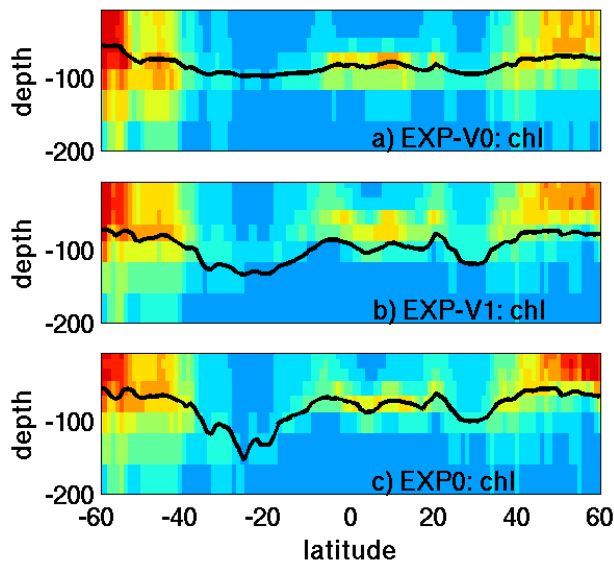
"4. Sensitivity experiments: Value of added model complexity.

We conduct two sensitivity experiments to highlight the importance of the extra level of complexities of this new version of the model. In the first experiment (designated EXP-V0) the biogeochemistry and ecosystem are the same as in the default experiment described above (designated EXP0) but there is only a single band of irradiation (400-700nm, summed over the original 25nm, so that total PAR is conserved); attenuation (c_{tot}) of PAR is a function only of absorption by water molecules and Chl-a summed over all phytoplankton types: $c_{tot}=a_{wo}+a_{chlo} Chl_{tot}$, where $a_{wo}=0.04$ m^{-1}, and $a_{chlo}=0.04$ m^2 (mg Chl)$^{-1}$. There is no explicit account taken for optical role of CDOM or detritus (though the value chosen for a_{chlo} implicitly include their role). Similar parameterizations have been used in previous versions of our model (e.g. Dutkiewicz et al., 2014), and are also common in many other biogeochemical models.

The results from EXP-V0 (Fig. 14a) reveals a much more latitudinally uniform penetration of light, and in particular the deep chlorophyll maximum in the subtropical gyre is too shallow relative to the default experiment (EXP0, Fig. 14c) and observations (Fig. 3a).

In experiment EXP-V1 we include all the optical constituents explicitly (as in EXP0), though with only a single band of PAR (as in EXP-V0). We assume the absorption and scattering coefficients for 500nm in this experiment. This experiment (Fig. 14 b) reveals substantial more realistic varying distribution of the deep chlorophyll maximum and penetration of PAR. The addition of spectral light leads to even deeper penetration of light in the subtropical gyres (default experiment, EXP0, Fig. 14c): deepest penetrating light is in the blue/green range and an average absorption across one waveband will not capture these differences.

These sensitivity experiments suggest that explicitly capturing regional changes in all optical constituents is essential for the realistic light penetration variations. Spectral light further enhances the realism of the results. The addition of the radiative transfer code is essential for obtaining upwelling irradiance that can link to satellite products."

"Figure 14: Sensitivity Experiments examining value of increased optical complexity in model. Chl-a (\unit{mg\,C\,m^{-3}}) along the extended AMT-15 transect for (a) {{EXP-V0}} with no radiative transfer, single waveband of PAR (400-700nm), no inclusion of optical effects of CDOM or detritus and no optical differences between phytoplankton. (b) {{EXP-V1}} with radiative transfer, explicit optical properties for CDOM and detritus, but only one waveband (400-700nm) and no optical differences between phytoplankton. (c) {{EXP0}}, the default experiment. Model 1% irradiance depth is shown as a black line."

2. Qualitative comparison should be performed (e.g. mean % or absolute deviations etc') , and not just computation of correlation coefficient. The later is strongly affected by dynamic range.

We now include the model bias in Figure 6 (shown below). We alter the text (pg 2622, line 18-21):
"The model also captures many of the global features in Chl~a (derived from MODIS satellite), primary production (derived using Behrenfeld and Falkowski, 1997) as well as macronutrients (from the World Ocean Atlas, Garcia et~al., 2006), though with notable biases (Fig. 6)."

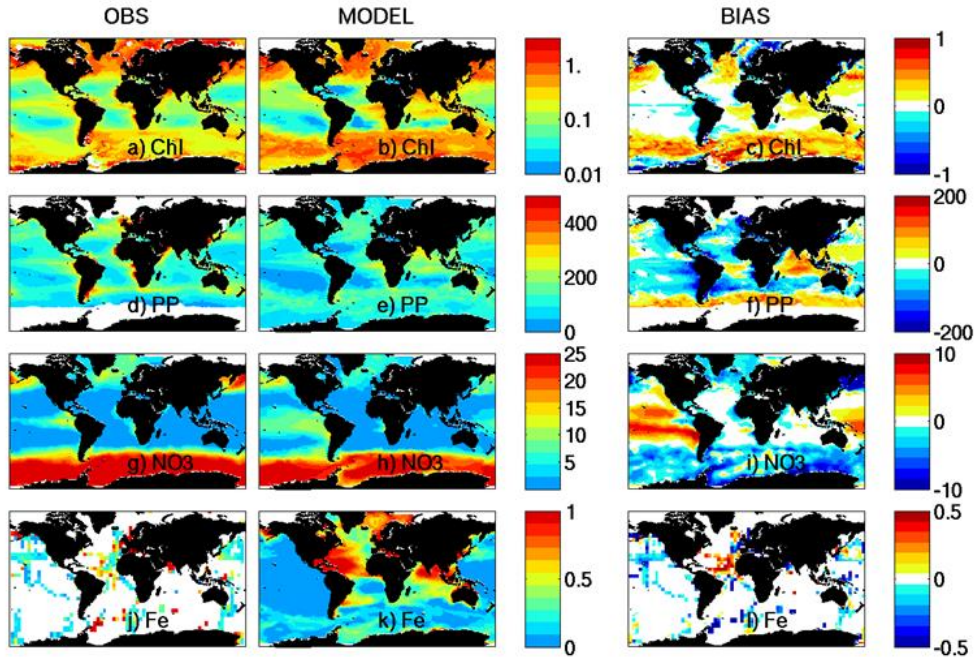The subsequent text in that section sums up the biases.

Figure 6. Model and satellite derived products and climatologies of in~situ measurements for annual mean and biases: \textbf{(a)}~satellite derived (MODIS) Chl~a (\unit{mg\,Chl\,m^{-2}}); \textbf{(b)}~modelled Chl~a (mean 0--50\,\unit{m}, \unit{mg\,Chl\,m^{-2}}); \textbf{(c)} bias of Chl~a (model-observations); \textbf{(d)}~satellite derived primary production (\unit{g\,C\,m^{-2}\,yr^{-1}}) (Behrenfeld and Falkowski, 1997); \textbf{(e)}~modelled primary production (column integrated, \unit{g\,C\,m^{-2}\,yr^{-1}}); \textbf{(f)} bias of primary production; \textbf{(g)}~World Ocean Atlas nitrate (mean 0--50\,\unit{m}, \unit{mmol\,m^{-3}}) (Garcia et~al., 2006); \textbf{(h)}~modelled nitrate (mean 0--50\,\unit{m}, \unit{mmol\,m^{-3}}); \textbf{(i)} bias of nitrate; \textbf{(j)}~compiled iron observations (composite 0--50\,\unit{m}, nM) (Tagliubue et~al., 2012); \textbf{(k)}~modelled iron (mean 0--50\,\unit{m}, nM); \textbf{(l)} bias in iron.

3. The limitations of the current model need to be spelled
out in a dedicated paragraph in the method section. E.g.: neglecting PIC and minerals,
neglecting the group specific changes of absorption coefficient with light and nutrients
(you model the changes in chl/C but not the ensuing modulation of the absorption
spectrum). Fixed parameters for CDOM and NAP rather than varying them. You ignore
inelastic scattering (e.g. Raman, Chlorophyll and CDOM). Raman has been found to
be important for chl<1mg mˆ-3, particularly in oligotrophic environments, where it would
increase the availability of blue and green light. You assume a fixed ratio of photopro-
tective to photosynthetic pigments (which, in nature, varies with light and nutrients).
You are ignoring non-phtosynthetic bacteria as having optical properties. You neglect
effects of sea surface on light entering/leaving the ocean.

We had mentioned several of these limitations in the older version (see for instance paragraph in the Discussion, pg 2634, lines 9-14). Given the reviewer's suggestion we now add a sub section in the Model description (new section 2.6) that includes those we already mention as well as additional points that the reviewer brings up. We note however that: CDOM and NAP vary in concentration in time and space in the model such that their effects do vary, though agree that the spectral shape does not vary. We had already made mention that NAP spectral qualities do not vary as they should (especially with size), but again make more of this in the new subsection. The OASIM model does take into account of the effect of sea surface on light entering the ocean. We make this clearer in the revised version (pg2612, line 25):
"OASIM includes the impact of clouds, water vapour and aerosols in the atmosphere and surface roughness and reflectance at the ocean-atmosphere interface."

Our model provides upwelling light just below the surface – thus we do not take into account the effect of sea surface on this model output. We add this limitation (as well as others already mentioned) in the new section as well.

New Section 2.6 reads:
"The inclusion of radiative transfer, spectral light and capturing several important optical constituents has been a significant development of the model. However, this version of the model is not without limitations. One major, though currently necessary simplification, is to assume constant absorption and scattering spectra (Fig. 1) for each constituent. For instance, absorption spectra for phytoplankton types do in reality change based on shifts in Chl:C ratios (MacIntyre et al., 2002; Morel et al., 1993; 1995) as well as changes in ratios of photoprotective to photosynthesis pigments as a result of light, temperature and nutrient stress (e.g. Stramski et al., 2002). However, these changes are likely to be small compared to the differences already captured by the representative spectra and photoacclimation component and there is not, as yet, enough systematic observations of these alterations to constrain model parameterisations. Additionally the CDOM absorption spectra has been observed to alter regionally (e.g. Kitidis et al., 2006; Twardowski et al, 2004; Bricuad et al 2010), though as yet we feel it is premature to attempt to capture this variability in the model parameterizations.

Scattering, particularly by detrital particles, remains the least well developed aspect of the model. In particular, we neglect variations in detrital particle size distributions which is likely to be important (Stramski et al, 2001). Additionally the spectra for b^{part}_{det} that we use (Stramksi et al., 2001, Fig. 1b) makes the assumption of homogeneous spheres. However it is likely that differences in shapes and internal structure of the particles will be important for altering the spectral shape (Stramski et al., 2004). We also do not take into account inelastic scattering which may be important for blue and green light in oligotrophic regions (e.g. Ge et al., 1993).

We additionally currently neglect other potentially important optical constituents such as minerals (e.g. Stramski et~al., 2001), particulate inorganic carbon (e.g. Balch and Itgoff, 2009), colloids and bubbles (e.g. Stramski et al., 2004), non-photosynthetic organism including

zooplankton, bacteria (e.g. Morel and Ahn, 1991), and viruses (e.g. Stramski et al., 2001). We felt that these are, as yet, not well enough constrained to include explicitly in the model.

The limitations list above should however not detract from the major enhancement to the model and are similar to those of other models (e.g. Fujii et al., 2007; Gregg and Casey, 2007). This new model provides a unique platform to examine global implication of optical properties to the phytoplankton ecosystem, feedbacks to the biogeochemistry, and links to satellite data that are not possible with limited observational data. Here we first validate the model in a standard "default" configuration. We then provide a series of studies exploring the significance of each of the optical constituents and our parameterization. Several studies in progress build on for these results."

4. The differences between
using a 3stream model compared to using a full RT model need to be quantified or
cited from other studies. The 3 stream model is an approximation and one would like
to know the likely biases associated with using it (ignoring the full RT calculations). The
full RT is the constituent equation in optics and models to solve it exist (e.g. Hydrolight).

While you will always have to assume thing (e.g. sky model), what you neglect by doing
approximations needs to and can be quantified.

The three stream model is indeed an irradiance model, not a radiance model: there is no angular dependence. In order to compare our results to hydrolight, we would need to make assumptions about the angular dependences of each of our optical constituents. This would lead to additional uncertainties and we believe that we would not gain much insight. We believe that it is more appropriate to compare to real data. We have in particular tried to compare against a detailed optical dataset to validate this model. In particular Fig 5 shows that we capture the spectral distribution of the depth of light penetration as found along the AMT-15. Adding a full radiance model would be a significant computational expense. The simplification of Mobley et al (2009) provide a justification for the simplifications we have undertaken. But we also note that these simplifications were also used by Ackelson et al (1994) and Gregg et al. (2007, 2009)

To provide the reader with sufficient background to understand that we have made specific assumptions on RT component we add in the revised version at the end of section 2.1:
"We note that radiative transfer component is a simplification from a full radiance model, and in particular does not resolve the angular distribution of light, nor angular dependence of scattering. These assumptions have been shown to be small in terms of the needs for ecosystem models in Mobley et al (2009). Though not a full radiative transfer model, our three-stream treatment does provides the relevant output for our needs: the light available for photosynthesis and an upwelling component that at the sea surface is similar to that seen by a satellite."

5. You are missing a large historical

7

body of literature that should be cited, as it specifically addresses the role and nature of the constituents you are focusing on. E.g. the works of Jerlov, Kale, and Bricaud and Stramski 1981 for CDOM and its parameterization. Many works comparing the relative absorption of different constituents have been published. I can think of works by Chang, Arnone, Barnard and Roesler among other. Arrigo has published on the effects of CDOM on phytoplankton (again, among others). Morel, 1988, has looked at the effect of H_2O on PAR. There are many studies that have been conducted showing that phytoplankton either photo-acclimate or are selected for the light field they experience (e.g. Moore and Chilsolm). Models capturing the chlorophyll max dynamics have also been published (e.g. Taylor et al., Fennel, Wang). I can't think of anything new that I learned from your paper about the role of optical constituents in the ocean, how they are affected by light or how they modulate the light field and reflectance.

We agree that we did not have enough references to previous studies when discussion the sensitivity studies (though had attempted to mention several in the introduction). We now remedy this as described below. However we disagree that there is "nothing" new in this paper. In particular the feedback from the optics to the productivity to the gyre size is (we believe) new and is a main conclusion of these studies. Also, though much of the different aspects of the constituents are known (and have a large literature behind them), we believe that our approach provides a level of synthetizing of prior knowledge (otherwise quite disparate) in a model that can explore the global impact of feedbacks. Yes, much of the mechanistic understanding is already known (we're not claiming to invent anything new in that regard), but 1) some of these issues may not be transparent to wider biogeochemical (modeling) community, 2) they haven't been brought together in a model such as this before, 3) many of these previous studies are regional observations and models, here we show how mechanistic understanding plays out globally (which in our opinion is novel). However we do now place these results in context of many previous results:

Pg 2626, Section 4 first paragraph (in new version this is Section 5) now reads:
"*Optical constituents play varying roles in their effect on irradiance attenuation (absorption and scattering). These roles have long been a topic of interest, though many studies have had limited observations and been of highly localized in character (e.g. Jerlov, 1953; Chang and Dickey, 1999) though it has also been recognized that they vary regionally (e.g. Barnard et al., 1998; Simeon et al., 2003; Zheng and Stramski, 2013). Targeted cruises have also provided larger scale observations indicating large range of value for each constituent and altering importance in different regions (e.g. BIOSOPE, Bricaud et al 2010) and several attempts have been made to construct algorithms to determine the relative contributions from more easily measured quantities, including those from satellite (e.g. Maritorena et al., 2002; Lee et al., 2002; 2007; Ciotti and Bricaud, 2006; Werdell et al., 2013; Zheng and Stramski, 2013). Our model provides a unique global 3-dimensional perspective. Here our results focus on an (extended) AMT transect (Figs. 15 and 16), however, they are also consistent with observations in other regions (e.g. Bricaud et al. 2010).*

Absorption by water molecules is most important at longer wavebands (Pope and Fry, 1997), but still has an impact at shorter wavebands (Fig 15a,~b,~i,~j). It is relatively more important in lower productive waters (e.g. South Atlantic gyre) because the concentrations of other constituents are relatively low . Absorption by detrital matter plays a~role, especially near the 1% depth in highly productive regions and at shorter wavebands (Fig 15 c,~d,~i,~j). Absorption by phytoplankton plays a~significant role where Chl~a is highest (e.g. the deep Chl~a maximum as suggested by observations, e.g. Chang and Dickey, 1999) at wavelengths less than $550\,\unit{nm}$, and little role at longer wavelength (Fig 15 g,~h,~i,~j, see also Fig. 1). Absorption by CDOM at short wavebands is important (as seen in observations e.g. Jerlov, 1953) in most regions, particularly where productivity is high where it is the dominant absorber. It also has, relative to other constituents, a~large role at depth (as seen in observations e.g. Simeon et al., 2003; Bricaud et al., 2010). At long wavebands CDOM plays very little role. Scattering by phytoplankton is relatively most important at shallower depths, while scattering by detrital matter is dominant deeper at all wavelengths (Fig. 16)."
(Note Fig 15 and 16 refer to old figures 14 and 15).

We start Section 5.1. (old text pg 2627, line 14, old section 4.1) with:
"Observations have determined that detrital matter does play a role in light attenuation, though with varying regional importance (e.g. Jerlov 1953; Bricaud et al., 2010)"

And in this same section when discussing the change in community structure (old text, pg 2628, line 13) we add reference to Moore et al (1995):
"This favours phytoplankton, at least in the subtropics, which absorb more efficiently in the blue part of the spectrum (i.e. \textit{Prochlorococcus}, Fig 16c) as anticipated from laboratory studies (e.g. Moore et al., 1995)"

We start Section 5.2 (Old text, pg 2630, line 26, old section 4.2) with the following new text:
"CDOM and its contribution to light absorption is observed to vary in different regions of the ocean (e.g. Jerlov 1953, Bricuad 1981, Nelson and Seigel, Morel et al., 2010) and many studies have attempted to empirically link a_{cdom} to other more easily measured quantities such as Chl-a (e.g. Morel, 2009). However these studies are still regional or include only sparse data. We conduct a~series of sensitivity experiments that test assumption and importance of a_{cdom} globally and its feedback to the biogeochemistry."

Also in this section we modify pg 2631, lines 15-17 to:
"In the parameterizations that either tie χ_{cdom} to Chl~a ({{EXP-C3}}) or to DOM ({{EXP-C4}}), a_{cdom} is almost non-existent below the $1\,{\%}$ light level (Fig. 17), at odds with observations (e.g. Simeon et al., 2003; Bricaud et al., 2010)."

And we also include an additional sentence (old text, pg 2631, at line 9):
"The model experiments thus reveal a potentially important role for CDOM in setting phytoplankton community structure via alteration of the visible light spectrum, building on previous studies (e.g. Arrigo and Brown 1996)."

9

We already included (Introduction, pg 2610, lines 17-18) several references on the issue of selection of phytoplankton by light environment (Bidigare et~al., 1990a; Huisman and Weissing, 1995; Stomp et~al., 2004; Hickman et~al., 2010). We add here the Moore et al references as well. However, we now also include this list of papers in section 5.3 (old section 4.3, sensitivity studies with a_phy and b_phy):

"Community structure is also altered (Fig. 19c) showing that the photosynthetetic absorption specific to each type is important for the emergent biogeography as has been suggested by previous studies (Bidigare et~al., 1990a; Huisman and Weissing, 1995; Moore et al, 1995; Stomp et~al., 2004; Hickman et~al., 2010)."

We include reference to Fennel and Boss (2003), Wang et al (2009) in the Discussion (old text pg 2634, line 26):

"The subsurface chlorophyll maximum can indeed be captured without including all constituents and spectral light (as seen in EXP-V0, and in other models, e.g. Fennel and Boss, 2003; Wang et al., 2009). However, the model developments presented were necessary for capturing the regional variability in depth of the subsurface chlorophyll maximum, in particular, by resolving the deep penetration of blue-green wavelengths in the subtropical gyres."

We note that Taylor et al (1997), Fennel and Boss (2003), Wang et al (2009) did not resolve spectral nature of light at the DCM. We look at this issue further in a paper in preparation (Hickman et al).

We now cite the following additional papers on the above subjects:
Arrigo, K.R. and Brown, C.W.: Impact of chromophoric dissolved organic matter on UV inhibition of primary productivity in the sea Mar. Ecol. Prog. Series, 140, 207-216, 1996.

Barnard, A.H., Pegua, W.S., and Zaneveld, J.R.V.: Global relationships of the inherent optical properties of the oceans, J. Geophys. Res., 103, 24,955--24,968.

Bricaud, A., Babin, M., Claustre, H., Ras, J., and Tieche, F., Light absorption properties and absorption budget of the Southeast Pacific waters. J. Geophys. Res., 115, C08009, doi:10.1029/2009JC005517, 2010.

Bricaud, A., Morel, A., and Prieur, L: Absorption by dissolved organic matter of the sea (yellow substance) in the UV and visible domains, Limnol. Oceanogr., 26, 43-53, 1981.

Chang, G.C. and Dickey, T.D.: Partitioning in situ total spectral absorption by use of moored spectral absorption-attenuation meters, Applied Optics, 38, 3876--3887.

Ciotti, A. M., and Bricaud, A.: Retrievals of a size parameter for phytoplankton and spectral light absorption by colored detrital matter from water-leaving radiances at SeaWiFS channels in a continental shelf region off Brazil, Limnol. Oceanogr. Methods, 4, 237–253, 2006.

10

Fennel, K. and Boss, E.: Subsurface maxima of phytoplankton and chlorophyll: Steady-state solutions from a simple model, Limnol. Oceanogr., 48, 1521-1534, 2003.

Jerlov, N.G.: Influence of suspended and dissolved matter on the transparency of sea water, Tellus, 5, 59--65, 1953.

Maritorena, S., Siegel, D.A., and Peterson, A.R.: Optimization of a semianalytical ocean color model for global-scale applications, Applied Optics, 41, 2705--2714, 2002.

Moore,~L.~R., Goericke,~R., and Chisholm,~S.~W.: Comparative physiology of^M \textit{Synechococcus} and \textit{Prochlorococcus}: influence of light and^M temperature on growth, pigments, fluorescence and absorptive properties, Mar.^M Ecol.-Prog. Ser., 116, 259--275, 1995

Morel,~A., and Ahn,~Y.-H.: Optics of heterotrophic nanoflagellates and ciliates: A tentative assessment of their scattering role in oceanic waters compared to those of bacterial and algal cells, J. Mar. Res., 49, 177--202, 1991

Simeon, J., Roesler, C., Pegau, W.S., and Dupouy, C.: Sources of spatial variability in light absorbing components along an equatorial transect from 165°E to 150°W, J. Geophys. Res., 108, doi:10.1029/2002JC001613, 2003.

Wang, X.J., Behrenfeld, M., Le Borgne., R., Murtugudde, R., and Boss, E.: Regulation of phytoplankton carbon to chlorophyll ratio by light, nutrients and temperature in the Equatorial Pacific Ocean: a basin-scale model. Biogeosciences, 6, 391-404, 2009.

Werdell, P.J., Franz, B.A., Bailey, S.W., Feldman, G.C., Boss, E., Brando, V.E., Dowell, M., Hirata, T., Lavender, S.J., Lee, Z., Loisel, H., Maritorena, S., Mélin, F., Moore, T.S., Smyth, T.J., Antoine, D., Devred, E., d'Andon, O.H.F. and Mangin, A.: Generalized ocean color inversion model for retrieving marine inherent optical properties, Applied Optics, 52, 2019--2037.

Zheng, G., and Stramski, D.: A model based on stacked-constraints approach for partitioning the light absorption coefficient of seawater into phytoplankton and non-phytoplankton components. J. Geophys. Res, 118, 2155–2174, doi:10.1002/jgrc.20115, 2013

6. There exist more comprehensive optical data from AMT that has already been published (e.g. by Dall'Olmo, Martinez-Vicente). Why not use it? If I understand correctly that you are modeling an 'average' year (not a specific year), you could aggregate all the data.

The AMT-15 had a particularly diverse and relevant set of optical measurements. In particular the light penetration data used in Fig 5 has been very useful in model development. We

decided to stick to just one cruise to avoid interannual variability and the differences in cruise tracks which we believe would have distracted from the main points that we want to make. We believe that adding additional cruise data would not have provided sufficiently in the validation to justify sacrificing clarity of the manuscript. We acknowledge that Martinez-Vicente et al (2013) do have additional scattering data (e.g. total backscattering), but that cruise lacked other datasets (e.g. phytoplankton light absorption measurements). We now reference that there are other AMT cruises but explain why we stick to just this one cruise. We add this just after old text pg 2620 line 25

"Though there are other AMT cruises that include some similar and/or different combinations of optical data (e.g. AMT-19, Dall'Olmo et al., 2012, Martinez-Vicente et al., 2013), we chose to look at only a single transect for clarity. In particular, the combination of data on spectral irradiance penetration, a_{CDOM}, and light absorption by phytoplankton were of particular use in model validation."

7. It will be very interesting if you could show the species succession in the spring in key locations (e.g NABE) and whether light and/or nutrients are the culprits (and whether the more explicit model is needed compared to the previous one). I am not aware that this question has been ever studied in a model framework.

We agree that this would be a very interesting study, and in fact we are working on two manuscripts that explore the relative role of nutrients and light on controlling growth. One focusing on the spring bloom at high latitudes, and another considering these controls both at the surface and the DCM. However this is beyond the scope of this paper. We do provide a figure here on the species succession for the reviewer's benefit. We decided however that we have too many figures in the text as it is, and so do not include it in the paper.
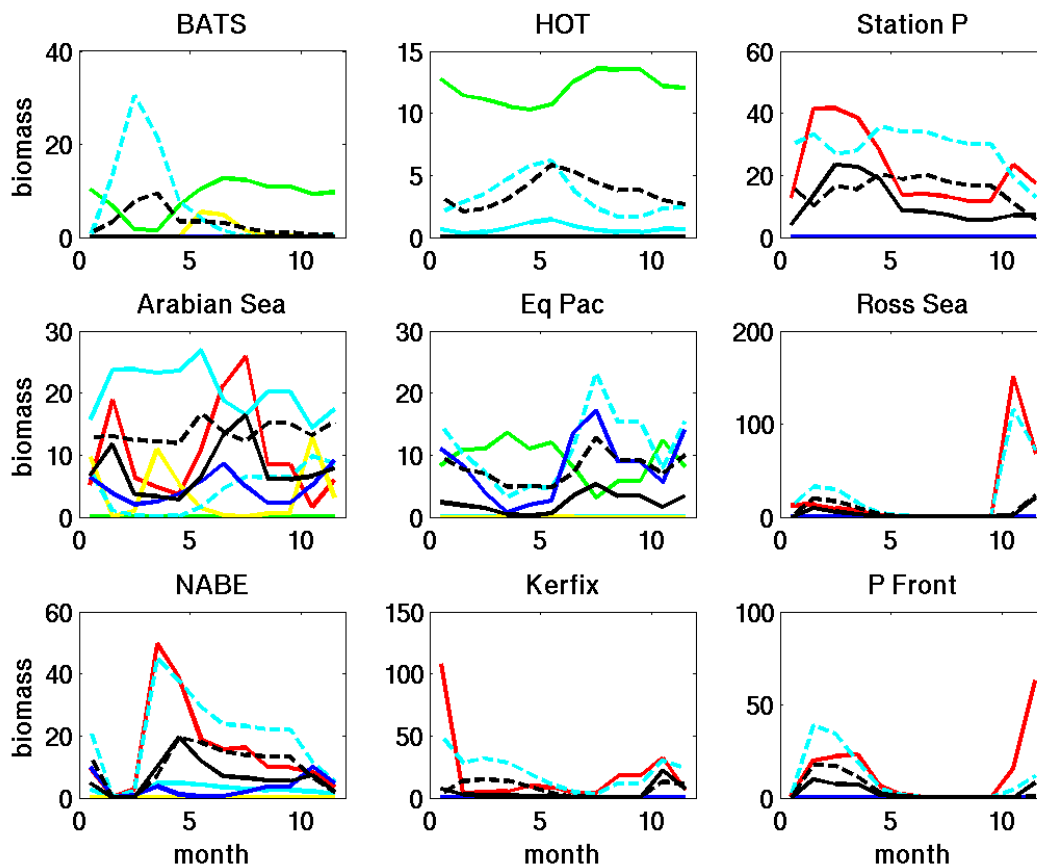
Figure A: Biomass (mgC/m3) of plankton types at the JGOFS stations (locations shown in Figure 1 of the BGD paper). Colours indicate different plankton types: red(diatoms), dark blue (cocco), yellow (diaz), dashed light blue (pico euks), solid light blue (Syn), green (Pro), dashed black (small zooplankton), solid black (large zooplankton). Total Chl is compared to satellite and in situ in Fig 8 of the BGD paper.

Minor comments:

1. Title: I think that 'Modeling' rather than 'Capturing' will better describe the content of the paper.

The title already includes the word "model" – we believe that the goal of the paper is to "capture" the optical properties in a model. As such we believe the current title is more relevant.

2. Abstract: Qualify what you mean by 'important' in your abstract. It seems it is related to domination of the absorption coefficient.

Good point. We now include this in the abstract (in place of old sentence pg 2609 lines 15 onward):

13

"CDOM has proportionally more importance at attenuating light at short wavelengths and in more productive waters, phytoplankton absorption is especially important at attenuation at the deep chlorophyll~a (Chl~a) maximum, and absorption by water molecules is relatively most important in the highly oligotrophic gyres."

3. Abstract: Line 23: Eu/Ed is referred to as the 'irradiance reflectance' not the reflectance of the irradiance.

In the abstract we used the words "sea surface reflectance", but did find other occasions where indeed we said "reflectance of irradiance" (e.g. pg 2611, line23). We endeavor throughout the manuscript to now use the term "irradiance reflectance" or simply "reflectance" where this is obvious.

4. What is the time step of the model?

3 hour. We tested this against a 1 hour timestep. We add this detail to the revised version of the paper in the "Simulation design" subsection (old 2.6, now 2.7):
"The model timestep is 3 hours. We tested this against smaller timesteps with almost identical results."

5. 2.3.2.: Rather than detritus or detrital matter, the ocean optics community now uses the term non-algal particles which is a much better terms (does not assume anything about these particles). Notice that given our methods, cell wall materials and cytoplasm are counted as NAP. Bacteria and viruses are also NAP.

This is a tricky issue. The numerical modeling community use "detritus". We also suggest that since we are not capturing bacteria or viruses in the model that it might be incorrect to use NAP. We also note that Stramski used "detritus" in his 2001 paper (where we get the spectra from for this constituent). In the revised version we elected to keep the word "detritus" as this links directly to our POM pool (which would include cell walls and cytoplasm of dead organic matter). However we make the distinction and the link to the optics community terminology in the revised text. Appended below (old) pg 2615, line 22 we add:
"We note that in the optical community the term "non-algal particles" or NAP is frequently used for any non phytoplankton particles. In this paper we specifically use the term "detritus" instead, as we link to the non-living organic matter pool and do not include other non-algal particles such as viruses and heterotrophic bacteria"

6. 2.3.2.: It is not clear why you have to define a 'detrital material' particle. You can refer to it as a pool of carbon with specific absorption and scattering w/o having to define such 'idealized' particle.

14

We define a detrital material particle size spectrum (not a single particle) so as to convert from our POM pool (in terms of concentration) to particles so as to use the spectrum from Stramski et al 2001. We are clearer on this point in the revised version (added to pg 2615, line 12-14): *"These spectra were deduced by assuming an assemblage of particles with size distribution described by a power function with slope of -4, and the values are given in terms of absorption or scattering per particle. Thus we introduce the coefficient p_part to convert the model particulate organic carbon (POC) to number of particles, making the crude assumption that the size distribution of particles is uniform everywhere."*

7. 2.3.3 A CDOM spectral slope of $0.02nm^{-1}$ is rather high. $0.0145nm^{-1}$ is more representative (studies by
Babin, Roesler, Bricaud, and Carder among other). Specific values are also method dependent, e.g. what spectral range and what fit method is used (e.g. Twardowski et al., 2004). The specific value you use ($0.02061nm^{-1}$) contains at least 2 insignificant digits

We specifically used this value as it was taken from measurement of Kitidis et al (2006) as an average value over the AMT. This did seem appropriate given that we were using AMT data for model validation. We now acknowledge that S_ACDOM does vary regionally in the new section 2.6 referencing Bricaud et al (2010) and Kitdis et al (2006) (see above).

We remove the "insignificant digits" from the revise text and table (though note that this is the value we actually use in the model and given by Kitidis et al 2006).

8. Equ. 20 is not clear to me (unitwise). A. Maximum quantum yield of absorption is 0.4 (I assume unitless) – what is this representing? If units of a^{chl}_ps,j are m^2/mg Chl and Eo mol quanta per nm the units ofn Lambda_E,j, integrated over wavelength, will be quanta m^2 per mg chl.

Quantum yield has units of mmol C/mol photon (see Table 3). Thus units of Eq 2 are mmolC/mgChl /d. This is now included in the revised text.

9. Nowhere do explain the use of mmolP (I assume phosphate is the maine currency of your model). – e.g. Table 1. Why not keep every-thing to mmolC (as you assumed Redfield).?

Yes, phosphorus is the main currency of the model (we do mention this in the appendix, pg 2637, line 11-12). But we agree it would be easier to keep as much as possible in carbon for the main text and the tables and have done so in the revised version. However several things (e.g. matrix of P:all other elements) makes more sense to keep as it is – will be much easier for anyone using this paper as documentation for the model.

15

10. Sec. 3.1/3.2 . Is the realism observed different from when you did not used a sophisticated optical model?

See our new section 4. (quoted above in response to major comment 1)

11. 3.3 numerical domination by picoplankton is well known. Do they dominate a_ph (they usually do not)?

It is likely that picoplankton dominate a_ph because a) the aphy* for picos is higher than for larger cells (Ciotti et al. 2002) and b) picos dominate the chl-a along the AMT transect (Poulton et al 2006). Consequently, since aphy = aphy* x chla, it is very likely that picos dominate the aphy as well. An interesting question would be where do different types dominate the absorption, but not the biomass. But we believe this is an issue beyond the scope of the current paper.

Ciotti A.M., Lewis M.R. & Cullen J.J. 2002. Assessment of the relationships between dominant cell size in natural phytoplankton communities and the spectral shape of the absorption coefficient. *Limnology And Oceanography* 404-417.

Poulton A.J., Holligan P.M., Hickman A., Kim Y.N., Adey T.R., Stinchcombe M.C., Holeton C., Root S. & Woodward E.M.S. 2006. Phytoplankton carbon fixation, chlorophyll-biomass and diagnostic pigments in the Atlantic Ocean. *Deep-Sea Research Part II* 53: 1593-1610.

12. 12 p.2625 l. 4. Could you use HPLC to estimate the larger phyto? Could you use other AMT cruises where such data is available?

We use HPLC to compare to pigments directly in a paper we are just about to submit (Hickman et al). Since there are many uncertainties when trying to relate HPLC pigments to specific groups however, we decide not to include these here.

Again, we could use different AMT cruise data, but instead choose to refer to these data in the new text (We believe using different cruise data would get messy because there are measured along different transects).

We alter old text pg 2625. Lines 3-4 to:
"The model distribution of large phytoplankton biomass (e.g. diatoms, Coccolithophores) compared well to observations made along other AMT cruises (Tarran et al. 2006; Cermeño et al. 2008)"

13. Variability in Chl/CDOM has been reported in Bricaud and Morel 1981.

16

We do acknowledge that there is variability between CDOM and Chl – in fact this is a significant reason to include explicit CDOM-like tracer (mentioned several times in the text). The experiment EXP-C3 was designed precisely to look at how important it is that CDOM and Chl vary. We do already reference Kitidis et al 2006 and Morel et al 2010 on this issue (see old text, pg 2630, line 15). We now also add the Bricaud et al (1981) (note, not Bricaud and Morel) paper as well in this location.

14. Fujji is Fujii (several instances throughout).

Apologies, these have been corrected.

15. Discussion: your treatment of light, while more comprehensive in species, is less comprehensive in RT (e.g. compared to Hydro or EcoLight). Question is always: are the advantages of being comprehensive important and worth the computational cost. I don't think you answered this important question in this version of your manuscript.

Our interest here is about interaction between ecosystem and light field. In this case complexity in species is needed but we believe RT requires less emphasis. See our comments and additional text mentioned above (Major Point 4). Additionally, the MITgcm is open source code, and thus we also feel it is important to include an open source radiative transfer component.

16. Note that while Stramski's data base include measured optical data, certain optical parameters are based on simulations with Mie theory (homogeneous spheres). It is known that shape and internal structure will increase backscattering compared to spheres (e.g. Stramski's 2004 review on backscattering).

We include this limitation (and the Stramski et al, 2004 reference) in the new section 2.6 (see reply to major point 3).

Dear authors, I am often wrong. If you feel I have misunderstood the paper and that comments are off base or not clear, feel free to contact me directly. –Best, Emmanuel

Thank you for your comments. Your suggestions have definitely improved the paper. Where we do not include your comments, we believe that the issues are beyond the scope of the paper – though several are directions we are currently working on.

17

Interactive comment on "Capturing optically important constituents and properties in a marine biogeochemical and ecosystem model"

by S. Dutkiewicz et al.

Interactive comment on Biogeosciences Discuss., 12, 2607-2695.

Response to Reviewer 2:

Reviewer's comments are in black, our replies are in blue.

The manuscript describes an update version of the MIT biogeochemistry and ecosystem model that contains explicit treatments of the main optically active constituents (OAC) of seawater, including 9 different phytoplankton functional groups. One important feature is the independent treatment of detritus and CDOM. The model is presented, and simulation results are compared to selected field data. By changing the relative importance or optical characteristics of each OAC, the numerical experiments allow to estimate feeds back to the system's biogeochemistry, and that is the main goal of the manuscript. The work is well written and relevant, and the model will be much improved by discussions and input from the scientific community, making Biogeosciences Discussions a good forum for the paper. I thus recommend the publication of this work.

We thank the reviewer for the positive comments and we do welcome input on this model and the results from the scientific community. The comments below were very useful and we have adjusted the revised version of the paper to take these into account.

Questions and Comments:
1- Introduction: It is not clear to me the choice of using a specific AMT-15 cruise, as oppose to the others.

The AMT-15 had a particularly diverse and relevant set of optical measurements. In particular the light penetration data used in Fig 5 has been very useful in model development. We decided to stick to just one cruise to avoid interannual variability and the differences in cruise tracks which we believe would have distracted from the main points that we want to make. To retain a clear manuscript – and with just one transect on the figures – we chose to stick with just this cruise. We discuss this choice further in the revised text (going just after old text pg 2620 line 25)
"*Though there are other AMT cruises that include some similar and/or different combinations of optical data (e.g. AMT-19, Dall'Olmo et al., 2012, Martinez-Vicente et al., 2013), we chose to look at only a single transect for clarity. In particular, the combination of data on spectral irradiance penetration, a_{CDOM} and light absorption by phytoplankton were of particular use in model validation*"

1

We already had in the introduction (pg 2611, line 14-19):
"In particular we use a comprehensive data set from an Atlantic Meridional Transect cruise which includes detailed concurrent optical, biogeochemical, and ecosystem observations between the UK and South Africa in September/October of 2004 (AMT-15). Some of the observations are published here for the first time. The data set is ideal for evaluating how our model captures the amount and nature of the light that penetrates the water column across basin scale along with the relevant ecological properties."

2- Model description:
a. are the 25 nm bands averages?

Yes, we make this clear in the revised text (pg 2612, line 27):
"*Irradiances are provided averaged in 25nm wavebands from 400 to 700 nm.*"

b. What are the spectral resolution of the absorption and scattering coefficients used?

We use the same resolution (25nm) for the absorption and scattering coefficients. We make this clearer in the revised text (old text, pg 2615, line 5, i.e. just below the equations):
"*In the model we use absorption and scattering coefficients averaged over 25nm bands to match the irradiance input (Fig. 1) from a variety of sources, detailed below.*"

And at the end of the caption of Figure 1:
"*Spectra are shown here with 1nm resolution for clarity, the model uses the average over the 25nm bands (vertical grey lines)."*

c. Phytoplankton functional types – throughout the text, the term is sometimes replaced by community or species. I would suggest to keep as PFT, to be consistent with the objectives of the work.

We agree that using "species" is not consistent, and have changes this in the revised version as suggested. Occasionally we do want to use the term "community" to address the combination of PFT's in any location.

d. How should the reader interpret the "phytoplankton establish a repeating pattern after about 3 years".

We make this statement to assure the reader that by year 10 (from which we show the results) the model has already reached a quasi-steady state in the ecosystem. We make this clearer in the revised version by adding the following (at old text pg 2620 lines18)
"*The phytoplankton establish a repeating pattern after about 3 years such that we can assume a "quasi-steady state" by year 10.*"

3- Model results a. I found section 3 too long, and I am also not too sure what new can be learned from the individual comparisons with PHYSAT results and MAREDAT dataset

2

In the revised version we have shortened section 3 (from 5 ¾ pages to 4 3/4). We have however decide to keep the comparison to PHYSAT and MAREDAT, though now the discussion is significantly shorter (23 lines compares to 39 previously). Though we agree that these give little extra input, it is important to show that our results do not disagree with other established observations (or inferred observations). We also believe that it is important to engage with the communities that have produced these output. It is however also noteworthy that the insitu observations are very sparse – we make this point as a call for more observations in the revised version. Near old text pg 2626, line 12:
"*These global "observations" contain many uncertainties stemming mainly from the scarcity of insitu data, but the model does not disagree with their findings*"

4- Sensitivity experiments a. I missed a discussion for probable causes for the experiments dealing with bb of phytoplankton had no apparent feedback on the system

Changes to scattering had minimal result on the depth (or spectrum) of light penetration as absorption is the main form of attenuation. Scattering does however have a major impact on the amount and spectrum of the upwelling light. To make this clear in the revised version we have added to the abstract (old pg2609, lines 22-24):
"*Absorption is the main cause of attenuation of irradiance with depth, and as such changes to scattering does not as strongly affect the ecosystem and biogeochemistry fields within the water column but since scattering is important for the amount and type of upwelling irradiance, it is important for setting sea surface reflectance.*"

And by altering the paragraph (old version) pg 2629, lines15-18 to:
"*The main attenuation of light with depth is through absorption, and as such alterations to the backscattering by detrital matter (EXP-D3 and EXP-D4) have little effect on the irradiance fields at depth (Fig. 16a) and thus little change to the dominant functional type (Fig. 16c). However scattering has major impact on the amount and quality of the upwelling light and as such the changes to the reflectance is large (Fig 16d).*"

And similarly (old) pg 2632 lines 22-25:
"*As discussed above, the main attenuation of light is through absorption, and thus when we assume no scattering by phytoplankton (EXP-P3) there is almost no change in dominant functional type, but because scattering does substantially affect the upwelling light there is some (though small) change to reflectance compared to the default run (EXP0). An experiment with four times b_phy has similar results (not shown here).*"

3

Capturing optically important constituents and properties in a marine biogeochemical and ecosystem model

S. Dutkiewicz[1]**, A. E. Hickman**[2]**, O. Jahn**[3]**, W. W. Gregg**[4]**, C. B. Mouw**[5]**, and M. J. Follows**[3]

[1]Center for Global Change Science and Department of Earth, Atmospheric and Planetary Sciences, Massachusetts Institute of Technology, Cambridge, MA 02139, USA
[2]Ocean and Earth Science, University of Southampton, National Oceanography Centre Southampton, Southampton, SO14 3ZH, UK
[3]Department of Earth, Atmospheric and Planetary Sciences, Massachusetts Institute of Technology, Cambridge, MA 02139, USA
[4]Global Modeling and Assimilation Office, NASA Goddard Space Flight Center, Greenbelt, MD, 20771 USA
[5]Department of Geological and Mining Engineering and Sciences, Michigan Technological University, Houghton, MI, 49931, USA

Correspondence to: S. Dutkiewicz (stephd@mit.edu)

Abstract

We present a numerical model of the ocean that couples a three-stream radiative transfer component with a marine biogeochemical-ecosystem in a dynamic three-dimensional physical framework. The radiative transfer component resolves the penetration of spectral irradiance as it is absorbed and scattered within the water column. We explicitly include the effect of several optically important water constituents (different phytoplankton functional types~~the phytoplankton community~~, detrital particles, and coloured dissolved organic matter, CDOM). The model is evaluated against in situ observed and satellite derived products. In particular we compare to concurrently measured biogeochemical, ecosystem and optical data along a meridional ~~north–south~~ transect of the Atlantic Ocean. The simulation captures the patterns and magnitudes of these data, and estimates surface upwelling irradiance analogous to that observed by ocean colour satellite instruments. We find that incorporating the different optically important constituents explicitly and including spectral irradiance was crucial to capture the variability in the depth of the subsurface chlorophyll a (Chl a) maximum. We conduct a series of sensitivity experiments to demonstrate, globally, the relative importance of each of the water constituents, as well as ~~and~~ the crucial feedbacks between the light field, ~~and~~ the relative fitness of phytoplankton types, and the biogeochemistry of the ocean. CDOM has proportionally more importance at attenuating light at short wavelengths and in more productive waters, phytoplankton absorption is relatively more ~~especially~~ important at the deep ~~chlorophyll a (~~Chl a ~~)~~ maximum, and water molecules have the greatest contribution when concentrations of other constituents are low, such as in the ~~absorption by water molecules is relatively most important in the highly~~ oligotrophic gyres. Scattering had less effect on attenuation, but since it is important for the amount and type of upwelling irradiance, it is crucial for setting sea surface reflectance. Strikingly, sensitivity ~~Sensitivity~~ experiments in which absorption by any of the optical constituents was increased led to a decrease in the size of the oligotrophic regions of the subtropical gyres: lateral nutrient supplies were enhanced as a result of decreasing high latitude productivity. This new model that captures ~~Scattering does not as~~

~~strongly affect the ecosystem and biogeochemistry fields within the water column but is important for setting the surface upwelling irradiance, and hence sea surface reflectance. Having a model capable of capturing~~ bio-optical feedbacks will be important for improving our understanding of the role of light and optical constituents on ocean biogeochemistry, especially in a changing environment. <u>Further, resolving</u> ~~The potential benefits of capturing~~ surface upwelling irradiance will <u>make is easier to connect</u> ~~be important for making closer connections~~ to satellite derived products in the future.

1 Introduction

Light is fundamental to phytoplankton and photosynthesis. Understanding ocean <u>productivity</u> ~~production~~ therefore requires detailed knowledge of how light penetrates through ~~the~~ seawater. Attenuation of light within the water column is an interaction of absorption and scattering by "optically important constituents", including water molecules, detrital matter, coloured dissolved organic matter (CDOM) and the phytoplankton themselves.

Phytoplankton absorb light in the visible spectrum (400 and 700 nm). The optical constituents attenuate these wavelengths differently. For instance, water molecules absorb very strongly in the longer wavelengths (Fig. 1a), while detrital matter and CDOM absorb more in the shorter wavelengths (Fig. 1b, c). Thus the spectrum of light at any location is a complex function of the combination of different optical constituents in the overlying water. Previous studies have highlighted the importance of resolving the spectral light field (e.g. Fujii et al., 2007; Kettle and Merchant, 2009), especially as different species of phytoplankton have different light absorption spectra (e.g. Stramksi et al., 2001; Sathyendranath and Platt, 2007). This difference in efficiency of light absorption by phytoplankton is important for their relative fitness and biogeography (Bidigare et al., 1990a; Huisman and Weissing, 1995; <u>Moore and Chisholm, 1999;</u> Stomp et al., 2004; Hickman et al., 2010).

Much is known about the optics of water (e.g. Pope and Fry, 1997; Smith and Baker, 1981; Morel, 1974; Zhang and Hu, 2009; Kirk, 1994). Although much is known about the distributions of coloured ~~colored~~ dissolved (Nelson and Siegel, 2013), detritus (Loisel, 2002) and phytoplankton (IOCCG report 15, 2014) it remains unclear how their distributions feed back to phytoplankton community structure and biogeochemistry. Numerical models provide useful tools to explore these interactions, but to do so requires an appropriately detailed description of the photosynthetically available radiation (PAR).

Several recent models resolve the light spectrum and some of the absorption and scattering properties of different constituents (e.g. Mobley et al., 2009; Fujii et al., 2007; Gregg and Casey, 2007; Bisset et al., 1999). Such models include fully coupled radiative transfer, but differ in the levels of simplification for computational efficiency (e.g. Fujii et al., 2007; Gregg and Casey, 2007) and differ in which and how they treat the different water constituents. For instance CDOM is treated as uniform in Fujii et al. (2007), and linked to chlorophyll a (Chl a) in Gregg and Casey (2007). Fujii et al. (2007) suggested that including explicit optics in an ecosystem model allowed a more accurate subsurface light field and allowed additional constraints on model parameters. Several additional studies have demonstrated the value of adding optics to biogeochemical models (e.g. Babin et al, 1993; Sathyendranath and Platt, 2007; Kettle and Merchant, 2008).

In Sect. 2 we introduce an updated version of the MIT biogeochemistry and ecosystem model (Follows et al., 2007; Dutkiewicz et al., 2012) with a radiative transfer component as well as the explicit treatment of several optical constituents (water molecules, detrital matter, CDOM, and a community of optically-distinct phytoplankton types). Specifically each constituent is treated independently. The fully coupled radiative transfer allows us to calculate spectral surface upwelling irradiance; a product similar to that measured by ocean colour satellites. We show results from this new coupled model where the light field is a dynamic function of the different optical constituents and evaluate against several data sets (Sect. 3). In particular we use a comprehensive data set from an Atlantic Meridional Transect cruise which includes detailed concurrent optical, biogeochemical, and ecosystem observations between the UK and South Africa in September/October of 2004 (AMT-15).

Some of the observations are published here for the first time. The data set is ideal for evaluating how our model captures the amount and nature of the light that penetrates the water column across basin scale along with the relevant ecological properties.

We perform a number of sensitivity experiments that explore the value of the additional model complexity (Sect. 4) the role of each of the water constituents (Sect. 5) and their relative importance. The model allows us to investigate changes to any constituent feeds back to the system, impacting phytoplankton biogeography, biogeochemistry and surface irradiance reflectancereflectance of irradiance .

2 Model description

The biogeochemical/ecosystem model resolves the cycling of carbon, phosphorus, nitrogen, silica, iron, and oxygen through inorganic, living, dissolved and particulate organic phases as discussed in Follows et al. (2007), Dutkiewicz et al. (2009, 2012), and Hickman et al. (2010). The biogeochemical and biological tracers are transported and mixed by a the MIT general circulation model (MITgcm) (Marshall et al., 1997). The physical framework is flexible, but here we employ a global configuration which is constrained to be consistent with altimetric and hydrographic observations (the ECCO-GODAE state estimates, Wunsch and Heimbach, 2007). This three dimensional configuration has $1° \times 1°$ horizontal resolution and 23 24 levels ranging from 10 m in the surface to 500 m at depth. These physical fields have been used in many previous biogeochemical/ecosystem studies (e.g. Follows et al., 2007; Dutkiewicz et al., 2009, 2012; Ward et al., 2012; Prowe et al., 2012).

Similar to several of these previous studies, we resolve several phytoplankton types, P_j as well as two simple grazers, Z_k. The biogeochemical and biological tracers interact through the formation, transformation and remineralization of organic matter. Excretion and mortality transfer living organic material into sinking particulate and dissolved organic detritus which are respired back to inorganic form. Aeolian iron fluxes to the ocean surface are provided by Luo et al. (2008).

We provide complete model equations, description and parameter values in Appendix A and Tables 1 to 6. Here we focus on the relevant new features: in particular an explicit radiative transfer component that allows us to consider absorption and scattering of light spectrally and with attention to each of the relevant optical constituents.

2.1 Radiative transfer model

Irradiance just below the surface of the ocean is provided by the Ocean–Atmosphere Spectral Irradiance Model (OASIM) (Gregg and Casey, 2009) in two downward streams: direct ($E_{d_o}^{\text{below}}$) and diffuse ($E_{s_o}^{\text{below}}$). OASIM includes the impact of clouds, water vapour and aerosols in the atmosphere and surface roughness and reflectance at the ocean-atmosphere interface. Irradiances are provided averaged ~~ocean surface. Irradiance are provided~~ in 25 nm wavebands from 400 to 700 nm. The two downward light streams (direct and diffuse, E_d, E_s) in each waveband are followed through the water column. Irradiance is attenuated by absorption (a), and scattering (b), which includes both forward (b_f), and backwards (b_b) components. Scattering diverts irradiance from the direct and diffuse beams and partitions it between the downward diffuse and an upwelling stream (E_u).

We parameterize this "three-stream" irradiance model following Aas (1987), Ackleson et al. (1994), and Gregg (2002). The model is described by the simultaneous equations for the light streams in each waveband (λ) with depth (z):

$$\frac{dE_d(\lambda)}{dz} = -\frac{a(\lambda) + b(\lambda)}{\overline{v_d}} E_d(\lambda) \tag{1}$$

$$\frac{dE_s(\lambda)}{dz} = -\frac{a(\lambda) + r_s b_b(\lambda)}{\overline{v_s}} E_s(\lambda) + \frac{r_u b_b(\lambda)}{\overline{v_u}} E_u(\lambda) + \frac{b_f(\lambda)}{\overline{v_d}} E_d(\lambda) \tag{2}$$

$$-\frac{dE_u(\lambda)}{dz} = -\frac{a(\lambda) + r_u b_b(\lambda)}{\overline{v_u}} E_u(\lambda) + \frac{r_s b_b(\lambda)}{\overline{v_s}} E_s(\lambda) + \frac{b_b(\lambda)}{\overline{v_d}} E_d(\lambda) \tag{3}$$

where r_s, r_u and r_d are the effective scattering coefficients, normalized by backward scattering coefficients, $\overline{v_d}$, $\overline{v_s}$, and $\overline{v_u}$ are the average cosines (definition in Appendix B), and the radiance is separated in the a direct beam and a diffuse component.

This set of equations can be simplified following Aas (1987) by approximating r_s, r_u, r_d, $\overline{v_s}$ and $\overline{v_u}$ with constant values (see Appendix B). With these assumptions, the set of equations can be reduced to a tri-diagonal system. In contrast to Aas (1987), Ackleson et al. (1994), and Gregg (2002) we solve $E_d(\lambda)$, $E_s(\lambda)$ and $E_u(\lambda)$ directly at each location and at each depth using Gaussian elimination.

We calculate total scalar irradiance, $E_0(\lambda)$ in each waveband at each location and layer (averaged, multiplicatively, between the top and bottom) by scaling the irradiance by the inverse average cosines:

$$E_0(\lambda) = \frac{E_d(\lambda)}{\overline{v_d}} + \frac{E_s(\lambda)}{\overline{v_s}} + \frac{E_u(\lambda)}{\overline{v_u}} \tag{4}$$

This is the light available to the phytoplankton.

We note that the radiative transfer component is a simplification from a full radiance model, and in particular does not resolve the angular distribution of light, nor angular dependence of scattering. These assumptions have been shown to be small in terms of the needs for ecosystem models (Mobley et al, 2009). Though not a full radiative transfer model, our three-stream treatment does provides the relevant output for our needs: the spectral light available for photosynthesis and an upwelling component, that at the sea surface is similar to that seen by a satellite.

2.2 Surface reflectance

Since the model resolves an upwelling stream of irradiance, we can calculate a surface reflectance (unitless):

$$R(\lambda) = \frac{E_u^{\mathsf{below}}(\lambda)|_{k=0}}{E_{d_o}^{\mathsf{below}}(\lambda) + E_{s_o}^{\mathsf{below}}(\lambda)} \tag{5}$$

where $E_\mathsf{u}^\mathsf{below}(\lambda)|_{k=0}$ is upwelling irradiance just below the surface and $E_{\mathsf{d}_o}^\mathsf{below}(\lambda)+E_{\mathsf{s}_o}^\mathsf{below}(\lambda)$ are the downward (direct and diffuse) irradiance just below the surface as provided by OASIM.

To compare to remotely sensed reflectance (R_RS) we convert between model subsurface reflectance and the slant upward radiance seen by satellite by using a bidirectional function Q:

$$R_\mathsf{RS}(\lambda) = \frac{R(\lambda)}{Q} \tag{6}$$

The bidirection function Q has values 3.5 and 5 sr depending on many variables, including inherent optical properties of the water, wavelength and solar zenith angles (Morel et al., 2002; Voss et al., 2007). For simplicity here we assume that $Q = 4$ sr. Model R_RS is therefore analogous, but not exactly the same as that measured by satellite. R_RS has units of 1/sr.

2.3 Treatment of water constituents

Attenuation of irradiance results from absorption by water molecules (a_w), phytoplankton (a_phy), detrital particles (a_det) and coloured dissolved organic matter (a_cdom) and by scattering by water molecules (b_w), phytoplankton (b_phy) and detrital particles (b_det). The absorption (a), total scattering (b) and backward scattering (b_b) (all with units of m^{-1}) are represented as a function of waveband:

$$a(\lambda) = a_\mathsf{w}(\lambda) + a_\mathsf{phy}(\lambda) + a_\mathsf{det}(\lambda) + a_\mathsf{cdom}(\lambda) \tag{7}$$
$$b(\lambda) = b_\mathsf{w}(\lambda) + b_\mathsf{phy}(\lambda) + b_\mathsf{det}(\lambda) \tag{8}$$
$$b_\mathsf{b}(\lambda) = b_\mathsf{bw}(\lambda) + b_\mathsf{bphy}(\lambda) + b_\mathsf{bdet}(\lambda) \tag{9}$$

In the model we use absorption and scattering coefficients (Fig. 1) averaged over 25nm bands to match the irradiance input from a variety of sources, detailed below.

8

2.3.1 Water molecules

We assume absorption by water molecules (a_w, b_w, b_bw) to follow the spectra of Pope and Fry 1997). Scattering is taken from Smith and Baker (1981) and Morel (1974), and backscattering from Morel (1974) and Morel et al. (2007). The spectra for these are shown in Fig. 1a.

2.3.2 Detrital matter

The model uses the absorption and scattering spectrum for detrital matter (Fig. 1b) from Stramski et al. (2001). These spectra were deduced by assuming an assemblage of particles with size distribution described by a power function with slope of -4, and the values are given in terms of absorption or scattering per particle (Stramski et al., 2001). Thus Since these spectra (Fig. 1b) were calculated as a function of concentration of particles, we introduce the coefficient p_part to convert the model particulate organic carbon (POC) to number of particles, making the crude assumption that the size distribution of particles is uniform everywhere. The absorption and scattering by particles is described as:

$$a_\text{det}(\lambda) = a_\text{det}^\text{part}(\lambda)\frac{\text{POC}}{p_\text{part}} \tag{10}$$

$$b_\text{det}(\lambda) = b_\text{det}^\text{part}(\lambda)\frac{\text{POC}}{p_\text{part}} \tag{11}$$

$$b_\text{bdet}(\lambda) = b_\text{bdet}^\text{part}(\lambda)\frac{\text{POC}}{p_\text{part}} \tag{12}$$

Here we use the convention that the superscript on the a, b, and b_b terms refers to the normalization variable, here particle concentration. Units of $a_\text{det}^\text{part}(\lambda)$, $b_\text{det}^\text{part}(\lambda)$ and $b_\text{bdet}^\text{part}(\lambda)$ are m^2 particle^{-1}.

We note that in the optical community the term "non-algal particles" or NAP is frequently used for any non phytoplankton particles. In this paper we specifically use the term "detrius"

instead, as we link to the non-living organic matter pool and do not explicitly resolve other non-algal particles such as viruses and heterotrophic bacteria.

2.3.3 Coloured dissolved organic matter

CDOM absorbs highly in the short wavelengths and absorption decreases exponentially with increasing wavelength (Kitidis et al., 2006; Nelson and Siegel, 2013). CDOM is not usually explicitly resolved in marine ecosystem models (exceptions are Xiu and Chai, (2014)-and Bissett et al., 1999). Here we have resolved an explicit CDOM-like tracer (denoted "CDOM") similar to Bissett et al. (1999). The model CDOM has units of concentration (mmol $C\,m^{-3}$), and is assumed have a source that is a fraction (f_{cdom}) of DOM production, to have a long remineralization time scales (d_{cdom}) and to be bleached under high light conditions. The bleaching is parameterized to reach a maximum rate, ι_{cdom}, when PAR is above I_{cdom}, and linearly decrease at lower PAR. The sources and sinks of this CDOM-like tracer are therefore parameterized as:

$$S_{CDOM} = f_{cdom}S_{DOM_s} - \left[\gamma_T d_{cdom} + \iota_{cdom} \min\left(\frac{\sum_{\lambda=400}^{\lambda=700} E_0(\lambda)}{I_{cdom}}, 1 \right) \right] CDOM \tag{13}$$

where S_{DOM_s} is the sources of DOM (see Appendix A), and γ_T is the temperature function affecting biological rates.

We parameterize $a_{cdom}(\lambda)$ as function of "CDOM" such that:

$$a_{cdom}(\lambda) = a_{cdom}^{CDOM}(\lambda)CDOM \tag{14}$$

and

$$a_{cdom}^{CDOM}(\lambda) = c_{cdom}(\lambda_o)e^{(-s_{cdom}(\lambda-\lambda_o))} \tag{15}$$

where $a_{cdom}^{CDOM}(\lambda)$ is the concentration specific absorption of the CDOM-like tracer (Fig. 1c). The value for the spectral slope, s_{cdom} is taken from literature (Kitidis et al., 2006), and

$c_{\text{cdom}}(\lambda_o)$ is the CDOM specific absorption at reference waveband, λ_o. Although CDOM is also strongly linked to terrestrial matter, we do not provide any land sources at present. We discuss the sensitivity of the function and parameters, and compare to previous model parameterizations in Sect. 5.

2.3.4 Phytoplankton

The absorption and scattering by phytoplankton is the net effect of each phytoplankton type resolved in our model, j:

$$a_{\text{phy}}(\lambda) = \sum_j a_{\text{phy}_j}^{\text{chl}}(\lambda)\text{Chl}_j \tag{16}$$

$$b_{\text{phy}}(\lambda) = \sum_j b_{\text{phy}_j}^{\text{C}}(\lambda)M_{\text{C}j}P_j \tag{17}$$

$$b_{\text{bphy}}(\lambda) = \sum_j b_{\text{bphy}_j}^{\text{C}}(\lambda)M_{\text{C}j}P_j \tag{18}$$

The Chl a specific absorption spectra $a_{\text{phy}_j}^{\text{chl}}(\lambda)$ has units of $\text{m}^2\,(\text{mg Chl})^{-1}$. The , and the scattering ($b_{\text{phy}_j}^{\text{C}}(\lambda)$) and backscattering ($b_{\text{bphy}_j}^{\text{C}}(\lambda)$) coefficients are assumed to be functions function of phytoplankton biomass (e.g. Martinez-Vincent et al., 2013) and has units $\text{m}^2\,(\text{mol C})^{-1}$. These spectra are specific to each of the phytoplankton types j (Fig. 1d–f) as taken from literature. See discussion in Sect. 2.5 and Appendix C. $M_{\text{C}j}$ is the C : P ratio in each phytoplankton type (see Appendix A).

2.4 Phytoplankton growth

Phytoplankton growth is modelled as a function of temperature, irradiance, and nutrients as in Hickman et al. (2010) following Geider et al. (1998). The growth rate is equal to the

carbon specific photosynthesis rate:

$$\mu_j = \mathcal{P}^{\mathsf{C}}_{mj} \left(1 - \exp \left(\frac{-\Lambda_{Ej}\theta_j}{\underset{\sim}{\mathcal{P}^{\mathsf{C}}_{mj}}} \frac{-\Lambda_{Ej}\theta_j}{\underline{\mathsf{P}^{\mathsf{C}}_{mj}}} \right) \right) \tag{19}$$

where $\underset{\sim\sim}{\mathcal{P}^{\mathsf{C}}_{mj}}$ $\underline{\mathsf{P}^{\mathsf{C}}_{mj}}$ is the light saturated photosynthesis rate that is a function of temperature and nutrient limitation (see Appendix A), θ_j is the ratio of Chl a to C within each phytoplankton j (discussed further below). Λ_{Ej} the scalar irradiance absorbed by each phytoplankton, j (units are mmolC (mg Chl)$^{-1}$ d^{-1})

$$\Lambda_{Ej} = \phi_{\mathsf{max}_j} \sum_{\lambda=400}^{\lambda=700} a^{\mathsf{chl}}_{\mathsf{ps}j}(\lambda) E_0(\lambda) \tag{20}$$

where ϕ_{max_j} is the maximum quantum yield, and $a^{\mathsf{chl}}_{\mathsf{ps}j}(\lambda)$ is the Chl a specific photosynthetic absorption spectra in each waveband λ (Fig. 1e), and $E_0(\lambda)$ comes from the radiative transfer code (see Eq. 4).

Since some pigments are photo-protective, phytoplankton do not use all the light that they absorb for photosynthesis. Similar to Hickman et al. (2010) and Bisset et al. (1999) the total absorption spectra is therefore greater than the photosynthetic absorption spectra, $a^{\mathsf{chl}}_{\mathsf{phy}j} > a^{\mathsf{chl}}_{\mathsf{ps}j}$ (Fig. 1d, e). See discussion in Sect. 2.5. We also allow for photo-inhibition, as in Hickman et al. (2010), such that $\underset{\sim\sim}{\mathcal{P}^{\mathsf{C}}_{mj}}$ $\underline{\mathsf{P}^{\mathsf{C}}_{mj}}$ reduces above a critical value at high light (see Appendix A).

2.5 Plankton types

We resolve 9 phytoplankton "functional" types: these include analogues of diatoms, other large eukaryotes, coccolithophores, pico-eukaryotes, *Synechococcus*, high and low light *Prochlorococcus*, nitrogen fixing *Trichodesmium* and unicellular diazotrophs. These phytoplankton differ in their elemental composition (e.g. diatoms require silica), maximum

12

growth rate, nutrient half saturation constants, sinking rates, maximum Chl a:C, and palatability to grazers (see Tables 3 and 4).

Cell size governs many traits. Smaller phytoplankton have lower nutrient half saturation constants and sink more slowly. The maximum growth rates are guided by observations; diatoms having the highest rates and *Prochlorococcus* having the lowest (see e.g. Irwin et al., 2006). The parameter values are within ranges found in the literature and previous ecosystem model (Dutkiewicz et al., 2012; Ward et al., 2013; Monteiro et al., 2010).

In this model we treat the phytoplankton light absorption and scattering explicitly (Sect. 2.3.4). The Chl a specific absorption spectra $a_{\text{phy}j}^{\text{chl}}(\lambda)$ (units, $\text{m}^2\,\text{mg Chl}^{-1}$) varies between functional group ~~species~~ (Fig. 1d). These spectra were obtained from representative phytoplankton types ~~species~~ in cultures grown at similar growth irradiance (see references in Appendix C). The spectra capture differences in pigment composition and other taxon specific differences, including the "package effect" (Berner et al., 1989). For instance, the larger diatom has a flatter spectrum than the smaller phytoplankton (e.g. *Prochlorococcus*). Total light scattering spectra ($b_{\text{phy}j}^{\text{C}}$, Fig. 1f) were also obtained from representative phytoplankton types ~~species~~ in culture, as were the backscatter to total scatter for each phytoplankton ($b_{\text{bphy}j}^{\text{C}}$, units $\text{m}^2\,\text{mol C}^{-1}$) (Stramski et al., 2001; Subramaniam et al., 1999).

Spectra for absorption by photosynthetic pigments ($a_{\text{ps}j}^{\text{chl}}$, Fig. 1e) were derived using the pigment reconstruction technique (following Hickman et al., 2010; Babin et al., 1996). Light absorption spectra were reconstructed by scaling the weight-specific absorption coefficients for Chl a, Chl b and Chl c, photosynthetic carotenoids and non-photosynthetic carotenoids, phycoeryththrobilin and phycourobilin-rich phycoerythrins (Bidigare et al., 1990b) to obtain the lowest sum of residuals between reconstructed and observed spectra. $a_{\text{ps}j}^{\text{chl}}$ was then calculated by adjusting the measured $a_{\text{phy}j}^{\text{chl}}$ by the spectral ratio of the reconstructed spectra with and without non-photosynthetic pigments (Hickman et al., 2010).

We parameterize all phytoplankton to have the same maximum quantum yield (ϕ_{max_j}, units mol C fixed per moles photons) and all but diatoms to have the same maximum Chl a:C (θ_{max_j}, units $\text{mg Chl}\,(\text{mmol C})^{-1}$) (MacIntyre et al., 2002). We parameterize low

light *Prochlorococcus* as being photo-inhibited, as this is a distinct feature of the difference between high and low light strains (Moore and Chisholm, 1999; Hickman et al., 2010).

We resolve two zooplankton classes (large and small) that graze on the phytoplankton using a Holling III scheme (Holling, 1959). The large class preys preferentially on the diatoms, coccolithophores, and *Trichodesmium*, while the smaller class preys preferentially on the smaller phytoplankton. We additionally parameterize diatoms and coccolithophores (hard shells) and *Trichodesmium* (toxicity) as having lower palatibility. Zooplankton grazing parameters are similar to those used in Prowe et al. (2012) which were determined from a mechanistic model of zooplankton feeding (see Table 6).

2.6 Enhancements and Limitations of Optics Component~~Simulation design~~

The inclusion of radiative transfer, spectral light and capturing several important optical constituents has been a significant development of the model. However, this version of the model is not without limitations. One major, though currently necessary simplification, is to assume constant absorption and scattering spectra (Fig. 1) for each constituent. For instance, absorption spectra for phytoplankton types do in reality change based on shifts in Chl:C ratios (e.g. MacIntyre et al., 2002; Morel et al., 1993; 1995) as well as changes in ratios of photoprotective to photosynthesis pigments as a result of light, temperature and nutrient stress (e.g. Stramski et al., 2002). However, these changes are likely to be small compared to the differences already captured by the representative spectra and photoacclimation component and there is not, as yet, enough systematic observations of these alterations to constrain model parameterizations. Additionally the CDOM absorption spectra has been observed to alter regionally (e.g. Kitidis et al., 2006; Twardowski et al, 2004; Bricaud et al 2010), though as yet we feel it is premature to attempt to capture this variability in the model parameterizations.

Scattering, particularly by detrital particles, remains the least well developed aspect of the model. In particular, we neglect variations in detrital particle size distributions which is likely to be important (Stramski et al., 2001). Additionally the spectra for b_{det}^{part} that we use (Stramksi et al., 2001, Fig. 1b) makes the assumption of homogeneous spheres. However

14

it is likely that differences in shapes and internal structure of the particles will be important for altering the spectral shape (Stramski et al., 2004). We also do not take into account inelastic scattering which may be important for blue and green light in oligotrophic regions (e.g. Ge et al., 1993).

We additionally currently neglect other potentially important optical constituents such as minerals (e.g. Stramski et al., 2001), particulate inorganic carbon (e.g. Balch and Itgoff, 2009), colloids and bubbles (e.g. Stramski et al., 2004), non-photosynthetic organisms including zooplankton, bacteria (e.g. Morel and Ahn, 1991), and viruses (e.g. Stramski et al., 2001). We felt that these are, as yet, not well enough constrained to include explicitly in the model.

The limitations list above should however not detract from the major enhancement to the model and are similar to those of other models (e.g. Fujii et al., 2007; Gregg and Casey, 2007). This new model provides a unique platform to examine global implication of optical properties to the phytoplankton ecosystem, feedbacks to the biogeochemistry, and links to satellite data that are not possible with limited observational data. Here we first validate the model in a standard "default" configuration. We then provide a series of studies exploring the significance of each of the optical constituents and our parameterization. Several studies in progress build on for these results.

3   Default Simulation and Validation

We initialize the macronutrient fields (nitrate, phosphate and silicic acid) from World Ocean Atlas (Garcia et al., 2006) climatologies and the iron from previous model output. We also use previous model output to provide distribution of the ammonium, nitrite, dissolved and particulate matter. The total phytoplankton biomass is initialized from previous model output, divided equally between groups, except for the diazotrophs who are initialized at a much lower value so as not to flood the system with new nitrogen in the first few timesteps. Zooplankton are similarly initialized with equal distribution in both groups.

15

The model timestep is 3 hours. We tested this against smaller timesteps with almost identical results. We run the simulation forward for 10 years with a repeating generic "year" from the physical ECCO-GODAE products (Wunsch and Heimbach, 2007). Model results shown in this section are from the last year of the simulation. The phytoplankton establish a repeating pattern after about 3 years such that we can assume a "quasi-steady state" by year 10. A slow drift as deep water nutrient distributions adjust does not significantly change the results over the remaining time period.

4 ~~Model results~~

We evaluate the model results against a range of in situ observations and satellite derived products. In particular we focus on the unique data set including biogeochemical, ecological and (some previously unpublished) optical properties that were obtained as part of the AMT-15 cruise. Though there are other AMT cruises that include some similar and/or different combinations of optical data (e.g. AMT-19, Dall'Olmo et a;l., 2012, Martinez-Vicente et al., 2013), we chose to look at only a single transect for clarity. In particular, the combination of data on spectral irradiance penetration, a_{CDOM}, and light absorption by phytoplankton were of particular use in model validation.

3.1 Atlantic meridional transect

The model broadly reproduces the horizontal gradients at the surface, but importantly also captures the deep Chl a maximum (Fig. 3a, b), and in particular its deepening in the subtropical gyres, especially in the South Atlantic. ~~It does not capture the high Chl a values in the North Africa upwelling zone since the coarse resolution model does not adequately represent the physics of these features. Model Chl a is too high just south of the equator, where the physical model captures an upwelling area that is not in the observations. The model also has a mixing event in October at about 35S that mixes Chl a to depth, a feature not seen in the observations.~~ The model captures the depth of the nitricline across the transect (Fig. 3c, d), especially the deep section (200 m) in the South Atlantic gyres. The

16

model does not adequately resolve the North Atlantic upwelling (a resolution issue in the physical model) and nitrate and Chl a are too low in this region. Additionally the physical model has too strong upwelling ~~Again, as expected due the physical model issues, we do not capture the high nitrate supply in the North Africa upwelling zone, and nitrate is too high~~ just south of the equator leading to nitrate and Chl a being too high.

The model also captures observed variability of a_{cdom} along the AMT-15 transect: low in the surface waters where CDOM is quickly bleached, and higher in deeper waters where CDOM accumulates. Values and regional patterns compare well between model and observations (Fig. 3e, f), except just south of the equator where Chl a, and nutrient supply are also too high (as discussed above). Absorption by phytoplankton (Fig. 3g) was only measured at the surface and the deep Chl a maximum. The model captures the higher value near the deep Chl a maximum (Fig. 3h).

We have used the AMT-15 measured downwelling irradiance and upwelling zenith radiance together with the inverse-modelling procedure of Gordon and Boynton (1997, 1998) to estimate the total absorption and total backscattering in several wavelengths (Fig. 4a, c, e, g). We discuss this inversion further in Appendix D. There is a large degree of uncertainty in this inversion process, and additional noisiness provides several spurious high/low values that are not realistic. Given this caveat, we find that the model qualitatively captures (Fig. 4b, d, f, h) the magnitudes and the pattern of higher absorption/lower scattering at the higher wavebands.

Since the model realistically captures much of the variability in optical constituents, it also accurately resolves the penetration of light through the water column (Fig. 5) as found in the AMT-15 data. We compare the depth of the 1% light level: the depth where the downwelling irradiance in each waveband is 1% of the surface value ($E_{\mathrm{d}_o}^{\mathrm{below}} + E_{\mathrm{s}_o}^{\mathrm{below}}$). We find the shortest wavebands (e.g. purple line and symbols in Fig. 5) reach deepest in the South Atlantic gyre where concentrations of the optical constituents are lowest and less deep than medium wavebands (e.g. light and dark blue lines) in more equatorial regions. The penetration of blue wavebands leads to the the very deep Chl a maximum and draw down of nutrients at depth as observed in the AMT-15 transect and in the model. The 1%

depths are too deep in the North Atlantic upwelling region, since we do not capture this feature in the physics.

The model captures intricate patterns of absorption and scattering that develop from the interplay of different optical constituents and suggests the importance of treating each constituent separately for reproducing the in situ light field. We explore this further in Sect. 5.

3.2 Global results

That the model captures much of the Chl a, nutrient and optical properties on basin scale and with depth as observed during the AMT-15 is very encouraging. The model also captures many of the global features ~~(Fig. 6)~~ in Chl a (derived from MODIS satellite), primary production (derived using Behrenfeld and Falkowski, 1997) as well as macronutrients (from the World Ocean Atlas, Garcia et al., 2006), though with notable biases (Fig. 6). The broad scale features of high nutrient, high Chl a and high productivity in the high latitudes and equatorial regions, and low nutrients, low Chl a in the subtropical gyres are resolved. We do not however capture coastal features as the physical model is too coarse to resolve the important mesoscale processes. This is also true in frontal zones (such as the Western boundary currents) where primary production is too low.

Relative to the composite of iron data (Taglibue et al., 2012), we also capture high iron in the Atlantic Ocean and lower iron over much of the Pacific (Fig. 6j, ~~kg, h~~). However, iron may be too low in the tropical South Pacific and Pacific equatorial regions. Here the model aeolian dust supply (based on Luo et al., 2008) may be too low, however the physical model also does not adequately resolve equatorial undercurrents which are likely responsible for supplying sedimentary iron to this region (Radic et al., 2011; Slemons et al., 2009). Since iron limitation is too strong in this region, productivity is ~~and Chl a are~~ too low, and nitrate too high. The model also overestimates Chl a in the Southern Ocean and other high latitudes relative to the satellite product. However, the satellite Chl a algorithm have ~~have~~ a factor of 2 range error (Campbell et al., 2002) and are especially problematic in the Southern Ocean (Szeto et al., 2011).

We find that the spatial SD (between 0.85 and 1.15) and correlation (greater than 0.9) of the model vs. observed nutrients are encouraging (Fig. 7). Though we capture much of the spatial variability in the Chl a the correlations to satellite derived products are not as good. The primary production is universally too low and too uniform relative to the satellite derived product. However, we note that the satellite products of Chl a and primary production have large error margins associated with them that are not spatially homogeneous (Szeto et al., 2011).

The model ecosystem has distinctive seasonal cycles (Fig. 8) that mostly match the observed satellite derived and in situ Chl a at nine timeseries sites (locations shown in Fig. 2) collected as part of JGOFS (Kleypas and Doney, 2001). In many locations the model overestimates the satellite derived peak of the bloom (consistent with annual mean Chl a being too high), but capture the non-bloom values more accurately. However, the in situ data broadly encompass the model values. We also capture the satellite derived timing of the spring bloom, though notably do not get correct blooms at Station P, Kerfix, NABE~~miss the late summer bloom in the northern Pacific (Station P), and instead have a spring bloom. At Kerfix(in the Southern Ocean) we also do not capture the bloom timing or magnitude. The spring bloom at NABEis too early relative to both in situ and satellite derived data. It is likely that the model does not capture all the physical process occurring in these regions~~.

A unique feature of this model is irradiance reflectance output, which we have converted to remotely sensed reflectance (R_{RS}) using a fixed bidirectional function Q (see Sect. 2.2). We compare this model output to MODIS remotely sensed reflectance, $R_{RS}(\lambda)$. Despite the mismatch in wavelength and bandwidth and the oversimplification of a fixed Q, the model qualitatively captures the pattern of high reflectance in the subtropics relative to the higher productivity regions in low wavebands and the opposite pattern in higher wavebands. These initial results suggests that the model framework will be a useful laboratory for exploring satellite-like semi-analytical inversion algorithms (e.g. IOCCG report 5, 2006).

3.3 Phytoplankton biogeography

Eight of the 9 phytoplankton functional groups that we resolve have distinct biogeography (Fig. 10). This biogeography encompasses both horizontal and vertical patterns of phytoplankton biomass. The large eukaryote group does not survive in this model as it was given no specific trade off. It was large (low nutrient affinity) and had a low growth rate (typical of dinoflagellates).

We compare simulated biomass of the pico-phytoplankton to observations from the AMT-15 (Fig. 11). AMT-15 cell counts were measured by analytical flow cytometry following methods of Heywood et al. (2006) and converted to biomass using constant factors (Zubkov et al., 1998) for comparison purposes. The model captures the smallest autotrophs, *Prochlorococcus* as having smallest autotroph, *Prochlorococcus* has significant abundances through the subtropics and tropic, *Synechococcus* were more abundant at the northern poleward fringe of the subtropics, and Pico-eukaryotes were more ubiquitous and more dominant in the deep Chl a maximum that is largely captured by the model. The model *Prochlorococcus* dominate in the most oligotrophic regions (Dutkiewicz et al., 2009). In the 20 to 5° S region the model nutrient source is too high (discussed above) and *Synechococcus*-analogues unrealistically dominate instead in the model. The model distribution . This is also indicated by the Chl a and nitrate which is too high in this region (Fig. 3), discussed above. Other than this region, the model *Synechococcus* are only found in high concentration in African upwelling region and the northern poleward fringes of the subtropics as is observed in the AMT-15 data. Pico-eukaryotes are more ubiquitous and are especially found in the deep Chl a maximum both in the observations and the model . Estimates of large phytoplankton biomass (e.g. diatoms, Coccolithophores) compared well to observations made along other AMT cruises (Tarran et al. 2006; Cermeño et al. 2008) were not available from this cruise.

The MAREDAT (MARine Ecosystem DATa, Buitenhuis et al., 2013) compilation provides a comprehensive, though still sparse, climatological distribution of several plankton functional groups. Here we re-grid the MAREDAT compilation onto a 5° grid with all

observations between 0 and 50 m averaged together and compare this to the model output (Fig. 12). For the model results we sum the *Prochlorococcus*, *Synechococcus* and pico-eukaryote groups to compare to the observations of pico-phytoplankton. The model captures the ubiquitous nature of the pico-phytoplankton, lack of Coccolithophores in the subtropical gyres and polar extent of the Southern Ocean, high diatom values in the high latitudes and in the equatorial upwelling regions, low (or lack) of diazotrophs in the southern Pacific gyres. However, model coccolithophore biomass is in general too high and diazotroph biomass has a peak too far south in the North Atlantic. Though the MAREDAT compilation includes micro, meso and macro zooplankton, the former and the latter data are very sparse. Since we do not have direct analogues in the model, we show here only the meso zooplankton biomass observations (Fig. 12i). The model captures the patterns of high and low values of zooplankton biomass.

Given the sparsity of in situ measurements of phytoplankton types, it is natural to attempt to capture aspects of biogeography from space (IOCCG report 15, 2014; IOCCG report 9, 2009). Here we compare the model output to the PHYSAT product (Alvain et al., 2008) which empirically relates optical properties to specific (probably dominant) phytoplankton types (Fig. 13a, c) for January and July and compare to model dominant types (Fig. 13). In both model and PHYSAT we find that cyanobacteria dominate the tropics and subtropics, diatoms play a substantial role in the summer biomass. and

PHYSAT also resolves Haptophytes (which includes coccolithophores) and *Phaeocystis*, while the model separates out instead pico eukaryotes and coccolithophores. The model captures a combination of coccolithophores and pico-eukaryotes dominate as dominant in the mid-latitudes.

These global "observations" contain many uncertainties stemming mainly from the scarcity of in situ data, but the model does not disagree with their findings. The model captures key patterns of observed optical and ecological properties. It provides a tool to explore aspects of the ocean biogeochemistry and ecosystem that are not possible with models that do not explicitly resolve radiative transfer, spectral irradiance, and an explicit resolution of the different water optical properties. In the next section we explore the role of the various water constituents on the irradiance spectrum and how they impact biogeochemistry and ecosystem structures.

4 Sensitivity experiments: Value of added model complexity.

We conduct two sensitivity experiments to highlight the importance of the extra level of complexities of this new version of the model. In the first experiment (designated EXP-V0) the biogeochemistry and ecosystem are the same as in the default experiment described above (designated EXP0) but there is only a single band of irradiation (400-700nm, summed over the original 25nm, so that total PAR is conserved); attenuation (c_{tot}) of PAR is a function only of absorption by water molecules and Chl-a summed over all phytoplankton types: $c_{tot} = a_{wo} + a_{chlo}Chl_{tot}$, where $a_{wo} = 0.04$ m^{-1}, and $a_{chlo} = 0.04$ m^2 (mg Chl)$^{-1}$. There is no explicit account taken for optical role of CDOM or detritus (though the value chosen for a_{chlo} does implicitly include their role). Similar parameterizations have been used in previous versions of our model (e.g. Dutkiewicz et al., 2014), and are also common in many other biogeochemical models.

The results from EXP-V0 (Fig. 14a) reveals a much more latitudinally uniform penetration of light, and in particular the deep chlorophyll maximum in the subtropical gyre is too shallow relative to the default experiment (EXP0, Fig. 14c) and observations (Fig. 3a).

In experiment EXP-V1 we include all the optical constituents explicitly (as in EXP0), though with only a single band of PAR (as in EXP-V0). We assume the absorption and scattering coefficients for 500nm in this experiment. This experiment (Fig. 14 b) reveals substantial more realistic varying distribution of the deep chlorophyll maximum and penetration of PAR. The addition of spectral light leads to even deeper penetration of light in the subtropical gyres (default experiment, EXP0, Fig. 14c): deepest penetrating light is in the blue/green range and an average absorption across one waveband will not capture these differences.

These sensitivity experiments suggest that explicitly capturing regional changes in all optical constituents is essential for the realistic light penetration variations. Spectral light further enhances the realism of the results. The addition of the radiative transfer code is essential for obtaining upwelling irradiance that can link to satellite products.

5 Sensitivity experiments: role of optical constituents

Optical ~~The optical~~ constituents play varying roles in their effect on irradiance attenuation (absorption and scattering). These roles have long been a topic of interest, however many studies have included only limited observations and been of highly localized in character (e.g. Jerlov, 1953; Chang and Dickey, 1999), but have however recognized that they vary regionally (e.g. Barnard et al., 1998; Simeon et al., 2003). Targeted cruises have also provided larger scale observations indicating a wide range of value for each constituent and altering importance in different regions (e.g. BIOSOPE, Bricaud et al 2010). Additionally, several attempts have been made to construct algorithms to determine the relative contributions from more easily measured quantities, including those from satellite (e.g. Maritorena et al., 2002; Lee et al., 2002; 2007; Ciotti and Bricaud, 2006; Werdell et al., 2013; Zheng and Stramski, 2013). Our model provides a unique global 3-dimensional perspective. Here our results focus on an (extended) AMT transect ~~differ between regions and depth~~ (Figs. 15 and 16), however, they are also consistent with observations in other regions (e.g. Bricaud et al. 2010).

Absorption by water molecules is most important at longer wavebands (Pope and Fry, 1997), but still has an impact at shorter wavebands (Fig. 15a, b, i, j). It is relatively more important in lower productive waters (e.g. South Atlantic gyre) because the concentrations of other constituents are relatively low. Absorption by detrital matter plays a role, especially near the 1% depth in highly productive regions and at shorter wavebands (Fig. 15c, d, i, j) as suggested by observations (e.g. Jerlov 1953). Absorption by phytoplankton plays a significant role where Chl a is highest (e.g. the deep Chl a maximum, as found in observations, e.g. Chang and Dickey, 1999) at wavelengths less than 550 nm, and little role at longer wavelength (Fig. 15g, h, i, j, see also Fig. 1). Absorption by CDOM at short wavebands is important (as seen in observations e.g. Jerlov, 1953) in most regions, particularly where productivity is high where it is the dominant absorber. It also has, relative to other constituents, a large role at depth (as seen in observations e.g. Simeon et al., 2003; Bricaud et al., 2010; Nelson and Siegel, 2013). At long wavebands CDOM plays very little role. Scattering by phytoplankton is relatively most important at shallower depths, while scattering by detrital matter is dominant deeper at all wavelengths (Fig. 16).

We perform a series of sensitivity experiments to explore the role of each constituent in setting the irradiance field in the ocean and on surface reflectance, and see how changes to these constituents feed back to the ecosystem and biogeochemistry. The range of values for these experiments are designed to cover and go be beyond the natural range of the absorption and scattering by the water constituents. We additionally explore how different assumptions and parameterizations for the optical constituents affects the simulation results.

5.1 Detrital matter

Observations have determined that detrital matter does play a role in light attenuation, though with varying regional importance (e.g. Jerlov 1953; Bricaud et al., 2010). We conduct several sensitivity studies to explore the relative importance of a_{det} and b_{det} (Fig. 17) globally in the model. We run each experiment from the same initial conditions as the "default" (EXP0) discussed in Sect. 3, and present results for the final year after 10 years

of integration. We artificially alter $a_{\mathsf{det}}^{\mathsf{part}}(\lambda)$ or $b_{\mathsf{det}}^{\mathsf{part}}(\lambda)$ as noted below, such that a_{det} and b_{det} are manipulated. The experiments include the feedbacks to nutrients and productivity. In experiment EXP-D5 we explore a different parameterization for $a_{\mathsf{det}}(\lambda)$ that was used in Fujii et al. (2007).

1. EXP0: this is the default run where

$$a_{\mathsf{det}}(\lambda) = a_{\mathsf{det}}^{\mathsf{part}}(\lambda)\frac{\mathsf{POC}}{p_{\mathsf{part}}}$$
$$b_{\mathsf{det}}(\lambda) = b_{\mathsf{det}}^{\mathsf{part}}(\lambda)\frac{\mathsf{POC}}{p_{\mathsf{part}}}$$
$$b_{\mathsf{dbet}}(\lambda) = b_{\mathsf{bdet}}^{\mathsf{part}}(\lambda)\frac{\mathsf{POC}}{p_{\mathsf{part}}}$$

2. EXP-D1: we set $a_{\mathsf{det}}^{\mathsf{part}}(\lambda) = 0$

3. EXP-D2: we set $a_{\mathsf{det}}^{\mathsf{part}}(\lambda)$ artificially to four times the values used in EXP0

4. EXP-D3: we set $b_{\mathsf{det}}^{\mathsf{part}}(\lambda) = 0$

5. EXP-D4: we set $b_{\mathsf{det}}^{\mathsf{part}}(\lambda)$ four times the value EXP0

6. EXP-D5: as in Fujii Fujii et al. (2007) we represent:

$$a_{\mathsf{det}}(\lambda) = a_{\mathsf{det}}^{\mathsf{POC}}(\lambda_o)\mathsf{POC}e^{(-0.01(\lambda - \lambda_o))}$$

where $a_{\mathsf{det}}^{\mathsf{POC}} = 0.1\,\mathrm{m}^2\,\mathrm{g\,C}^{-1}$ (Fujii et al., 2007) and $\lambda_o = 450\,\mathrm{nm}$.

Removing the detrital absorption (EXP-D1) leads to bluer wavebands reaching to greater depth (Fig. 17a). This favours phytoplankton, at least in the subtropics, which absorb more efficiently in the blue part of the spectrum (i.e. *Prochlorococcus*, Fig. 17c) as anticipated from laboratory studies (e.g. Moore et al., 1995). On the other hand, having stronger

detrital absorption (EXP-D2) leads to shallower 1 % light levels for the blue wavebands. The corresponding red-shifted light favours *Synechococcus* which absorb more efficiently in this part of the spectrum. With less irradiance absorbed in EXP-D1, we find a higher percentage is reflected at the shorter wavebands (Fig. 17d). Similarly as more irradiance is absorbed (EXP-D2), there is a reduction in the reflectance.

We observe distinct biogeochemical feedbacks. With lower absorption by detritus (EXP-D1) the depth integrated phytoplankton biomass in the high latitudes increases (Fig. 17b), leading to higher nutrient utilization in these locations. Thus the transport of nutrients to the lower latitudes is reduced (see e.g. Sarmiento et al., 2004; Dutkiewicz et al., 2005) reducing biomass in those locations. This will even further increase the 1 % light depth for the blue wavebands and consequently favour *Prochlorococcus* more. The lower absorption by detritus therefore leads to expansion of the oligotrophic subtropical gyres. Conversely, with more absorption (EXP-D2), we find lower depth integrated productivity in the high latitudes, higher nutrient supply to subtropics, reduced oligotrophic regions and stronger favouring of *Synechococcus*. This feedback between the light field and the biogeochemistry can only be captured by a fully three-dimensional coupled ecosystem-radiative transfer model.

The main attenuation of light with depth is through absorption, and as such alterations Alterations to the backscattering by detrital matter (EXP-D3 and EXP-D4) have little effect on the irradiance fields at depth (Fig. 17a) and thus little change to the dominant functional type community structure (Fig. 17c). However scattering has major impact on the amount and quality of the upwelling light and as such the changes to the irradiance reflectance is large (Fig. 17d).

In EXP0, a_{det} is calculated relative to number of detrital particles, whereas in EXP-D5 we parameterized it relative to particulate organic carbon (POC) concentrations (following Fujii et al., 2007). We find very similar patterns and magnitudes of $a_{det}(450)$ using these two methods. Slight difference in magnitude can be attributed the values chosen for a_{det}^{POC} and p_{part} in the respective parameterizations. There is consequently little difference to biomass, phytoplankton distributions and reflectance between the two experiments.

5.2 Coloured dissolved organic matter

CDOM and its contribution to light absorption is observed to vary in different regions of the ocean (e.g. Jerlov 1953, Bricaud 1981, Nelson and Seigel, Morel et al., 2010) and many studies have attempted to empirically link a_{cdom} to other more easily measured quantities such as Chl-a (e.g. Morel, 2009). However these studies are still regional or include only sparse data. We conduct a series of sensitivity experiments that test assumptions and importance of ~~about~~ a_{cdom} globally and its feedback to the biogeochemistry. In two experiments (EXP-C1) and (EXP-C2) we assume no and significantly more absorption by CDOM respectively. In additional sensitivity experiments (EXP-C3, EXP-C4, and EXP-C6) we explore the consequences of different parameterization of a_{cdom} as used in previous model studies (e.g. Greg and Casey, 2009; Mouw et al., 2012; Fujii et al., 2007; Hickman et al., 2010).

In all experiments $a_{\text{cdom}}(\lambda)$ is an exponential function with wavelength:

$$a_{\text{cdom}} = \chi_{\text{cdom}} e^{(-s_{\text{cdom}}(\lambda - \lambda_o))}$$

In the series of experiments we make different assumption on χ_{cdom}:

1. EXP0: $\chi_{\text{cdom}} = c_{\text{cdom}}(\lambda_o)\text{CDOM}$
   This is our default experiment detailed in previous sections.

2. EXP0-C1: $\chi_{\text{cdom}} = 0$
   This experiment artificially assumes that there is no a_{cdom}.

3. EXP-C2: $\chi_{\text{cdom}} = 4 \cdot c_{\text{cdom}}(\lambda_o)\text{CDOM}$
   This experiment is the same as the default (EXP0), but with CDOM artificially able to absorb four times as much light in each waveband.

4. EXP-C3: $\chi_{\text{cdom}} = c_{\text{chl}}(a_{\text{w}}(\lambda_o) + \sum_j a_{\text{phy}j}^{\text{chl}}(\lambda_o)\text{Chl}_j)$
   Studies (e.g. Morel, 2009) have noted an empirical relationship between mean Chl a and a_{cdom}. But regionally there is a large variation in the ratio of Chl a and a_{cdom} (e.g.

27

Bricaud et al., 1981; Kitidis et al., 2006; Morel et al., 2010). Here, as is done in Gregg and Casey (2007), we assume that a_{cdom} is a function of Chl a, and $c_{chl} = 0.8$ (unitless) to match the magnitudes of EXP0.

5. EXP-C4: $\chi_{cdom} = c_{cdom} f_{cdom} DOM$
   Since CDOM is part of the DOM pool, a previous model-based study (Mouw et al., 2012) has assumed that some portion of the DOM pool (f_{cdom}) is CDOM. Here we assume $c_{dom} = 0.00508\,\mathrm{m^2\,mg^{-1}}$ and $f_{dom} = 0.0323$ following Bisset et al. (1999).

6. EXP-C5: $\chi_{cdom} = 0.016\,(\mathrm{m^{-1}})$
   Other studies (e.g. Fujii ~~Fujii~~ et al., 2007; Hickman et al., 2010) have assumed a uniform aCDOM at each wavelength. For specific regions of the ocean (e.g. clear subtropical water, Hickman et al., 2010) or for regional studies this may be appropriate. Here for comparison we use $\chi_{cdom} = 0.016\,(\mathrm{m^{-1}})$ as in Fujii et al. (2007).

Community structure shifts significantly in response the the amount of irradiance that the CDOM absorbs (Fig. 18c). No CDOM absorption (EXP0-C1) favours bluer adapted *Prochlorococcus* and high absorption (EXP0-C2) leads to more *Synechococcus*. There is also similar impact on the biogeochemistry and shifting boundaries of the oligotrophic subtropical gyres as in the detrital experiments (Fig. 18b). The model experiments thus reveal a potentially important role for CDOM in setting phytoplankton community structure via alteration of the visible light spectrum, building on previous studies (e.g. Arrigo and Brown 1996). The amount of absorption by CDOM impacts the reflectance, again similar to the results seen with detrital absorption (Fig. 18d).

The three alternative parameterizations of χ_{cdom} (EXP-C3, EXP-C4, and EXP-C5) lead to very different a_{cdom} fields (Fig. 18a). There are consequently shifts in the light fields and penetration depths of different wavebands, and corresponding regional shifts in the dominant functional type~~community structure~~. In the parameterizations that either tie χ_{cdom} to Chl a (EXP-C3) or to DOM (EXP-C4), a_{cdom} is almost non-existent below the 1% light level (Fig. 18), at odds with observations (e.g. Simeon et al., 2003; Bricaud et al., 2010~~Fig. 18~~). Above the 1% light level the patterns of a_{cdom} are relatively realistic in these

experiments, with higher a_{cdom} in productive regions and lower in less productive regions. However, there are significant differences to the default run and ~~dominant functional types are~~ community structure is altered (Fig. 18c). The uniform a_{cdom} simulation (EXP-C5) has a more uniform 1 % light depth along the transect, reflecting the importance of CDOM for spatial variability in the depth of the euphotic zone. Since alterations to a_{cdom} significantly affect the irradiance propagation, leading to changes in the upwelling, the impact of CDOM on the reflectance is important, and all experiments show a strong response (Fig. 18d).

These experiments illustrate that the parameterization of CDOM has very significant impact on community structure and reflectance, and suggests that it is crucial to explicitly include CDOM in models and that we learn more about its variability in the ocean (Morel et al., 2010; Nelson and Siegel, 2013).

5.3 Phytoplankton

Idealized experiments were also conducted to explore the sensitivity due to phytoplankton absorption and scattering (Fig. 19). We artificially manipulate $a_{\mathrm{phy}j}^{\mathrm{chl}}(\lambda)$ and $b_{\mathrm{phy}j}^{\mathsf{C}}$ affecting a_{phy} and b_{phy}.

1. EXP0: this is the default run with each phytoplankton type has a specific absorption and scattering spectra (Fig. 1d, e, f).

2. EXP-P1: we artificially set $a_{\mathrm{phy}j}^{\mathrm{chl}}(\lambda) = 0$ for irradiance attenuation process, but still assume that phytoplankton growth depends on light as in EXP0. This is a highly hypothetical experiment.

3. EXP-P2: we artificially set $a_{\mathrm{phy}j}^{\mathrm{chl}}(\lambda)$ to four times that of EXP0 for irradiance attenuation process, but still assume that phytoplankton growth depends on light as in EXP0. This is therefore also a highly hypothetical experiment.

4. EXP-P3: we set $b_{\mathrm{phy}j}^{\mathsf{C}} = 0$.

5. EXP-P4: we assume all phytoplankton have the same absorption properties (the mean, black lines, in Fig. 1d, e) for both $a_{\mathrm{phy}j}^{\mathrm{chl}}(\lambda)$ and $a_{\mathrm{ps}j}^{\mathrm{chl}}(\lambda)$.

29

6. EXP-P5: we assume all phytoplankton types have the same scattering and backscattering properties (the mean, black line, in Fig. 1f).

Altering the absorption by phytoplankton (EXP-P1 and EXP-P2) has a similar impact as altering CDOM or detritus (Fig. 19). There are similar changes to the irradiance field, dominant functional type ~~community structure~~, and reflectance with consequent feedbacks to the biogeochemsitry.

As discussed above, the main attenuation of light is through absorption, and thus when ~~When~~ we assume no scattering by phytoplankton (EXP-P3) there is almost no change in dominant functional type. However, since scattering does substantially affect the upwelling light there is ~~community structure, but~~ some (though small) change to reflectance compared to the default run (EXP0). An experiment with four times b_{phy} has similar results (not shown here).

In EXP-P4 and EXP-P5 we explore the importance of the phytoplankton type specific absorption and scattering spectra in setting their biogeography and biogeochemical consequences. Total a_{phy}, the irradiance field and light penetration depths of each waveband are altered when we assume a mean absorption for all phytoplankton (EXP-P4). Total a_{phy} is generally increased in the high latitudes and decreases at low latitudes (Fig. 19a). This occurs because diatoms (which dominate the high latitudes) have lower absorption per unit Chl a than the mean spectra (see Fig. 1e), and pico-phytoplankton (that dominate the lower latitudes) have a higher absorption than the mean. Community structure is also altered (Fig. 19c) showing that the photosynthetic ~~photosynthetetic~~ absorption specific to each type is important for the emergent biogeography as has been suggested by previous studies (Bidigare et al., 1990a; Huisman and Weissing, 1995; Moore et al., 1995; Stomp et al., 2004; Hickman et al., 2010). In this study ~~. In particular~~, coccolithophores have a spectra that absorbs well in the blue-green light (Fig. 1a.) ~~.~~ Once this advantage is removed diatoms take over their domain. Changes to irradiance reflectance also occur as a direct result (Fig. 19d).

When assuming a mean scattering spectra for all phytoplankton (EXP-P5) we find, similar to EXP-P3, almost no difference to the irradiance field, dominant functional type ~~community~~

or biogeography. There are, however, small changes to the reflectance. Changes in the reflectance are also apparent when the mean a_{phy} was used (EXP-P4). Differences in reflectance caused by phytoplankton optical properties underpin many efforts to map phytoplankton functional groups from space (see e.g. IOCCG report 15, 2014).

6 Discussion

In this paper we have presented a version of the MIT biogeochemistry-ecosystem model (the "Darwin Project" model) which now incorporates radiative transfer, spectrally resolved irradiance, and explicit representation of optically important water constituents. Our treatment of optical properties combines many features from prior studies (e.g. Gregg et al., 2007; Fujii ~~Fujii~~ et al., 2007; Mobley, 2011; Bissett et al., 1999, 2004), but is more comprehensive than most. In particular we include a detailed absorption by several different types of phytoplankton as in Gregg and Casey (2007), explicitly resolve a CDOM like tracer as in Xiu and Chai (2014) and Bisset et al. (1999), and also resolve detrital particulate matter similar to Fujii et al. (2007).

We have evaluated our model against a range of in situ observations and satellite derived products. The model captures the large scale biogeochemical, ecosystem and optical characteristics as suggested by these datasets. In particular we have used a unique dataset collected during AMT-15 which includes concurrent optical, biogeochemical and ecosystem measurements. The model captures the observed basin scale and vertical distribution. In many of the instances where the model does not compare well to the observations, we find that the physics of the model is at least partly responsible.

The model captures spatial light absorption by different optical constituents, and the relative magnitude of the scattering. However, the scattering, particularly by detrital particles, remains the least well constrained aspect (see Section 2.6). ~~At the moment, we neglect variations in detrital particle size distributions. We resolve the main optically important water constituents, but still neglect minerals (e.g. Stramski et al., 2001) and particulate inorganic carbon (e.g. Balch and Itgoff, 2009)that may also be important~~.

Each of the optical constituents resolved in the model (water, CDOM, detrital particles and phytoplankton) have an important role in attenuating irradiance through the water column: but the relative importance differs between region, with depth, and with wavelength (Fig. 15). CDOM was relatively more important to light absorption in high productive regions, phytoplankton were important at the deep Chl a maximum and absorption by water was most important in the clear oligotrophic waters.

Our sensitivity experiments suggest that models that neglect the explicit and independently varying absorption by detrital particulate matter and CDOM are missing important components that have implications for the biogeochemistry and productivity of the model. For instance we find that the magnitude of the light absorption of any of the water constituents that we resolve is important in setting the penetration of irradiance in different wavebands. The subsurface chlorophyll maximum can indeed be captured without including all constituents and spectral light (as seen in EXP-V0, and in other models, e.g. Fennel and Boss, 2003; Wang et al., 2009). However, the model developments presented were necessary for capturing the regional variability in depth of the subsurface chlorophyll maximum, in particular, by resolving the deep penetration of blue-green wavelengths in the subtropical gyres. Not including any of the constituents leads to an unrealistically regionally uniform depth of the deep chlorophyll maximum.

Changes to the irradiance spectrum will have important ramification for the community structure. Lower absorption by the optical constituents leads to deeper penetration of blue light and favours phytoplankton which absorb better in the shorter wavelengths (e.g. *Prochlorococcus*). However, the penetration of light also has a large impact on the biogeochemistry and biogeography on global scales. In the sensitivity studies with less light absorption, there was more primary production at the higher latitudes, and reduced nutrients transport to the lower latitudes. Thus changes in absorption could impact the size of the oligotrophic regions, which in turn impacted the community structure.

An important product of the model is the surface irradiance reflectance that provides a more direct comparison to satellite data than derived products such as Chl a or primary production. These derived products rely on empirical algorithms to convert from more

direct measurement of ocean colour (e.g. reflectance) which introduce a large degree of uncertainty to the output (see e.g. Campbell et al., 2002; Carr et al., 2006). Thus directly relating model output to satellite reflectance has exciting promise.

The absorption by any of the optical constituents strongly determines the amount of upwelling irradiance and consequently the surface reflectance. In particular, we found that the regional variations in CDOM are important in setting the patterns of reflectance (see EXP-C5). Though alterations to scattering appears to have little effect on the in-water optical fields, they have significant impact on the surface reflectance fields. Even slight changes to the scattering by phytoplankton (see EXP-P5) has an effect on the reflectance. Such changes are important when attempting to retrieve information on the community structure from ocean colour satellite products (e.g. IOCCG report 15, 2014).

7 Conclusions

The amount and type of irradiance that penetrates through the water column is an important issue when studying phytoplankton productivity and community structure. And yet, ocean models routinely offer very crude parameterizations of light attenuation and neglect the spectral quality. We have improved the MITgcm ecosystem and biogeochemistry model by incorporating spectral light, explicit radiative transfer and representations of several optical constituents. The model performed well when compared to observations. Capturing each of the optically important constituents explicitly, and including a spectrum of light was important for obtaining realistic variability in depth of the subsurface chlorophyll maximum, and in resolving the deep penetration of blue-green wavelengths in the subtropical gyres important for phytoplankton community structure~~The model provides a useful platform to explore the relative importance of different optical constituents for biogeography, biogeochemistry and optical properties such as those measured by satellite~~.

The sensitivity studies were intentionally hypothetical to provide a wide range of responses. They provide evidence that capturing how each of the optical constituents absorbs and scatters irradiance has important ramifications for biogeochemistry and

33

the phytoplankton community structure. This feedback between the light field and the biogeochemistry can only be captured by a fully three-dimensional coupled ecosystem-radiative transfer model.

The model provides a useful platform to explore the relative importance of different optical constituents for biogeography, biogeochemistry and optical properties such as those measured by satellite. We believe that this model will useful in examining the role of the irradiance spectrum and pigments in setting biogeography (Hickman et al., 2015), how changes in irradiance and/or optical constituents will impact the future oceans, and in providing a laboratory to explore the use of water leaving radiance as a marker of changes in the ecosystem.

Appendix A: Ecosystem and biogeochemical model equations

The model equations are based on those of Follows et al. (2007), Dutkiewicz et al. (2009, 2012), and Hickman et al. (2010). We consider the cycling of phosphorus, nitrogen, silica, iron as well as carbon, alkalinity, and dissolved oxygen (the latter three following Ullman et al., 2009). We also resolve here explicit dynamic Chl a (following Geider et al., 1998) and a tracer that mimics coloured dissolved organic matter (CDOM). We provide a complete set of the equations here.

Several nutrients N_i nourish many phytoplankton types P_j which are grazed by several zooplankton types Z_k. Mortality of and excretion from plankton, and sloppy feeding by zooplankton contribute to a dissolved organic matter DOM_i pool and a sinking particulate organic matter pool POM_i. Subscript i refers to a nutrient/element, j for a specific phytoplankton type, and k for a zooplankton type. Here $i = PO_4$, inorganic fixed nitrogen (includes NO_3, NO_2, NH_4), Fe, Si and C. Particulate inorganic carbon (PIC), Alkalinity (A) and dissolved oxygen (O_2) are also included in this framework. All tracers, X are advected and diffused by the three-dimensional flow fields:

$$\frac{\partial X}{\partial t} = -\nabla \cdot (\mathbf{u}X) + \nabla \cdot (\mathbf{K}\nabla X) + S_X \tag{A1}$$

where

$\mathbf{u} = (u, v, w)$, velocity in physical model,

$\mathbf{K}$ are the mixing coefficients used in physical model,

S_X are sources and sinks of tracer X.

The source and sinks of each tracer, S_X, are different and including biological transformations, chemical reactions and external sources and sinks. Phytoplankton are assumed to have fixed elemental ratios following Redfield (1934). The base currency of the plankton equations is phosphorus.

Nutrients:

$$S_{\text{PO}_4} = -\sum_j [\mu_j P_j] + r_{\text{dop}} \gamma_{\text{T}} \text{DOP} \tag{A2}$$

$$S_{\text{Si}} = -\sum_j [\mu_j P_j \mathbf{M}_{\text{Si}_j}] + r_{\text{dosi}} \gamma_{\text{T}} \text{POSi} \tag{A3}$$

$$S_{\text{FeT}} = -\sum_j [\mu_j P_j \mathbf{M}_{\text{FeT}_j}] + r_{\text{dofe}} \gamma_{\text{T}} \text{DOFe} - c_{\text{scav}} \text{Fe}' + F_{\text{atmos}} + F_{\text{sed}} \tag{A4}$$

$$S_{\text{NO}_3} = -\sum_j [\mu_j P_j \mathbf{M}_{\text{IN}_j} \Gamma_{\text{no3}_j}] + \zeta_{\text{no3}} \text{NO}_2 - (1 - H_{\text{ocrit}}) \frac{R_{\text{dno3}}}{R_{\text{denit}}} D_{\text{denit}} \tag{A5}$$

$$S_{\text{NO}_2} = -\sum_j [\mu_j P_j \mathbf{M}_{\text{IN}_j} \Gamma_{\text{no2}_j}] + \zeta_{\text{no2}} \text{NH}_4 - \zeta_{\text{no3}} \text{NO}_2 \tag{A6}$$

$$S_{\text{NH}_4} = -\sum_j [\mu_j P_j \mathbf{M}_{\text{IN}_j} \Gamma_{\text{nh4}_j}] + r_{\text{don}} \gamma_{\text{T}} \text{DON} \tag{A7}$$

$$S_{\text{C}} = -\sum_j [\mu_j P_j \mathbf{M}_{\text{C}_j}] - \sum_j [\mu_j P_j R_{rj}] + r_{\text{doc}} \gamma_{\text{T}} \text{DOC} + d_{\text{pic}} \text{PIC} + F_{\text{C}} + D_{\text{C}} \tag{A8}$$

Plankton:

$$S_{P_j} = \mu_j P_j - m_{\mathsf{p}j}\gamma_{\mathsf{T}} P_j - \sum_k [g_{jk} Z_{k,i=1}] - \frac{\partial(w_{\mathsf{p}j} P_j)}{\partial z} \tag{A9}$$

$$S_{Z_{ki}} = Z_{\mathsf{k}i} \sum_j [\zeta_{jk} g_{jk} \mathbf{M}_{ij}] - m_{\mathsf{z}k}\gamma_{\mathsf{T}} Z_{\mathsf{k}i} - m_{\mathsf{z}2k}\gamma_{\mathsf{T}} Z_{\mathsf{k}i}^2 \tag{A10}$$

Chlorophyll a:

$$S_{\mathsf{Chl}_j} = \mathbf{M}_{\mathsf{C}j} \left(\rho_j \mu_j P_j - \theta_j m_{\mathsf{p}j}\gamma_{\mathsf{T}} P_j - \theta_j \sum_k [g_{jk} Z_{k,i=1}] - \frac{\partial(w_{\mathsf{p}j}\mathsf{Chl}_j)}{\partial z} \right)$$
$$+ t_{\mathsf{chl}}(\theta_{oj} - \mathbf{M}_{\mathsf{C}j}\theta_j P_j) \tag{A11}$$

36

Particulate and dissolved matter:

$$
\begin{aligned}
S_{\mathsf{POM}_i} = & -\gamma_{\mathsf{T}} r_{\mathsf{pom}_i} \mathsf{POM}_i - \frac{\partial(w_{\mathsf{pom}_i} \mathsf{POM}_i)}{\partial z} + \sum_j [(1 - \varphi_{\mathsf{mp}_{ij}}) m_{\mathsf{p}j} P_j \mathbf{M}_{ij}] \\
& + \sum_k \left[(1 - \varphi_{\mathsf{mz}_{ik}}) \left(m_{\mathsf{z}k} Z_{ik} + m_{\mathsf{z}2k} Z_{ik}^2 \right) \right] \\
& + \sum_k \sum_j [(1 - \varphi_{\mathsf{g}_{ijk}})(1 - \zeta_{jk}) g_{ij} \mathbf{M}_{ij} Z_k]
\end{aligned}
\tag{A12}
$$

$$
\begin{aligned}
S_{\mathsf{DOM}_i} = & -\gamma_{\mathsf{T}} r_{\mathsf{dom}_i} \mathsf{DOM}_i + (1 - f_{\mathsf{cdom}}) \gamma_{\mathsf{T}} r_{\mathsf{pom}_i} \mathsf{POM}_i + \sum_j [\varphi_{\mathsf{mp}_{ij}} m_{\mathsf{p}j} P_j \mathbf{M}_{ij}] \\
& + \sum_k \left[\varphi_{\mathsf{mz}_{ik}} \left(m_{\mathsf{z}k} Z_{\mathsf{i}k} + m_{\mathsf{z}2k} Z_{\mathsf{i}k}^2 \right) \right] + \sum_k \sum_j [\varphi_{\mathsf{g}_{ijk}}(1 - \zeta_{jk}) g_{ij} \mathbf{M}_{ij} Z_{\mathsf{k}i}] \\
& + \gamma_{\mathsf{T}} C\mathsf{DOM}_i \left[d_{\mathsf{cdom}} + \iota_{\mathsf{cdom}} \min \left(\frac{\sum_{\lambda=400}^{\lambda=700} E_0(\lambda)}{I_{\mathsf{cdom}}}, 1 \right) \right]
\end{aligned}
\tag{A13}
$$

$$
\begin{aligned}
S_{C\mathsf{DOM}_i} = & \; f_{\mathsf{cdom}} \left(\gamma_{\mathsf{T}} r_{\mathsf{pom}_i} \mathsf{POM}_i + \sum_j [\varphi_{\mathsf{mp}_{ij}} m_{\mathsf{p}j} P_j \mathbf{M}_{ij}] + \sum_k \left[\varphi_{\mathsf{mz}_{ik}} \left(m_{\mathsf{z}k} Z_{\mathsf{k}i} + m_{\mathsf{z}2k} Z_{\mathsf{k}i}^2 \right) \right] \right. \\
& \left. + \sum_k \sum_j [\varphi_{\mathsf{g}_{ijk}}(1 - \zeta_{jk}) g_{ij} \mathbf{M}_{ij} Z_{\mathsf{k}i}] \right) \\
& - \gamma_{\mathsf{T}} C\mathsf{DOM}_i \left[d_{\mathsf{cdom}} + \iota_{\mathsf{cdom}} \min \left(\frac{\sum_{\lambda=400}^{\lambda=700} E_0(\lambda)}{I_{\mathsf{cdom}}}, 1 \right) \right]
\end{aligned}
\tag{A14}
$$

$$
S_{\mathsf{PIC}} = -d_{\mathsf{pic}} \mathsf{PIC} - \frac{\partial(w_{\mathsf{pic}} \mathsf{PIC})}{\partial z} \sum_j [m_{\mathsf{p}j} P_j R_{\mathsf{r}j}] + \sum_k \sum_j [g_{ij} R_{\mathsf{r}j} Z_{\mathsf{k}i}]
\tag{A15}
$$

37

Alkalinity:

$$S_A = \sum_j [\mu_j P_j \mathbf{M}_{NO_3 j}] - S_{NO_3} - 2\left(\sum_j [\mu_j P_j R_{rj}] + d_{pic} PIC\right) + D_A \tag{A16}$$

Dissolved oxygen:

$$S_{O_2} = F_{O_2} + \mathbf{M}_{O_j} \sum_j \mu_j P_j - H_{ocrit} M_{O_j} \gamma_T r_{dom_i} DOM_i \tag{A17}$$

where:

μ_j is the growth rate of phytoplankton j (function provided below),

$\mathbf{M}_{ij}$ is the matrix of ratios of element i to phosphorus for phytoplankton j

r_{dom_i} is remineralization rate of DOM for element i, here P, Fe, N, C

r_{pom_i} is degradation/remineralization rate of POM for element i, here P, Si, Fe, N, C

d_{cdom} is degradation rate of CDOM to DOM for element i, here P, Fe, N, C

γ_T is temperature regulation of biological rates (function provided below),

c_{scav} is scavenging rate for free iron (function provided below),

Fe$'$ is free iron (description provided below),

F_{atmos} is atmospheric deposition of iron dust on surface of model ocean,

F_{sed} is the sedimentary source of iron (function provided below),

ζ_{no3} is oxidation rate of NO$_2$ to NO$_3$ (function provided below),

ζ_{no2} is oxidation rate of NH$_4$ to NO$_2$ (function provided below),

Γ_{no3_j} is fraction inorganic nitrogen uptake from nitrate (function provided below),

Γ_{no2_j} is fraction inorganic nitrogen uptake from nitrite (function provided below),

Γ_{nh4_j} is fraction inorganic nitrogen uptake from ammonium (function provided below),

$H_{ocrit} = 1$ if $O > O_{crit}$ and 0 if $O =< O_{crit}$,

O$_{crit}$ is critical oxygen level for denitrification,

R_{denit} is N : P ratio in denitrification,

R_{dno3} is ratio of NO$_3$ relative to all N in denitrification,

D_{denit} is denitrification rate (function provided below),

$R_{\mathsf{r}j}$ is ratio of inorganic carbon to organic phosphorus produced by phytoplankton j,

F_{C} is air–sea flux of carbon dioxide (function provided below),

D_{C} is dilution/concentration of carbon by addition/loss freshwater,

D_{A} is dilution/concentration of alkalinity by addition/loss freshwater,

F_{O_2} is air–sea flux of oxygen (function provided below),

d_{pic} is dissolution rate of PIC,

$m_{\mathsf{p}j}$ is mortality/excretion rate for phytoplankton j,

$m_{\mathsf{z}k}$ is mortality/excretion rate for zooplankton k,

$m_{\mathsf{z}2k}$ is quadratic mortality for zooplankton k,

g_{jk} is grazing of zooplankton k on phytoplankton j (function provided below),

ζ_{jk} is grazing efficiency of zooplankton k on phytoplankton j (function provided below),

$w_{\mathsf{p}j}$ is sinking rate for phytoplankton j,

w_{pom_i} is sinking rate for POM i,

w_{pic} is sinking rate for PIC,

ρ_j is Chl a : C of new growth (function provided below),

θ_j is local Chl a : C ratio,

θ_{oj} is acclimated Chl a : C (function provided below),

t_{chl} is acclimation timescale for Chl a,

$\varphi_{\mathsf{mp}_{ij}}$ is fraction of dead/respired phytoplankton organic matter that goes to DOM$_i$,

$\varphi_{\mathsf{mz}_{ik}}$ is fraction of dead/respired zooplankton organic matter that goes to DOM$_i$,

$\varphi_{\mathsf{g}_{ijk}}$ is fraction of sloppy grazing that goes to DOM$_i$,

f_{cdom} is fraction of DOM produced that enters CDOM pool,

ι_{cdom} is bleaching rate for CDOM,

$\sum_{\lambda=400}^{\lambda=700} E_0(\lambda)$ is local total scale irradiance,

I_{cdom} is PAR above which CDOM bleaches.

A1   Temperature regulation of biological rates

Biological rates (plankton growth and the parameterization of remineralization of organic matter) are represented as a function of temperature, following the Arrenhius equation (Kooijman, 2000), similar to Eppley (1972):

$$\gamma_T = -\frac{1}{-\tau_1} e^{\left(A_E \left(\frac{1}{T+273.15} - \frac{1}{T_o} \right) \right)} \tag{A18}$$

where

τ_1 is coefficient to normalize the maximum value,

A_E, T_o regulate the form of the temperature modification function,

T is the local model ocean temperature.

A2   Phytoplankton growth

Phytoplankton growth is a function of temperature, irradiance, and nutrients. We follow Hickman et al. (2010), which in turn follows Geider et al. (1998), such that the growth rate is equal to the carbon specific photosynthesis rate:

$$\mathcal{P}_j^C = \mathcal{P}_{mj}^C \left(1 - e^{\left(\frac{-\Lambda_{Ej}\theta_j}{P_{mj}^C} \right)} \right) \tag{A19}$$

where

$\mathcal{P}_{mj}^C$ ~~P_{mj}^C~~ is light saturated photosynthesis rate (see function below),

Λ_{Ej} is light absorbed by each phytoplankton (see function below),

θ_j is Chl a : C for each phytoplankton (see function below).

The light saturated photosynthesis rate is a function of nutrients and temperatures:

$$\mathcal{P}_{mj}^C = \mathcal{P}_{m_{\max_j}}^C \gamma_T \gamma_{Nj} \tag{A20}$$

40

where:

$\mathcal{P}^C_{m_{max_j}}$ $P^C_{m_{max_j}}$ is maximum photosynthesis rate of phytoplankton j,

γ_T is modification of growth rate by temperature (see above)

γ_{Nj} is modification of growth rate by nutrients for phytoplankton j (see function below).

The light absorbed by each phytoplankton, j is

$$\Lambda_{Ej} = \phi_{\max_j} \sum_{\lambda=400}^{\lambda=700} a_{psj}^{chl}(\lambda) E_0(\lambda) \tag{A21}$$

where:

$\phi_{\max_j}$ is the maximum quantum yield

$a_{psj}^{chl}(\lambda)$ is the Chl a specific photosynthetic absorption spectra in each waveband λ.

The local Chl a : C ratio θ_j is:

$$\theta_j = \frac{Chl_j}{P_j \mathbf{M}_{Cj}} \tag{A22}$$

The increase of Chl a due to growth term ($\mathbf{M}_{Cj}\rho_j\mu_j P_j$) in Eq. (A11) follows Geider et al. (1998), with:

$$\rho_j = \theta_{\max j} \frac{\mathcal{P}_j^C}{\Lambda_{Ej}\theta_{oj}} \frac{P_j^C}{\Lambda_{Ej}\theta_{oj}} \tag{A23}$$

and the acclimated Chl a : C follows Geider et al. (1997):

$$\theta_{oj} = \frac{\theta_{\max j}}{1 + \frac{\Lambda_{Ej}\theta_{\max j}}{2\mathcal{P}_{mj}^C}} \frac{\theta_{\max j}}{1 + \frac{\Lambda_{Ej}\theta_{\max j}}{2P_{mj}^C}} \tag{A24}$$

where $\theta_{\max j}$ is maximum Chl a : C ratio each phytoplankton can reach.

41

Phytoplankton can be photo-inhibited (following Hickman et al., 2010), such that $\mathcal{P}_j^{\mathsf{C}}$ reduces to $\mathcal{P}_{\mathsf{inhib}_j}^{\mathsf{C}}$ ~~P$_j^{\mathsf{C}}$ reduces to P$_{\mathsf{inhib}_j}^{\mathsf{C}}$~~ above E_{kj}:

$$\mathcal{P}_{\mathsf{inhib}_j}^{\mathsf{C}} = \mathcal{P}_j^{\mathsf{C}} \kappa_{\mathsf{inhib}} \frac{E_{kj}}{\sum_{\lambda=400}^{\lambda=700} E_0(\lambda)} \tag{A25}$$

where κ_{inhib} is the inhibition coefficient and E_{kj} is the light saturation parameter.

$$E_{kj} = \frac{\mathcal{P}_{mj}^{\mathsf{C}}}{\theta_j \overline{a_{\mathsf{ps}j}^{\mathsf{chl}}(\lambda)}} \frac{P_{mj}^{\mathsf{C}}}{\theta_j a_{\mathsf{ps}j}^{\mathsf{chl}}(\lambda)} \tag{A26}$$

where $\overline{a_{\mathsf{ps}j}^{\mathsf{chl}}(\lambda)}$ is the mean light absorption by photosynthetic pigments between 400 and 700 nm.

Nutrient limitation is determined by the most limiting nutrient:

$$\gamma_{\mathsf{N}j} = \min(N_{\mathsf{lim}j_i}) \tag{A27}$$

Limitation by PO$_4$, Si, Fe are all parameterized following the Michaelis–Menton formulation:

$$N_{\mathsf{lim}j_i} = \frac{N_i}{N_i + \kappa_{\mathsf{N}_{ij}}} \tag{A28}$$

where $\kappa_{\mathsf{N}_{ij}}$ is the half saturation constant of nutrient $i = \mathsf{PO}_4$, Si, Fe, for phytoplankton j.

Nitrogen is available in three forms of which ammonia is the preferred type:

$$N_{\mathsf{Nlim}j} = \frac{\mathsf{NO}_3 + \mathsf{NO}_2}{\mathsf{NO}_3 + \mathsf{NO}_2 + \kappa_{\mathsf{in}_j}} e^{-\psi \mathsf{NH}_4} + \frac{\mathsf{NH}_4}{\mathsf{NH}_4 + \kappa_{\mathsf{nh}4_j}} \tag{A29}$$

where:
κ_{in_j} is the half saturation constant of $\mathsf{IN} = \mathsf{NO}_3 + \mathsf{NO}_2$,
$\kappa_{\mathsf{nh}4_j}$ is the half saturation constant of NH_4,
ψ reflects the fixed nitrogen uptake inhibition by ammonia.

A3 Zooplankton parameterization

Zooplankton grazing is parameterized as:

$$g_{jk} = g_{\mathsf{max}_{jk}} \gamma_T \frac{\eta_{jk} P_j}{G_k} \frac{G_k^n}{G_k^n + \kappa_{pk}^n} \tag{A30}$$

where

$g_{\mathsf{max}_{jk}}$ is maximum grazing rate of zooplankton k on phytoplankton j,

η_{jk} is palatibility of plankton j to zooplankton k,

G_k is palatibility (for zooplankton k) weighted total phytoplankton concentration, equal to $\sum_j [\eta_{jk} P_j]$

κ_{pk} is half-saturation constant for grazing of zooplankton k,

n is exponent for Holling Type II or III ($n = 1$ or 2), in this study $n = 2$.

The maximum grazing $g_{\mathsf{max}_{jk}}$ depends of the relative size of the phytoplankton j and zooplankton k, with a faster rate if they are both small or both big (g_{max_a}), and slower if they are in different size classes (g_{max_b}).

Zooplankton are assumed to have both a linear and quadratic loss term. The linear term represents mortality, the quadratic loss terms represents grazing by higher trophic levels (Steele and Henderson, 1992) that are not explicitly resolved in this model.

A4 Nitrogen cycle

Phytoplankton take up DIN in three forms (NH_4, NO_2 and NO_3). To separate out how much comes from each source we have the functions Γ in Eqs. (A5)–(A7):

$$\Gamma_{no3_j} = \frac{\frac{NO_3}{NO_3+NO_2+\kappa_{in_j}}e^{-\psi NH_4}}{N_{Nlim j}} \tag{A31}$$

$$\Gamma_{no2_j} = \frac{\frac{NO_2}{NO_3+NO_2+\kappa_{in_j}}e^{-\psi NH_4}}{N_{Nlim j}} \tag{A32}$$

$$\Gamma_{nh4_j} = \frac{\frac{NH_4}{NH_4+\kappa_{nh4_j}}}{N_{Nlim j}} \tag{A33}$$

The oxidation of NH_4 to NO_2 and NO_2 to NO_3 are parameterized as a function of the total scalar irradiance:

$$\zeta_{no3} = \zeta_{ono3}\left(1 - \frac{\sum_{\lambda=400}^{\lambda=700}E_0(\lambda)}{I_0}\right) \tag{A34}$$

$$\zeta_{no2} = \zeta_{ono2}\left(1 - \frac{\sum_{\lambda=400}^{\lambda=700}E_0(\lambda)}{I_0}\right) \tag{A35}$$

where ζ_{ono3} and ζ_{ono2} are maximum rates, and I_0 is critical light level below which oxidation occurs.

Denitrification occurs when $O < O_{crit}$ in which case O_2 is not used during remineralization, but instead NO_3 is used such that:

$$D_{denit} = R_{denit}r_{dop}\gamma_T DOP \tag{A36}$$

We assume the denitrification formula suggested by Anderson (1995) for determining R_{denit}:

$$C_{117}N_{16}P + 120NO_3 \Rightarrow 117CO_2 + PO_4 + 68N_2$$

44
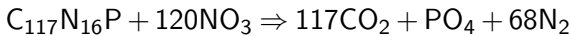
A5 Iron parameterization

The iron model we use is based on that of Parekh et al. (2004, 2005). We explicitly model the complexation of iron with an organic ligand:

$Fe' + L' \Leftrightarrow {}^{k_f}{}_{k_d} FeL$

$Fe_T = Fe' + FeL$

$L_T = L' + FeL$

where:

Fe', L' are free iron and ligand respectively
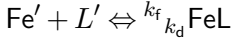
FeL is ligand bound iron

L_T is total organic ligand (assumed to be a constant)

$\beta_{fe} = \frac{k_f}{k_d}$ is ligand binding strength

k_f is the forward rate constant and k_d is the reverse rate constant.

We assume that only the free iron (Fe') can be scavenged, $c_{scav}Fe'$, and parametrize this as a function of the particulate organic carbon (POC) present (empirical values based on those found for Thorium, Honeyman et al., 1988), a similar approach was used in Parekh et al. (2005):

$$c_{scav} = c_o(R_{C:P}POP)^{\xi} \tag{A37}$$

where:

c_o determines maximum scavenging rate for iron

ξ empirically determined constant

$R_{C:P}$ is the carbon to phosphorus ratio of the POM.

The sedimentary source (F_{sed}) is parameterized as a function of the sinking organic matter reaching the ocean bottom as suggested by Elrod et al. (2004):

$$F_{sed} = R_{sed}\frac{\partial w_{pom}POP}{\partial z} \tag{A38}$$

45

where R_{sed} ratio of sediment iron to sinking organic matter.

A6 Air–sea exchange

Air–sea exchange of CO_2 and O_2 are given by:

$$F_C = k_{wc}([CO_2] - [CO_2]_{sat}) \tag{A39}$$
$$F_O = k_{wo}([O_2] - [O_2]_{sat}) \tag{A40}$$

where:
k_{wi} is the gas transfer velocity for $i = CO_2$, O_2,
$[CO_2]$ is sea surface concentration of carbon dioxide,
$[CO_2]_{sat}$ is the partial CO_2 in the water if it were fully saturated,
$[O_2]$ is sea surface concentration of oxygen,
$[O_2]_{sat}$ is the partial pressure of O_2 in the water if it were fully saturated.

Dissolved inorganic carbon (DIC) carried in the model is made up of carbon dioxide and carbonic acid and other carbonate species:

$$DIC = [CO_2{}^*] + [HCO_3] + [CO_3].$$

$[CO_2]$ is calculated from DIC and Alkalinity concentrations following Follows et al. (2006), which included deducing the pH at all surface locations. The gas transfer coefficient is parametrized following Wannikkof (1992) and is a function of the wind speed, and Schmidt number (a function of surface sea temperature). $[CO_2]_{sat}$ is determined as a function of partial pressures of CO_2 in the air, atmospheric pressure, sea surface temperature, and salinity. $[O_2]_{sat}$ is provided by Garcia and Gordon (1992). All coefficients of the air–sea flux calculations are determined using the algorithms used in the ocean carbon modeling inter-comparison project (OCMIP) (e.g. Matsumoto et al., 2004).

Appendix B: Ocean radiative transfer model: three-stream parameterization

The radiance in the ocean in its most general form, $L(\boldsymbol{x}, \theta, \varphi, \lambda)$, depends on location and orientation in addition to wavelength (units $W\,m^{-2}\,sr^{-1}\,nm^{-1}$). Neglecting horizontal gradients, the z dependence of L is described by the classical radiative transfer equation,

$$\frac{dL(\theta,\varphi)}{dz}\cos\theta = -cL(\theta,\varphi) + \int \beta(\theta,\varphi,\theta',\varphi')L(\theta',\varphi')d\Omega', \tag{B1}$$

where $\beta(\theta,\varphi,\theta',\varphi')$ is the rate of scattering of light from θ',φ' into θ,φ. We assume the ocean is optically isotropic, so β is invariant under simultaneous rotation of original and scattered angles (in fact it depends only on the relative angle). The integral over one set of angles therefore yields an angle-independent value,

$$\int\limits_{4\pi} \beta(\theta,\varphi,\theta',\varphi')\,d\Omega = \int\limits_{4\pi} \beta(\theta,\varphi,\theta',\varphi')\,d\Omega' = b.$$

Here, b is then the total scattering coefficient and the total scattered light is

$$\iint \beta(\theta,\varphi,\theta',\varphi')L(\theta',\varphi')\,d\Omega'\,d\Omega = b\int L(\theta',\varphi')\,d\Omega' = bE_0$$

and may be decomposed into forward and backward scattering coefficients, $b = b_f + b_b$, where

$$b_b = \int\limits_{\theta>\pi/2} \beta(\theta,\varphi,0,0)\,d\Omega. \tag{B2}$$

The attenuation coefficient c represents loss due to absorption and scattering, $c = a + b$.

At the sea surface, the downward part of $L(\theta,\varphi)$ for $\theta < \pi/2$ is required to equal the output of the atmospheric radiative transfer model (OASIM). The ocean is assumed to be

infinitely deep, with vanishing light at infinite depth.

Three-stream equations
Following Aas (1987) and Ackelson et al. (1994), we first separate out the direct (collimated) beam from the radiance,

$$L(\theta, \varphi) = \delta(\cos\theta - \cos\theta_d)\,\delta(\varphi - \varphi_d)\,E_{0d}(z) + L'(\theta, \varphi).$$

where the downward scalar irradiance is $E_{0d} = E_d / \cos\theta_d$. The scattering term in Eq. (B1) does not have a collimated part, so the equation for E_d separates,

$$\frac{\mathrm{d}E_d}{\mathrm{d}z} = -c\frac{E_d}{\cos\theta_d} \tag{B3}$$

The downward diffuse and upward irradiance are defined as,

$$E_s = \int\limits_{\theta < \pi/2} L'(\theta, \varphi)\cos\theta\,\mathrm{d}\Omega,$$

$$E_u = \int\limits_{\theta > \pi/2} L(\theta, \varphi)\cos\theta\,\mathrm{d}\Omega.$$

and Eq. (B1) is integrated over the downward hemisphere,

$$\frac{\mathrm{d}E_s}{\mathrm{d}z} = \int\limits_{\theta < \pi/2} \frac{\mathrm{d}L(\theta, \varphi)}{\mathrm{d}z}\cos\theta\,\mathrm{d}\Omega - \frac{\mathrm{d}E_d}{\mathrm{d}z}\cos\theta_d$$

$$= \int\limits_{\theta < \pi/2} \left[-cL(\theta, \varphi) + \int\limits_{4\pi} \beta(\theta, \varphi, \theta', \varphi')L(\theta', \varphi')\,\mathrm{d}\Omega' \right]\,\mathrm{d}\Omega.$$

48

The outer integral is split into contributions from E_d and down- and upwelling irradiance, using Eq. (B2) to rewrite the inner integral,

$$
\iint \cdots = \left(b - \int\limits_{\theta > \pi/2} \beta(\theta, \varphi, \theta_\mathsf{d}, \varphi_\mathsf{d}) \, \mathsf{d}\Omega \right) E_{0\mathsf{d}}
$$

$$
+ \int\limits_{\theta' < \pi/2} \left(b - \int\limits_{\theta > \pi/2} \beta(\theta, \varphi, \theta', \varphi') \, \mathsf{d}\Omega \right) L'(\theta', \varphi') \, \mathsf{d}\Omega'
$$

$$
+ \int\limits_{\theta' > \pi/2} \int\limits_{\theta < \pi/2} \beta(\theta, \varphi, \theta', \varphi') \, \mathsf{d}\Omega \, L(\theta', \varphi') \, \mathsf{d}\Omega'
$$

The effective backward scattering coefficients are defined as corrections to b_b,

$$
r_\mathsf{s} b_\mathsf{b} = \frac{1}{E_{0\mathsf{s}}} \int\limits_{\theta' < \pi/2} \int\limits_{\theta > \pi/2} \beta(\theta, \varphi, \theta', \varphi') \, \mathsf{d}\Omega \, L'(\theta', \varphi') \, \mathsf{d}\Omega',
$$

$$
r_\mathsf{u} b_\mathsf{b} = \frac{1}{E_{0\mathsf{u}}} \int\limits_{\theta' > \pi/2} \int\limits_{\theta < \pi/2} \beta(\theta, \varphi, \theta', \varphi') \, \mathsf{d}\Omega \, L(\theta', \varphi') \, \mathsf{d}\Omega',
$$

$$
r_\mathsf{d} b_\mathsf{b} = \int\limits_{\theta > \pi/2} \beta(\theta, \varphi, \theta_\mathsf{d}, \varphi_\mathsf{d}) \, \mathsf{d}\Omega,
$$

where

$$
E_{0\mathsf{s}} = \int\limits_{\theta < \pi/2} L'(\theta, \varphi) \, \mathsf{d}\Omega,
$$

$$
E_{0\mathsf{u}} = \int\limits_{\theta > \pi/2} L(\theta, \varphi) \, \mathsf{d}\Omega.
$$

49

In terms of the effective backscattering coefficients,

$$\frac{\mathrm{d}E_{\mathsf{s}}}{\mathrm{d}z} = -cE_{0\mathsf{s}} + (b - r_{\mathsf{s}}b_{\mathsf{b}})E_{0\mathsf{s}} + r_{\mathsf{u}}b_{\mathsf{b}}E_{0\mathsf{u}} + (b - r_{\mathsf{d}}b_{\mathsf{b}})E_{0\mathsf{d}}$$

Likewise,

$$-\frac{\mathrm{d}E_{\mathsf{u}}}{\mathrm{d}z} = -cE_{0\mathsf{u}} + (b - r_{\mathsf{u}}b_{\mathsf{b}})E_{0\mathsf{u}} + r_{\mathsf{s}}b_{\mathsf{b}}E_{0\mathsf{s}} + r_{\mathsf{d}}b_{\mathsf{b}}E_{0\mathsf{d}}.$$

$E_{0\mathsf{s}}$ is related to the downwelling irradiance E_{s} by the average cosine of the zenith angle,

$$\bar{v}_{\mathsf{s}} = \frac{E_{\mathsf{s}}}{E_{0\mathsf{s}}} = \frac{\int_{\theta < \pi/2} L' \cos\theta \, \mathrm{d}\Omega}{\int_{\theta < \pi/2} L' \, \mathrm{d}\Omega}$$

and similar for $E_{0\mathsf{u}}$. The radiative transfer equations become

$$\frac{\mathrm{d}E_{\mathsf{s}}}{\mathrm{d}z} = -\frac{a + r_{\mathsf{s}}b_{\mathsf{b}}}{\bar{v}_{\mathsf{s}}}E_{\mathsf{s}} + \frac{r_{\mathsf{u}}b_{\mathsf{b}}}{\bar{v}_{\mathsf{u}}}E_{\mathsf{u}} + \frac{b - r_{\mathsf{d}}b_{\mathsf{b}}}{\cos\theta_{\mathsf{d}}}E_{\mathsf{d}}, \tag{B4}$$

$$-\frac{\mathrm{d}E_{\mathsf{u}}}{\mathrm{d}z} = -\frac{a + r_{\mathsf{u}}b_{\mathsf{b}}}{\bar{v}_{\mathsf{u}}}E_{\mathsf{u}} + \frac{r_{\mathsf{s}}b_{\mathsf{b}}}{\bar{v}_{\mathsf{s}}}E_{\mathsf{s}} + \frac{r_{\mathsf{d}}b_{\mathsf{b}}}{\cos\theta_{\mathsf{d}}}E_{\mathsf{d}}. \tag{B5}$$

In general, $\bar{v}_{\mathsf{s}}$ and $\bar{v}_{\mathsf{u}}$ depend on the angular profile radiation field, and r_{s} and r_{u}, which describe the scattering of downward into upward and upward into downward radiation, depend on both the scattering function and the radiation field.

We close the system of equations by by making the following assumptions (following Aas, 1987):

$r_{\mathsf{d}} \approx 1.0$,
$r_{\mathsf{s}} \approx 1.5$,
$r_{\mathsf{u}} \approx 3.0$,
$\bar{v}_{\mathsf{s}} \approx 0.83$,
$\bar{v}_{\mathsf{u}} \approx 0.4$.

Equations (B3)–(B5) are the 3-stream equations (given in main text as Eqs. 1–3, though note that here we dispense with function of λ for simplicity).

The equation for E_d (Eqs. B3 or 1) is readily integrated,

$$E_d(z) = E_d(0) \exp \int\limits_0^z \frac{-c(z')}{\cos\theta_d} dz'$$

In contrast to Aas (1987), Ackelson et al. (1994) and Gregg (2002) we do not make further approximations, but instead solve the remaining equations explicitly. We can write the remaining two equations (Eqs. B4 and B5, also Eqs. 2 and 3) as

$$\frac{d}{dz}\mathbf{E} = M\mathbf{E} + \mathbf{I} \tag{B6}$$

where

$$M = \begin{pmatrix} -C_s & B_u \\ -B_s & C_u \end{pmatrix}, \quad \mathbf{E} = \begin{pmatrix} E_s \\ E_u \end{pmatrix}, \quad \mathbf{I} = \begin{pmatrix} F_d \\ -B_d \end{pmatrix} E_d \tag{B7}$$

and

$$C_s = \frac{a + r_s b_b}{\bar{v}_s}, \quad B_u = \frac{r_u b_b}{\bar{v}_u}, \quad F_d = \frac{b - r_d b_b}{\cos\theta_d},$$
$$C_u = \frac{a + r_u b_b}{\bar{v}_u}, \quad B_s = \frac{r_s b_b}{\bar{v}_s}, \quad B_d = \frac{r_d b_b}{\cos\theta_d}.$$

M, F_d and B_d are assumed to be piece-wise constant as a function of z.

Following Kylling (1995) we write the inhomogeneous solution as

$$\mathbf{E} = \begin{pmatrix} x \\ y \end{pmatrix} E_d$$

51

where x, y satisfy the equation

$$\begin{pmatrix} -C_s + c_d & B_u \\ -B_s & C_u + c_d \end{pmatrix} \begin{pmatrix} x \\ y \end{pmatrix} + \begin{pmatrix} F_d \\ -B_d \end{pmatrix} = 0 \tag{B8}$$

with solution

$$\begin{pmatrix} x \\ y \end{pmatrix} = \frac{1}{(c_d - C_s)(c_d + C_u) + B_s B_u} \cdot \begin{pmatrix} c_d + C_u & -B_u \\ B_s & c_d - C_s \end{pmatrix} \begin{pmatrix} -F_d \\ B_d \end{pmatrix}. \tag{B9}$$

The eigenvalues of M are

$$\kappa^- = D - C_s$$
$$-\kappa^+ = C_u - D = -C_s + \frac{B_s B_u}{D}$$

where

$$D = \frac{1}{2} \left(C_s + C_u + \sqrt{(C_s + C_u)^2 - 4 B_s B_u} \right)$$

Within a computational layer, the general solution can be written as

$$\begin{pmatrix} E_s(z) \\ E_u(z) \end{pmatrix} = c_k^+ \begin{pmatrix} 1 \\ r_k^+ \end{pmatrix} e^{-\kappa_k^+ (z - z_k)} + c_k^- \begin{pmatrix} r_k^- \\ 1 \end{pmatrix} e^{\kappa_k^- (z - z_{k+1})} + \begin{pmatrix} x_k \\ y_k \end{pmatrix} E_d(z)$$

where $r^+ = R_2 = B_s/D$, $r^- = 1/R_1 = B_u/D$. The offsets in the exponents have been introduced so that both exponentials are smaller than 1. The coefficients c^+ and c^- have to be determined from boundary conditions. At the sea surface, we require E_s and E_d coincide with the output of OASIM,

$$c_1^+ + r_1^- e^{-\kappa_1^- z_1} c_1^- = E_{s_o}^{\text{below}} - x_1 E_{d_o}^{\text{below}}.$$

In the bottom layer, k_{bot}, we require zero light at infinite depth, i.e., $c_{k_{\text{bot}}}^- = 0$. At layer boundaries, z_{k+1}, we require continuity,

$$e^{-\kappa_k^+(z_{k+1}-z_k)}c_k^+ + r_k^- c_k^- + x_k E_{\text{d}}(z_{k+1}) = c_{k+1}^+ + e^{\kappa_{k+1}^-(z_{k+1}-z_{k+2})}r_{k+1}^- c_{k+1}^- + x_{k+1} E_{\text{d}}(z_{k+1}),$$

$$e^{-\kappa_k^+(z_{k+1}-z_k)}r_k^+ c_k^+ + c_k^- + y_k E_{\text{d}}(z_{k+1}) = r_{k+1}^+ c_{k+1}^+ + e^{\kappa_{k+1}^-(z_{k+1}-z_{k+2})}c_{k+1}^- + y_{k+1} E_{\text{d}}(z_{k+1}).$$

In order to solve this coupled system of equations, we follow Kylling et al. (1995) and Toon et al. (1989) who observed that it can be transformed to tri-diagonal form by eliminating c_{k+1}^-,

$$e_k^+(1-r_k^+ r_{k+1}^-)c_k^+ + (r_k^- - r_{k+1}^-)c_k^- - (1-r_{k+1}^+ r_{k+1}^-)c_{k+1}^+ =$$
$$[x_{k+1} - x_k - (y_{k+1} - y_k)r_{k+1}^-]E_{\text{d}}(z_{k+1}) \tag{B10}$$

resp. c_k^+,

$$(1-r_k^- r_k^+)c_k^- - (r_{k+1}^+ - r_k^+)c_{k+1}^+ - e_{k+1}^-(1-r_{k+1}^- r_k^+)c_{k+1}^- =$$
$$[y_{k+1} - y_k - (x_{k+1} - x_k)r_k^+]E_{\text{d}}(z_{k+1}) \tag{B11}$$

where $e_k^+ = e^{-\kappa_k^+(z_{k+1}-z_k)}$ and $e_k^- = e^{-\kappa_k^-(z_{k+1}-z_k)}$. The reduced system is solved explicitly using Gaussian elimination.

Appendix C: Phytoplankton functional type specific absorption and scattering spectra

Phytoplankton total light absorption spectra show in Fig. 1d were obtained for representative phytoplankton types ~~species~~ in culture: Syn, *Synechococcus* WH7803 (Suggett et al., 2004); HLPro, *Prochlorococcus* MED4 (Moore et al., 1995); LLPro, *Prochlorococcus SS120* (Moore et al., 1995); Cocco, *Emiliania huxleyi* (Suggett et al., 2007); SmEuk, *Isochrysis galbana* (Ahn et al., 1992); Diat, *Thalassiosira weissflogii* (Suggett et al., 2004);

LgEuk, *Prorocentrum micans* (Ahn et al., 1992); Tricho, *Trichodesmium* sp. (Dupouy et al., 2008), Diaz, unicellular diazotroph absorption properties were assumed the same as Syn.

Total phytoplankton light scattering was also taken for representative <u>phytoplankton types</u> ~~species~~ in culture, with every attempt to match <u>types</u> ~~species~~ used for absorption: Syn, generic *Synechococcus* (Stramski et al., 2001, derived from Morel et al., 1993 and Stramksi et al., 1995); HLPro and LLPro, *Prochlorococcus* (Stramski et al., 2001, derived from Morel et al., 1993 and Stramski et al., 1995); Cocco, *Emiliania huxleyi* (Stramski et al., 2001, where original data are from Ahn et al., 1992); SmEuk, *Isochrysis galbana* (Stramski et al., 2001, where original data are from Ahn et al., 1992); Diat, *Chaetoceros curvisetus* (Stramski et al., 2001, derived from Bricaud et al., 1988); LgEuk, *Prorocentrum micans* (Stramski et al., 2001, where original data are from Ahn et al., 1992); *Trichodesmium* sp. (Dupouy et al., 2008), Diaz, unicellular diazotroph scattering properties were assumed the same as Syn. Backscattering to forward scattering ratios were obtained from Stramski et al. (2001), except for Tricho which was derived from <u>Subramaniam</u> ~~Subramanian~~ et al. (1999).

The absorption and scattering properties of the other optical constituents were also obtained from the literature, as outlined in the main text.

Appendix D: Inversion of AMT-15 light field

In order to estimate backscattering b_{b} from the observations made during AMT-15 we utilize the measured downwelling irradiance, E_{dn}, and upwelling, zenithward radiance, L_{u}. We use the procedure of Gordon and Boynton (1997, 1998) with the radiative transfer package DISORT, version 2.0β. We use the Gordon and Boynton (1997, 1998) parameterization rather than the the Quasi-Analytical Algorithm (Lee et al., 2002, 2007) since we are dealing with profiles not surface water leaving radiance.

Gordon and Boynton (1998) propose that $R = E_\mathsf{u}/E_\mathsf{dn}$ and $X = b_\mathsf{b}/a$ are related as

$$3R(z) \approx \frac{\int_z^\infty X(z)q(z,z')\,\mathrm{d}z'}{\int_z^\infty q(z,z')\,\mathrm{d}z'}$$

where

$$q(z,z') = \left(E_\mathsf{dn}(z')/E_\mathsf{dn}(z)\right)^2.$$

We drop $E_\mathsf{dn}(z)$ from numerator and denominator and discretize as

$$3R_i \approx \frac{\sum_{j=i}^\infty X_j q_j}{\sum_{j=i}^\infty q_j}$$

where

$$q_j = \int\limits_{z_j}^{z_{j+1}} E_\mathsf{dn}(z)^2\,\mathrm{d}z = \frac{E_j^2 - E_{j+1}^2}{2k_j}$$

and

$$k_j = \frac{1}{z_{j+1} - z_j}\ln\frac{E_j}{E_{j+1}}.$$

In order to solve for X, we write

$$3R_i \approx \frac{X_i q_i + 3R_{i+1}\sum_{j=i+1}^\infty q_j}{q_i + \sum_{j=i+1}^\infty q_j}$$

and get

$$X_i \approx 3R_i - 3\left(R_{i+1} - R_i\right)\frac{1}{q_i}\sum_{j=i+1}^\infty q_j.$$

For noisy data, this estimate of X may become negative. We drop the derivative term where this happens, i.e., X is approximated by $3R$.

55

References

Aas, E.: Two-stream irradiance model for deep waters, Appl. Optics, 26, 2095–2101, 1987.

Ahn, Y.-H., Bricaud, A., and Morel, A.: Light backscattering efficiency and related properties of some phytoplankters, Deep-Sea Res., 39, 1835–1855, 1992.

Ackleson, S. G., Balch, W. M., and Holligan, P. M.: Response of water-leaving radiance to particulate calcite and chlorophyll a concentrations: a model for Gulf of Maine coccolithophore blooms, J. Geophys. Res., 99, 7483007499, doi:10.1029/93JC02150, 1994.

Alvain, S., Moulin, C., Dandonneau, Y., and Loisel, H.: Seasonal distribution and succession of dominant phytoplankton groups in the global ocean: a satellite view, Global Biogeochem. Cy., 22, GB3001, doi:10.1029/2007GB003154, 2008.

Anderson, L.: On the hydrogen and oxygen content of marine phytoplankton, Deep-Sea Res. Pt. I, 42, 1675–1680, 1995.

Arrigo, K.R. and Brown, C.W.: Impact of chromophoric dissolved organic matter on UV inhibition of primary productivity in the sea, Mar. Ecol. Prog. Series, 140, 207-216, 1996.

Babin, M., Morel, A., Claustre, H., Bricaud, A., Kolber, Z., and Falkowski, P. G.: Nitrogen- and irradiance-dependent variations of the maximum quantum yield of carbon fixation in eutrophic, mesotrophic and oligotrophic marine systems, Deep-Sea Res. Pt. I, 43, 1241–1272, 1996.

Babin, M.A., Therrlujlt, J.-C., Legendre, L., and Condal, A.: Extent of variations in the specific absorption coefficient for natural phytoplankton assemblages: Impact on estimation of primary production, Limnol. Oceanogr. 38, 154-177, 1993

Balch, W. M. and Utgoff, P. E.: Potential interactions among ocean acidification, coccolithophores, and the optical properties of seawater, Oceanography~~Oceaography~~, 22, 146–159, 2009.

Barnard, A.H., Pegua, W.S., and Zaneveld, J.R.V.: Global relationships of the inherent optical properties of the oceans, J. Geophys. Res., 103, 24,955–24,968.

Behrenfeld, M. J. and Falkowski, P. G.: Photosynthetic rates derived from satellite-based chlorophyll concentration, Limnol. Oceanogr., 42, 1–20, 1997.

Berner, T., Dubinsky, Z., Wyman, K., and Falkowski, P. G.: Photoadaptation and the package effect in *Dunaliella-Tertiolecta* (*Chlorophyceae*), J. Phycol., 25, 70–78, 1989.

Bissett, W. P., Carder, K. L., Walsh, J. J., and Dieterle, D. A.: Carbon cycling in the upper waters of the Sargasso Sea: II. Numerical simulation of apparent and inherent optical properties, Deep-Sea Res. Pt. I, 46, 271–317, 1999.

Bissett, W. P., DeBra, S., and Dye, D.: Ecological Simulation (EcoSim) 2.0 Technical Description, Technical Document FERI-2004-0002-U.D., Florida Environmental Research Center, Tampa, Fl, 27 pp., 2004.

Bidigare, R. R., Marra, J., Dickey, T. D., Iturriaga, R., Baker, K. S., Smith, R. C., and Pak, H.: Evidence for phytoplankton succession and chromatic adaptation in the Sargasso Sea during spring 1985, Mar. Ecol.-Prog. Ser., 60, 113–122, 1990a.

Bidigare, R. R., Ondrusek, M. E., Morrow, J. H., and Kiefer, D. A.: In-vivo absorption properties of algal pigments, P. SPIE, 1302, 290, doi:10.1117/12.21451, 1990b.

Bricaud, A., Babin, M., Claustre, H., Ras, J., and Tieche, F., Light absorption properties and absorption budget of the Southeast Pacific waters. J. Geophys. Res., 115, C08009, doi:10.1029/2009JC005517, 2010.

Bricaud, A., Bedhomme, A.-L., and Morel, A.: Optical properties of diverse phytoplanktonic species: experimental results and theoretical interpretation, J. Plankton Res., 10, 851–873, 1988.

Bricaud, A., Morel, A., and Prieur, L: Absorption by dissolved organic matter of the sea (yellow substance) in the UV and visible domains, Limnol. Oceanogr., 26, 43-53, 1981.

Buitenhuis, E. T., Li, W. K. W., Vaulot, D., Lomas, M. W., Landry, M. R., Partensky, F., Karl, D. M., Ulloa, O., Campbell, L., Jacquet, S., Lantoine, F., Chavez, F., Macias, D., Gosselin, M., and McManus, G. B.: Picophytoplankton biomass distribution in the global ocean, Earth Syst. Sci. Data, 4, 37–46, doi:10.5194/essd-4-37-2012, 2012.

57

Buitenhuis, E. T., Vogt, M., Moriarty, R., Bednaršek, N., Doney, S. C., Leblanc, K., Le Quéré, C., Luo, Y.-W., O'Brien, C., O'Brien, T., Peloquin, J., Schiebel, R., and Swan, C.: MAREDAT: towards a world atlas of MARine Ecosystem DATa, Earth Syst. Sci. Data, 5, 227–239, doi:10.5194/essd-5-227-2013, 2013.

Campbell, J. W., Antoine, D., Armstrong, R., Arrigo, K., Balch, W., Barber, R., Behrenfeld, M., Bidigare, R., Bishop, J., Carr, M. E., Iverson, R., Kiefer, D., Lohrenz, S., Marra, J., Morel, A., Ryan, J., Vedernikov, V., Waters, K., Yentsch, C., and Yoder, J.: Comparison of algorithms for estimating ocean primary production from surface chlorophyll, temperature, and irradiance, Global Biogeochem. Cy., 16, 9-1–9-15, doi:10.1029/2001GB001444, 2002.

Carr, M.-E., Friedrichs, M. A. M., Schmeltz, M., Aita, M. N., Antoine, D., Arrigo, K. R., Asanuma, I., Aumont, O., Barber, R., Behrenfeld, M., Bidigare, R., Buitenhuis, E. T., Campbell, J., Ciotti, A., Dierssen, H., Dowell, M., Dunne, J., Esaias, W., Gentili, B., Gregg, W., Groom, S., Hoepffner, N., Ishizaka, J., Kameda, T., Le Quere, C., Lohrenz, S., Marra, J., Melin, F., Moore, K., Morel, A., Reddy, T. E., Ryan, J., Scardi, M., Smyth, T., Turpie, K., Tilstone, G., Waters, K., and Yamanaka, Y.: A comparison of global estimates of marine primary production from ocean color, Deep-Sea Res. Pt. II, 53, 741–770, 2006.

Cermeño, P. Dutkiewicz S, Harris, R.P., Follows, M., Schofield, O, and Falkowski, P.G.: The role of nutricline depth in regulating the ocean carbon cycle. Proc. Natl. Acad. Sci., 105, 20344–20349, 2008.

Chang, G.C. and Dickey, T.D.: Partitioning in situ total spectral absorption by use of moored spectral absorption-attenuation meters, Applied Optics, 38, 3876–3887.

Ciotti, A. M., and Bricaud, A.: Retrievals of a size parameter for phytoplankton and spectral light absorption by colored detrital matter from water-leaving radiances at SeaWiFS channels in a continental shelf region off Brazil, Limnol. Oceanogr. Methods, 4, 237–253, 2006.

Dall'Olmo, G., Boss, E., Behrenfeld, T.K., Westberry, M.J.: Particulate optical scattering coefficients along an Atlantic Meridional Transect. Optics Express, 20, 21532–21551, 2012.

Dupouy, C., Neveux, J., Dirberg, G., Rattgers, R., Barboza Tenario, M. M., and Ouillon, S.: Bio-optical properties of the marine cyanobacteria *Trichodesmium* spp., J. Appl. Remote Sens., 2, 023503, doi:10.1117/1.2839036, 2008.

Dutkiewicz, S., Follows, M. J., and Parekh, P.: Interactions of the iron and phosphorus cycles: a three-dimensional model study, Global Biogeochem. Cy., 19, GB1021, doi:10.1029/2004GB002342, 2005.

Dutkiewicz, S., Follows, M. J., and Bragg, J.: Modeling the coupling of ocean ecology and biogeochemistry, Global Biogeochem. Cy., 23, GB4017, doi:10.1029/2008GB003405, 2009.

Dutkiewicz, S., Ward, B. A., Monteiro, F., and Follows, M. J.: Interconnection between nitrogen fixers and iron in the Pacific Ocean: theory and numerical model, Global Biogeochem. Cy., 26, GB1012, doi:10.1029/2011GB004039, 2012.

Dutkiewicz, S., Ward, B. A., Scott, J.R., and Follows, M. J.: Understanding Predicted Shifts in Diazotroph Biogeography using Resource Competition Theory. Biogeosciences , 11, 5445-5461, doi:10.5194/bg-11-5445-2014.

Elrod, V. A., Berelson, W. M., Coale, K. H., and Johnson, K. S.: The flux of iron from continental shelf sediments: A missing source for global budgets, Geophys. Res. Lett., 31, L12307, doi:10.1029/2004GL020216, 2006.

Eppley, R. W.: Temperature and phytoplankton growth in the sea, Fish. Bull., 70, 1063–1085, 1972.

Fennel, K. and Boss, E.: Subsurface maxima of phytoplankton and chlorophyll: Steady-state solutions from a simple model, Limnol. Oceanogr., 48, 1521-1534, 2003.

Follows, M. J., Ito, T., and Dutkiewicz, S.: A compact and accurate carbonate chemistry solver for ocean biogeochemistry models, Ocean Model., 12, 290–301, 2006.

Follows, M. J., Dutkiewicz, S., Grant, S., and Chisholm, S. W.: Emergent biogeography of microbial communities in a model ocean, Science, 315, 1843–1846, doi:10.1126/science.1138544, 2007.

Fujii, M., Boss, E., and Chai, F.: The value of adding optics to ecosystem models: a case study, Biogeosciences, 4, 817–835, doi:10.5194/bg-4-817-2007, 2007.

Garcia, H. E. and Gordon, L. I.: Oxygen solubility in seawater: better fitting equations, Limnol. Oceanogr., 37, 1307–1312, 1992.

Garcia, H. E., Locarnini, R. A., Boyer, T. P., and Antonov, J. I.: World Ocean Atlas 2005, vol. 4, Nutrients (Phosphate, Nitrate, Silicate), NOAA Atlas NESDIS, vol. 64, 396 pp., edited by: Levitus, S., NOAA, Silver Spring, Md., 2006.

Ge, Y., Gordon, H.R., and Voss, K.J.: Simulations of inelastic-scattering contributions to the irradiance field in the ocean: variations in Fraunhofer line depths. Applied Optics, 32, 4028–4036, 1993.

Geider, R. J., MacIntyre, H. L., and Kana, T. M.: Dynamic model of phytoplankton growth and acclimation: responses of the balanced growth rate and the chlorophyll a:carbon ratio to light, nutrient-limitation and temperature. Mar. Ecol.-Prog. Ser., 148, 187–200, 1997.

Geider, R. J., MacIntyre, H. L., and Kana, T. M.: A dynamic regulatory model of photoacclimation to light, nutrient and temperature, Limnol. Oceanogr., 43, 679–694, 1998.

Gordon, H. R. and Boynton, G. C.: Radiance-irradiance inversion algorithm for estimating the absorption and backscattering coefficients of natural waters: homogeneous waters, Appl. Optics, 36, 2636–2641, 1997.

Gordon, H. R. and Boynton, G. C.: Radiance-irradiance inversion algorithm for estimating the absorption and backscattering coefficients of natural waters: vertically stratified water bodies, Appl. Optics, 37, 3886–3896, 1998.

Gregg, W. W.: A Coupled Ocean–Atmosphere Radiative Model for Global Ocean Biogeochemical Model, NASA Technical Report Series on Global Modeling and Data Assimilation, NASA/TM-2002-104606, 22, NASA, Goddard Space Flight Center, Greenbelt, MD, 2002.

Gregg, W. W. and Casey, N. W.: Modeling coccolithophores in the global ocean. Deep-Sea Res. Pt. II, 54, 447–477, 2007.

Gregg, W. W. and Casey, N. W.: Skill assessment of a spectral ocean–atmosphere radiative model, J. Marine Syst., 76, 49–63, doi:10.1016/j.jmarsys.2008.05.007, 2009.

Heywood, J. L., Zubkov, M. V., Tarran, G. A., Fuchs, B. M., and Holligan, P. M.: Prokaryoplankton standing stocks in oligotrophic gyre and equatorial provinces of the Atlantic Ocean: evaluation of inter-annual variability, Deep-Sea Res. Pt. II, 53, 1530–1547, 2006.

Hickman, A. E., Dutkiewicz, S., Williams, R. G., and Follows, M. J.: Modelling the effects of chromatic adaptation on phytoplankton community comunity structure in the oligotrophic ocean, Mar. Ecol.-Prog. Ser., 406, 1–17, doi:10.3354/meps08588, 2010.

Honeyman, B., Balistrieri, L., and Murray, J.: Oceanic trace metal scavenging and the importance of particle concentration, Deep-Sea Res. Pt. I, 35, 227–246, 1988.

Holling, C. S.: The components of predation as revealed by a study of small mammal predation on the European pine sawfly, Can. Entomol., 91, 293–320, 1959.

Huisman, J. and Weissing, F.: Competition for nutrients and light in a mixed water column: a theoretical analysis, Am. Nat., 146, 536–564, 1995.

IOCCG Report 5: Remote Sensing of Inherent Optical Properties: Fundamentals, Tests of Algorithms, and Applications, edited by: Lee, Z.-P., International Ocean-Colour Coordinating Group, Dartmouth, Nova Scotia, Canada, 126 pp., 2006.

IOCCG Report 9: Partition of the Ocean into Ecological Provinces: Role of Ocean-Colour Radiometry, edited by: Dowell, M. and Platt, T., International Ocean-Colour Coordinating Group, Dartmouth, Nova Scotia, Canada, 98 pp., 2009.

IOCCG Report Resport 15: Phytoplankton Functional Types from Space, edited by: Sathyendranath, S., International Ocean-Colour Coordinating Group, Dartmouth, Nova Scotia, Canada, 156 pp., 2014.

Irwin, A. J., Finkel, Z. V., Schofield, O. M. E., and Falkowski, P. G.: Scaling-up from nutrient physiology to the size-structure of phytoplankton communities, J. Plankton Res., 28, 459–471, 2006.

Jerlov, N.G.: Influence of suspended and dissolved matter on the transparency of sea water, Tellus, 5, 59–65, 1953.

Kettle, H. and Merchant, C. J.: Modeling ocean primary production: sensitivity to spectral resolution of attenuation and absorption of light. Prog. Oceanogr., 78, 135–146, 2008.

Kirk, J. T. O.: Light and Photosynthesis in Aquatic Ecosystems, Cambridge University Press, Cambridge, 1994.

Kitidis, V., Stubbins, A. P., Uher, G., Upstill Goddard, R. C., Law, C. S., and Woodward, E. M. S.: Variability of chromophoric organic matter in surface waters of the Atlantic Ocean, Deep-Sea Res. Pt. II, 53, 1666–1684, 2006.

Kleypas, J. A. and Doney, S. C.: Nutrients, Chlorophyll, Primary Production and Related Biogeochemical Properties in the Ocean Mixed Layer – a Compilation of Data Collected at Nine JGOFS Sites, NCAR Technical Note Change to TN-447+STR, National Center for Atmospheric Research, Boulder, CO, USA, 55 pp., 2001.

Kooijman, S. A. L. M.: Dynamic Energy and Mass Budget in Biological Systems, Cambridge Univ. Press, Cambridge, UK, 2000.

Kylling, A., Stamnes, K., and Tsay, S.-C.: A reliable and efficient two-stream algorithm for spherical radiative transfer: documentation of accuracy in realistic layered media, J. Atmos. Chem., 21, 115–150, 1995.

Leblanc, K., Arístegui, J., Armand, L., Assmy, P., Beker, B., Bode, A., Breton, E., Cornet, V., Gibson, J., Gosselin, M.-P., Kopczynska, E., Marshall, H., Peloquin, J., Piontkovski, S., Poulton, A. J., Quéguiner, B., Schiebel, R., Shipe, R., Stefels, J., van Leeuwe, M. A., Varela, M., Widdicombe, C., and Yallop, M.: A global diatom database – abundance, biovolume and biomass in the world ocean, Earth Syst. Sci. Data, 4, 149–165, doi:10.5194/essd-4-149-2012, 2012.

Lee, Z. P., Carder, K. L., and Arnone, R. A.: Deriving inherent optical properties from water color: a multi- band quasi-analytical algorithm for optically deep waters, Appl. Optics, 41, 5755–5772, 2002.

Lee, Z. P., Weidemann, A., Kindle, J., Arnone, R., Carder, K. L., and Davis, C.: Euphotic zone depth: its derivation and implication to ocean-color remote sensing, J. Geophys. Res., 112, C03009, doi:10.1029/2006JC003802, 2007.

Loisel, H.: Seasonal an inter-annual variability of particulate organic matter in the global ocean, Geophys. Res. Lett., 29, 2196, doi:10.1029/2002GL015948, 2002.

Luo, C., Mahowald, N., Bond, T., Chuang, P. Y., Artaxo, P., Siefert, R., Chen, Y., and Schauer, J.: Combustion iron distribution and deposition, Global Biogeochem. Cy., 22, GB1012, doi:10.1029/2007GB002964, 2008.

Luo, Y.-W., Doney, S. C., Anderson, L. A., Benavides, M., Berman-Frank, I., Bode, A., Bonnet, S., Boström, K. H., Böttjer, D., Capone, D. G., Carpenter, E. J., Chen, Y. L., Church, M. J., Dore, J. E., Falcón, L. I., Fernández, A., Foster, R. A., Furuya, K., Gómez, F., Gundersen, K., Hynes, A. M., Karl, D. M., Kitajima, S., Langlois, R. J., LaRoche, J., Letelier, R. M., Marañón, E., McGillicuddy Jr., D. J., Moisander, P. H., Moore, C. M., Mouriño-Carballido, B., Mulholland, M. R., Needoba, J. A., Orcutt, K. M., Poulton, A. J., Rahav, E., Raimbault, P., Rees, A. P., Riemann, L., Shiozaki, T., Subramaniam, A., Tyrrell, T., Turk-Kubo, K. A., Varela, M., Villareal, T. A., Webb, E. A., White, A. E., Wu, J., and Zehr, J. P.: Database of diazotrophs in global ocean: abundance, biomass and nitrogen fixation rates, Earth Syst. Sci. Data, 4, 47–73, doi:10.5194/essd-4-47-2012, 2012.

MacIntyre, H., Kana, T., Anning, T., and Geider, R.: Photoacclimation of photosynthesis irradiance response curves and photosynthetic pigments in microalgae and cyanobacteria, J. Phycol., 38, 17–38, 2002.

Maritorena, S., Siegel, D.A., and Peterson, A.R.: Optimization of a semianalytical ocean color model for global-scale applications, Applied Optics, 41, 2705–2714, 2002.

Marshall, J., Adcroft, A., Hill, C. N., Perelman, L., and Heisey, C.: A finite-volume, incompressible Navier–Stokes model for studies of the ocean on parallel computers, J. Geophys. Res., 102, 5753–5766, 1997.

Martinez-Vicente, V., Dall'Olmo, G., Tarran, G., Boss, E., and S. Sathyendranath: Optical backscattering is correlated with phytoplankton carbon across the Atlantic Ocean. J. Geophys. Res, 40, 1154–1158, doi:10.1002/grl.50252, 2013.

Matsumoto, K., Sarmiento, J. L., Key, R. M., Aumont, O., Bullister, J. L., Caldeira, K., Campin, J.-M., Doney, S. C., Drange, H., Dutay, J.-C., Follows, M. J., Gao, Y., Gnanadesikan, A., Gruber, N., Ishida, A., Joos, F., Lindsay, K., Maier-Reimer, E., Marshall, J. C., Matear, R. J., Monfray, P., Mouchet, A., Najjar, R., Plattner, G.-K., Schlitzer, R., Slater, R., Swathi, P. S., Totterdell, I. J.,

Weirig, M.-F., Yamanaka, Y., Yool, A., and Orr, J. C.: Evaluation of ocean carbon cycle models with data-based metrics, Geophys. Res. Lett., 31, L07303, doi:10.1029/2003GL018970, 2004.

Mobley, C. D.: Fast light calculations for ocean ecosystem and inverse models, Opt. Express, 19, 1827–1894, 2011.

Mobley, C. D., Sundman, L. K., Bissett, W. P., and Cahill, B.: Fast and accurate irradiance calculations for ecosystem models, Biogeosciences Discuss., 6, 10625–10662, doi:10.5194/bgd-6-10625-2009, 2009.

Moisander, P. H., Zhang, R., Boyle, E. A., Hewson, I., Montoya, J. P., and Zehr, J. P.: Analogous nutrient limitations in unicellular diazotrophs and *Prochlorococcus* in the South Pacific Ocean, ISME J., 6, 733–744, 2012.

Monteiro, F. M., Follows, M. J., and Dutkiewicz, S.: Distribution of diverse nitrogen fixers in the global ocean, Global Biogeochem. Cy., 24, GB3017, doi:10.1029/2009GB003731, 2010.

Moore, L. R. and Chisholm, S. W.: Photophysiology of the marine cyanobacterium *Prochlorococcus*: ecotypic differences among cultured isolates, Limnol. Oceanogr., 43, 628–638, 1999.

Moore, L. R., Goericke, R., and Chisholm, S. W.: Comparative physiology of *Synechococcus* and *Prochlorococcus*: influence of light and temperature on growth, pigments, fluorescence and absorptive properties, Mar. Ecol.-Prog. Ser., 116, 259–275, 1995.

Morel, A.: Optical properties of pure water and pure sea water, in: Optical Aspects of Oceanography, edited by: Jerlov, N. G. and Nielson, E. S., Academic Press, New York, 1–24, 1974.

Morel, A.: Are the empirical laws describing the bio-optical properties of Case 1 waters consistent and internally compatible?, J. Geophys. Res., 114, C01016, doi:10.1029/2008JC004803, 2009.

Morel, A., and Ahn, Y.-H.: Optics of heterotrophic nanoflagellates and ciliates: A tentative assessment of their scattering role in oceanic waters compared to those of bacterial and algal cells, J. Mar. Res., 49, 177–202, 1991.

Morel, A., Ahn, Y.-H., Partensky, F., Vaulot, D., and Claustre, H.: *Prochlorococcus* and *Synechococcus*: a comparative study of their optical properties in relation to their size and pigmentation, J. Mar. Res., 51, 617–649, 1993.

Morel, A., Antoine, D., and Gentili, B.: Bidirectional reflectance of oceanic waters: accounting for Raman emission and varying particle scattering phase function, Appl. Optics, 41, 6289–6306, 2002.

Morel, A., Gentili, B., Claustre, H., Babin, M., Bricaud, A., Ras, J., and Tieche, F.: Optical properties of the "clearest" natural waters, Limnol. Oceanogr., 52, 217–229, 2007.

Morel, A., Claustre, H., and Gentili, B.: The most oligotrophic subtropical zones of the global ocean: similarities and differences in terms of chlorophyll and yellow substance, Biogeosciences, 7, 3139–3151, doi:10.5194/bg-7-3139-2010, 2010.

Moriarty, R. and O'Brien, T. D.: Distribution of mesozooplankton biomass in the global ocean, Earth Syst. Sci. Data, 5, 45–55, doi:10.5194/essd-5-45-2013, 2013.

Mouw, C. B., Yoder, J. A., and Doney, S. C.: Impact of phytoplankton community size on a linked global ocean optical ecosystem model, J. Marine Syst., 89, 61–75, 2012.

Nelson, N. B. and Siegel, D. A.: The global distribution and dynamics of chromophoric dissolved organic matter, Annual Review of Marine Science, 5, 447–476, doi:10.1146/annurev-marine-120710-100751, 2013.

O'Brien, C. J., Peloquin, J. A., Vogt, M., Heinle, M., Gruber, N., Ajani, P., Andruleit, H., Arístegui, J., Beaufort, L., Estrada, M., Karentz, D., Kopczyńska, E., Lee, R., Poulton, A. J., Pritchard, T., and Widdicombe, C.: Global marine plankton functional type biomass distributions: coccolithophores, Earth Syst. Sci. Data, 5, 259–276, doi:10.5194/essd-5-259-2013, 2013.

Parekh, P., Follows, M. J., and Boyle, E. A.: Modeling the global ocean iron cycle, Global Biogeochem. Cy., 18, GB1002, doi:10.1029/2003GB002061, 2004.

Parekh, P., Follows, M. J., and Boyle, E. A.: Decoupling of iron and phosphate in the global ocean, Global Biogeochem. Cy., 19, GB2020, doi:10.1029/2004GB002280, 2005.

Pope, R. M. and Fry, E. S.: Absorption spectrum (380–700 nm) of pure water. II. Integrating cavity measurements, Appl. Optics, 36, 8710–8723, 1997.

Prowe, A. E. F., Pahlow, M., Dutkiewicz, S., Follows, M. J., Oschlies, A.: Top-down control of marine phytoplankton diversity in a global ecosystem model, Prog. Oceanogr., 101, 1–13, doi:10.1016/j.pocean.2011.11.016, 2012.

Radic, A., Lacan, F., and Murray, J. W.: Iron isotopes in the seawater of the equatorial Pacific Ocean: new constraints for the oceanic iron cycle, Earth Planet. Sc. Lett., 306, 1–10, 2011.

Redfield, A. C.: On the proportions of organic derivations in sea water and their relation to the composition of plankton, in: James Johnstone Memorial Volume, edited by: Daniel, R. J., University Press of Liverpool, UK, 177–192, 1934.

Sarmiento, J. L., Gruber, N., Brzezinski, M., and Dunne, J. P.: High-latitude controls of thermocline nutrients and low latitude biological productivity, Nature, 427, 56–60, 2004.

Sathyendranath, S. and Platt, T.: Spectral effects in bio-optical control on the ocean system, Oceanologia, 49, 5–39, 2007.

Simeon, J., Roesler, C., Pegau, W.S., and Dupouy, C.: Sources of spatial variability in light absorbing components along an equatorial transect from 165^oE to 150^oW, J. Geophys. Res., 108, doi:10.1029/2002JC001613, 2003.

Slemons, L., Gorgues, T., Aumont, O., Menkes, C., and Murray, J. W.: Biogeochemical impact of a model western iron source in the Pacific Equatorial Undercurrent, Deep-Sea Res. Pt. I, 56, 2115–2128, 2009.

Smith, R. C. and Baker, K. S.: Optical properties of the clearest natural water (200–800 nm), Appl. Optics, 20, 177–184, 1981.

Steele, J. H. and Henderson, E. W.: The role of predation in plankton models, J. Plankton Res., 14, 157–172, 1992.

Stomp, M., Huisman, J., de Jongh, F., Veraart, A. J., Gerla, D., Rijkeboer, M., Ibelings, B. W., Wollenzien, U. I. A., and Stal, L. J.: Adaptive divergence in pigment composition promotes phytoplankton biodiversity, Nature, 432, 104–107, 2004.

Stubbins, A., Uher, G., Law, C. S., Mopper, K., Robinson, C., and Upstill-Goddard, R. C.: Open-ocean carbon monoxide photoproduction, Deep-Sea Res. Pt. II, 53, 1695–1705, doi:10.1016/j.dsr2.2006.05.011, 2006.

Stramski, D., Boss, E., Bogucki, D., and Voss, K.J.: The role of seawater constituents in light backscattering in the ocean. Prog. Oceanogr., 61, 27–56, 10.1016/j.pocean.2004.07.001, 2004.

Stramski, D., Sciandra, A., and Claustre, H.: Effects of temperature, nitrogen, and light limitation on the optical properties of the marine diatom *Thalassiosira pseudonana*. Limnol. Oceanogr., 47, 392–403.

Stramski, D., Bricaud, A., and Morel, A.: Modeling the inherent optical properties of the ocean based on the detailed composition of the planktonic community, Appl. Optics, 40, 2929–2945, 2001.

Stramski, S., Shalapyonok, A., and Reynolds, R. A.: Optical characterization of the oceanic unicellular cyanobacterium *Synechococcus* grown under a day-night cycle in natural irradiance, J. Geophys. Res., 100, 13295–13307, 1995.

Subramaniam, A., Carpenter, E. J., and Falkowski, P. G.: Bio-optical properties of the marine diazotrophic cyanobacteria *Trichodesmium* spp. II. A reflectance model for remote sensing, Limnol. Oceanogr., 44, 618–627, 1999.

Suggett, D., MacIntyre, H., and Geider, R.: Evaluation of biophysical and optical determinations of light absorption by photosystem II in phytoplankton, Limnol. Oceanogr.-Meth., 2, 316–332, 2004.

Suggett, D. J., Le Floch, E., Harris, G. N., Leonardos, N., and Geider, R. J.: Different strategies of photoacclimation by two strains of *Emiliania huxleyi* (Haptophyta), J. Phycol., 43, 1209–1222, doi:10.1111/j.1529-8817.2007.00406.x, 2007.

Suggett, D. J., Moore, C. M., Hickman, A. E., and Geider, R. J.: Interpretation of fast repetition rate (FRR) fluorescence: signatures of phytoplankton community structure versus physiological state, Mar. Ecol.-Prog. Ser., 376, 1–19, 2009.

Szeto, M., Werdell, P. J., Moore, T. S., and Campbell, J. W.: Are the world's oceans optically different?, J. Geophys. Res., 116, C00H04, doi:10.1029/2011JC007230, 2011.

Tagliabue, A., Mtshali, T., Aumont, O., Bowie, A. R., Klunder, M. B., Roychoudhury, A. N., and Swart, S.: A global compilation of dissolved iron measurements: focus on distributions and processes in the Southern Ocean, Biogeosciences, 9, 2333–2349, doi:10.5194/bg-9-2333-2012, 2012.

Tarran G.A., Heywood, J.L., and Zubkov, M.V.: Latitudinal changes in the standing stocks of nano- and picoeukaryotic phytoplankton in the Atlantic Ocean. Deep Sea Res. II, 53, 1516-1529, 2006.

Toon, O. B., McKay, C. P., and Ackerman, T. P.: Rapid calculation of radiative heating rates and photodissociation rates in inhomogeneous multiple scattering atmospheres, J. Geophys. Res., 94, 16287–16301, 1989.

Ullman, D. J., McKinley, G. A., Bennington, V., and Dutkiewicz, S.: Trends in the North Atlantic carbon sink: 1992–2006, Global Biogeochem. Cy., 23, GB4011, doi:10.1029/2008GB003383, 2009.

Voss, K. J., Morel, A., and Antoine, D.: Detailed validation of the bidirectional effect in various Case 1 waters for application to ocean color imagery, Biogeosciences, 4, 781–789, doi:10.5194/bg-4-781-2007, 2007.

Wang, X.J., Behrenfeld, M., Le Borgne., R., Murtugudde, R., and Boss, E.: Regulation of phytoplankton carbon to chlorophyll ratio by light, nutrients and temperature in the Equatorial Pacific Ocean: a basin-scale model. Biogeosciences, 6, 391-404, 2009.

Wanninkhof, R.: Relationship between wind speed and gas exchange over the ocean, J. Geophys. Res., 97, 7373–7382, 1992.

Ward, B. A., Dutkiewicz, S., Jahn, O., and Follows, M. J.: A size structured food-web model for the global ocean, Limnol. Oceanogr., 57, 1877–1891, 2012.

Ward, B. A., Dutkiewicz, S., Moore, C. M., and Follows, M. J.: Nutrient supply ratios define ocean biomes, Limnol. Oceanogr., 58, 2059–2075, 2013.

Werdell, P.J., Franz, B.A., Bailey, S.W., Feldman, G.C., Boss, E., Brando, V.E., Dowell, M., Hirata, T., Lavender, S.J., Lee, Z., Loisel, H., Maritorena, S., Mélin, F., Moore, T.S., Smyth, T.J., Antoine,

66

D., Devred, E., d'Andon, O.H.F. and Mangin, A.: Generalized ocean color inversion model for retrieving marine inherent optical properties, Applied Optics, 52, 2019–2037.

Wunsch, C. and Heimbach, P.: Practical global ocean state estimation, Physica D, 230, 197–208, 2007.

Xiu, P. and Chai, F.: Connections between physical, optical and biogeochemical processes in the Pacific Ocean, Prog. Oceanogr., 122, 30–53, 2014.

Zhang, X. and Hu, L.: Estimating scattering of pure water from density fluctuation of the refractive index, Opt. Express, 17, 1671–1678, 2009.

Zheng, G., and Stramski, D.: A model based on stacked-constraints approach for partitioning the light absorption coefficient of seawater into phytoplankton and non-phytoplankton components. J. Geophys. Res, 118, 2155–2174, doi:10.1002/jgrc.20115, 2013

Zubkov, M. V., Sleigh, M. A., Tarran, G. A., Burkill, P. H., and Leakey, R. J. G.: Picoplanktonic community structure on an Atlantic transect from 50° to 50° S, Deep-Sea Res. Pt. I, 45, 1339–1355, 1998.

Table 1. Fixed biogeochemical/ecosystem model parameters (1).

Parameter	Symbol	Fixed value	Units
temperature coefficients	A_E	-4000	K
	T_o	293.15	K
temperature normalization	$1/\tau_1$	0.5882	unitless
DOM remineralization	r_{dop}	0.0333	d^{-1}
rate at 30 °C	r_{don}	0.0333	d^{-1}
	r_{dofe}	0.0333	d^{-1}
	r_{doc}	0.0333	d^{-1}
POM remineralization	r_{pop}	0.05	d^{-1}
rate at 30 °C	r_{pon}	0.0333	d^{-1}
	r_{pofe}	0.0333	d^{-1}
	r_{posi}	0.0067	d^{-1}
	r_{poc}	0.0333	d^{-1}
PIC dissolution rate	d_{pic}	0.0033	d^{-1}
POM sinking rate	w_{pom}	10	$m\,d^{-1}$
PIC sinking rate	w_{pic}	15	$m\,d^{-1}$
fraction DOM to CDOM	f_{cdom}	0.02	unitless
bleaching rate for CDOM	ι_{cdom}	0.167	d^{-1}
degradation rate for CDOM	d_{cdom}	0.003	d^{-1}
light level for bleaching CDOM	I_{cdom}	60	$\mu\text{Ein}\,m^{-2}\,s^{-1}$
CDOM absorption at λ_o	$c_{\text{cdom}}(\lambda_o)$	0.18 ~~20.5~~	$m^2\,(\text{mmol C})^{-1}$
reference waveband	λ_o	450	nm
CDOM absorption spectral slope	s_{cdom}	0.021 ~~0.02061~~	$(\text{nm})^{-1}$
POP to particle conversion	p_{part}	$1 \times 10^{-15}\ ^{-17}$	$\text{mmol C}\,(\text{particle})^{-1}$

Table 2. Fixed biogeochemical/ecosystem model parameters (2).

Parameter	Symbol	Fixed value	Units
NH_4 to NO_2 oxidation rate	ζ_{no2}	0.1	d^{-1}
NO_2 to NO_3 oxidation rate	ζ_{nh4}	0.1	d^{-1}
critical PAR for oxidation	I_{ox}	10	$\mu Ein\,m^{-2}\,s^{-1}$
critical oxygen for denitrification	O_{crit}	6	$\mu M\,O_2$
ratio N : P in denitrification	R_{denit}	120	unitless
ratio NO_3 to all N in denitrification	R_{dno3}	104	unitless
ligand binding strength	β_{fe}	2×10^5	$(\mu M\,Fe)^{-1}$
total ligand	L_T	1×10^{-3}	$\mu M\,Fe$
scavenging rate coefficient	c_o	1.2×10^{-3}	d^{-1}
scavenging power coefficient	ξ	0. 58	unitless
sedimentation rate ratio	R_{sed}	6.8×10^{-4}	$\mu M\,Fe(\mu M\,POC)^{-1}$
Chl a acclimation timescale	t_{chl}	0.5	d^{-1}
ammonia inhibition	ψ	4.6	$(\mu M\,N)^{-1}$

Table 3. Phytoplankton specific parameters description.

Parameter	Symbol	Units
max photosyn rate at 30 °C	$P^C_{m_{\max_j}}$	d^{-1}
~~max growth rate at 30~~ $\mu_{\max_j}$~~~~ elemental ratios	$M_{\mathsf{Si}:\mathsf{P}_j}$	mol Si $(\text{mol P})^{-1}$
	$M_{\mathsf{N}:\mathsf{P}_j}$	mol N $(\text{mol P})^{-1}$
	$M_{\mathsf{Fe}:\mathsf{P}_j}$	mmol Fe $(\text{mol P})^{-1}$
	$M_{\mathsf{C}:\mathsf{P}_j}$	mol C $(\text{mol P})^{-1}$
ratio IC to OP	R_{rj}	mol C $(\text{mol P})^{-1}$
growth half saturation	κ_{po4_j}	µM P
	κ_{in_j}	µM N
	κ_{nh4_j}	µM N
	κ_{fe_j}	nM Fe
	κ_{si_j}	µM Si
max quantum yield	$\phi_{\max_j}$	mmol C $(\text{mol photons})^{-1}$
max Chl a:C	$\theta_{\max_j}$	mg Chl $(\text{mmol C})^{-1}$
Chl a specific absorption	$a^{\mathsf{chl}}_{\mathsf{phy}_j}(\lambda)$	$\text{m}^2\,\text{mg Chl}^{-1}$
photosyn absorption	$a^{\mathsf{chl}}_{\mathsf{ps}j}(\lambda)$	$\text{m}^2\,\text{mg Chl}^{-1}$
carbon specific scattering	$b^C_{\mathsf{phy}_j}(\lambda)$	$\text{m}^2\,\text{mol C}^{-1}$
backscattering	$b^C_{\mathsf{bphy}_j}(\lambda)$	$\text{m}^2\,\text{mol C}^{-1}$
sinking rate	$w_{\mathsf{p}j}$	m d^{-1}
light inhibition	κ_{inhb_j}	unitless
mortality rate at 30 °C	$m_{\mathsf{p}j}$	d^{-1}
DOM/POM partitioning	$\varphi_{\mathsf{mp}_{ij}}$	unitless
grazing palatibility	η_{jk}	unitless

Table 4. Phytoplankton specific parameter values.

Parameter	Diatom	Lg Euk	Tricho	Coccol	Uni Diaz	Sm Euk	Syn	HL/LL Pro
$P^{\mathsf{C}}_{m_{\max_j}}$	3.45	1.67	0.31	1.03	0.61	1.82	1.22	1.09
$M_{\mathsf{Si:P}_j}$	16	0		0	0	0	0	0
$M_{\mathsf{N:P}_j}$	16	16	40	16	40	16	16	16
$M_{\mathsf{Fe:P}_j}$	1	1	4	1	4	1	1	1
$M_{\mathsf{C:P}_j}$	120	120	120	120	120	120	120	120
$R_{\mathrm{r}j}$	0	0	0	0.8	0	0	0	0
κ_{po4_j}	0.0187	0.0069	0.0034	0.0046	0.0011	0.0018	0.0011	0.0004
κ_{in_j}	0.300	0.110	0	0.074	0	0.029	0.018	0.007
κ_{nh4_j}	0.150	0.055	0	0.037	0	0.015	0.090	0.035
κ_{fe_j}	0.0187	0.0069	0.0136	0.0046	0.0052	0.0018	0.0081	0.0004
κ_{si_j}	0.300	0	0	0	0	0	0	0
ϕ_{max_j}	0.4	0.4	0.4	0.4	0.4	0.4	0.4	0.4
θ_{max_j}	0.3	0.2	0.2	0.2	0.2	0.2	0.2	0.2
$w_{\mathrm{p}j}$	0.36	0.23	0.45	0.23	0.10	0.07	0.06	0.03
κ_{inhb_j}	0	0	0	0	0	0	0	0/0.9
$m_{\mathrm{p}j}$	0.1	0.1	0.1	0.1	0.1	0.1	0.1	0.1
$\varphi_{\mathsf{mp}_{ij}}$	0.5	0.5	0.5	0.5	0.2	0.2	0.2	0.2
$\eta_{jk},\, k=\mathsf{lg}$	0.86	0.90	0.5	0.85	0.2	0.2	0.2	0.2
$\eta_{jk},\, k=\mathsf{sm}$	0.17	0.18	0.1	0.17	1.0	1.0	1.0	1.0

Table 5. Zooplankton/grazing specific parameter description.

Parameter	Symbol	Units
max grazing rate	$g_{\mathsf{max}_{jk}}$	d^{-1}
DOM/POM partitioning	$\varphi_{\mathsf{g}_{ijk}}$	unitless
	$\varphi_{\mathsf{mz}_{ik}}$	unitless
mortality at 30 °C	$m_{\mathsf{z}k}$	d^{-1}
	m_{z2k}	d^{-1} (µM P)$^{-1}$
grazing efficiency	ζ_{jk}	unitless
grazing half saturation	κ_{pk}	µM P

Table 6. Zooplankton/grazing specific parameter values.

Parameter	$k =$ large	$k =$ small
$g_{\max_{jk}}$	$j =$ large, 1; $j =$ small, 0.1	$j =$ large, 0.1; $j =$ small, 1.
$\varphi_{g_{ijk}}$	0.7	0.2
$\varphi_{mz_{ik}}$	0.5	0.2
m_{zk}	0.067	0.067
m_{z2k}	22.4	22.4
ζ_{jk}	$j =$ large, 0.85; $j =$ small, 0.95	$j =$ large, 0.5; $j =$ small, 0.85
κ_{pk}	0.027	0.027

Figure 1. Spectra for **(a)** absorption and scattering by water molecules (a_w, b_w, m^{-1}); **(b)** particle specific absorption and scattering by detritus (a_{det}^{part}, b_{det}^{part}, m^2 particle^{-1}); and **(c)** CDOM-specific absorption by CDOM (a_{cdom}^{CDOM}, m^2 mmol P^{-1}); **(d)** Chl a specific total absorption by phytoplankton ($a_{phy j}^{chl}$, m^2 mg Chl^{-1}); **(e)** Chl a specific absorption by photosynthetic pigments ($a_{ps j}^{chl}$, m^2 (mg Chl)$^{-1}$); and **(f)** biomass specific scattering by phytoplankton ($b_{phy j}^C$, m^2 (mg C)$^{-1}$). Details on data sources are included in the main text and Appendix C. The black line in **(d–f)** is the mean of the coloured lines (i.e. the mean spectrum). Spectra are shown here with 1nm resolution for clarity, the model uses the average over the 25nm bands (vertical grey lines).

Figure 2. Satellite (MODIS) derived Chl a (mg m^{-3}) overlain with the cruise track of the 15th Atlantic Meridional Transect (AMT-15) solid black line and 9 JGOFS timeseries site (black circles). We also show with dashed line the extension to the AMT-15 which is used in some transect figures to include model subpolar results.

Figure 3. Comparison of model output (right column, October mean) with data collected during AMT-15 (left column, collected from late September to late October): **(a, b)** Chl a (mg Chl m^{-3}); **(c, d)** nitrate (mmol N m^{-3}); **(e, f)** absorption by colored dissolved matter (a_{cdom}) (m^{-1}); **(g, h)** absorption by phytoplankton (a_{phy}) (m^{-1}). The AMT-15 data is plotted as dots for each observation taken. Model data is presented across the whole transect. The black crosses indicate the depth where the total PAR is 1 % of the surface value in the AMT-15. Model 1 % irradiance depth is shown as a black line. Transect location is shown in Fig. 2. (AMT-15 optical data G. Moore, unpublished; CDOM, Stubbins et al., 2006).

Figure 4. Comparison of model output (right column, October mean) with data collected during AMT-15 (left column): **(a)** derived total absorption at 443 nm (m^{-1}); **(b)** model total absorption at 450 nm (m^{-1}); **(c)** derived total absorption at 555 nm (m^{-1}); **(d)** model total absorption at 550 nm (m^{-1}); **(e)** derived total backscattering at 443 nm (m^{-1}); **(f)** model total backscattering at 450 nm (m^{-1}). **(g)** derived total backscattering at 555 nm (m^{-1}); **(h)** model total backscattering at 550 nm (m^{-1}). The derived properties were calculated with an inverse model of the downwelling and upwelling irradiance measured during AMT-15 (see text, and Appendix D). 1 % light level indicated with black lines/symbols. (AMT-15 optical data G. Moore, unpublished).

Figure 5. Comparison of data collected along AMT-15 **(a)** and model (October mean) **(b)**; black symbols in **(a)**, and black line in **(b)** indicate the depth of where the total irradiance is 1 % of the surface value. Colored lines/symbols indicate where the irradiance in each of several wavelengths are 1 % of the surface values. Model results are interpolated to same wavelength as the AMT-15 data. (AMT-15 optical data G. Moore, unpublished.)

Figure 6. Model ~~Comparison of model~~ and satellite derived products and climatologies of in situ measurements for annual mean and biases: **(a)** satellite derived (MODIS) Chl a ($\mathrm{mg\,Chl\,m^{-2}}$); **(b)** modelled Chl a (mean 0–50 m, $\mathrm{mg\,Chl\,m^{-2}}$); **(c)** model bias of Chl a (model-observations); **(d)** satellite derived primary production ($\mathrm{g\,C\,m^{-2}\,yr^{-1}}$) (Behrenfeld and Falkowski, 1997); **(e)**~~(d)~~ modelled primary production (column integrated, $\mathrm{g\,C\,m^{-2}\,yr^{-1}}$); **(f)** model bias of primary production; **(g)**~~(e)~~ World Ocean Atlas nitrate (mean 0–50 m, $\mathrm{mmol\,m^{-3}}$) (Garcia et al., 2006); **(h)**~~(f)~~ modelled nitrate (mean 0–50 m, $\mathrm{mmol\,m^{-3}}$); **(i)** model bias of nitrate; **(j)**~~(g)~~ compiled iron observations (composite 0–50 m, nM) (Tagliubue et al., 2012); **(k)**~~(h)~~ modelled iron (mean 0–50 m, nM); **(l)** model bias in iron.

Figure 7. Taylor diagram showing correlation and normalized SD between annual mean modelled Chl a, primary production (PP), macro nutrient (NO_3, PO_4 and silicic acid (SIL)). Satellite derived products (Chl a from MODIS and primary production following Behrenfeld and Falkowski, 1997) and World Ocean Atlas (Garcia et al., 2006) nutrients. A perfect match would be a correlation of 1 (i.e. on the x axis) and normalized SD of 1: this point is shown as "REF".

Figure 8. Comparison of monthly model Chl a (mg m^{-3}) (dark blue) at nine sites (JGOFS data, Kleypas and Doney, 2001) with satellite (MODIS) derived Chl a (mg m^{-3}) (black) and in situ (light blue). In situ show monthly mean of 0–15 m with symbol and line indicates range of values. Locations of sites are shown in Fig. 1.

Figure 9. Comparison of model with satellite (MODIS) derived remotely sensed reflectance, R_{RS} (sr^{-1}): **(a)** MODIS at 443 nm; **(b)** model at 450 nm; **(c)** MODIS at 547 nm; **(d)** model at 550 nm; **(e)** MODIS at 678 nm; **(f)** model at 675 nm. Note that the wavebands do not exactly match between model and MODIS output.

Figure 10. Model annual mean biomass ($\mathrm{mg\,C\,m^{-3}}$) of the plankton types for AMT-15 transect extended north and south to show the subpolar regions (left) and 0–50 m average (right). Shown are the 8 surviving phytoplankton types and the two zooplankton types.

Figure 11. Comparison of model output (October mean) with data collected along AMT-15: **(a, b)** *Prochlorococcus*; **(c, d)** *Synechococcus*; **(e, f)** pico-eukaryotes. Results are shown in $mg\,C\,m^{-3}$; AMT-15 observations were converted from cell count to biomass (Zubkov et al., 1998). AMT-15 data from Heywood et al. (2006).

Figure 12. Comparison of model plankton type biomass (mg C m^{-3}) with compilation of biomass from MAREDAT (pico-phytoplankton; Buitenhuis et al., 2012; coccolithophores, O'Brien et al., 2013; diatoms, Leblanc et al., 2012; diazotrophs, Luo et al., 2012; meso-zooplankton, Moriarty and O'Brien, 2013). Note that model output is annual average from 0 to 50 m; right column is compilation of all MAREDAT data in 5° bins between 0 and 50 m and does not represent an annual average.

Figure 13. Comparison of model phytoplankton type dominate type with dominant type found from PHYSAT (Alvain et al., 2008) satellite derived product for **(a, b)** January and **(c, d)** July. Note that Haptophytes and *Phaeocystis* are not specifically resolved in the model, so are only shown in the PHYSAT plots. Coccolithophores (a subset of Haptophytes) and pico-eukaryotes are not resolved by the PHYSAT algorithm, so are only shown in the model results.

Figure 14. Sensitivity Experiments examining value of increased optical complexity in model. Chl-a ($mg\,C\,m^{-3}$) along the extended AMT-15 transect (see Fig. 2) for (a) EXP-V0 with no radiative transfer, single waveband of PAR (400-700nm), no inclusion of optical effects of CDOM or detritus and no optical differences between phytoplankton. (b) EXP-V1 with radiative transfer, explicit optical properties for CDOM and detritus, but only one waveband (400-700nm) and no optical differences between phytoplankton. (c) EXP0, the default experiment. Model 1 % irradiance depth is shown as a black line.

Figure 15. Model output along extended AMT-15 transect (annual mean) of **(a–h)** ratio of optical constituents contribution to total absorption: **(a)** water molecules, a_w/a at 450 nm; **(b)** a_w/a at 550 nm; **(c)** detrital matter, a_det/a at 450 nm; **(d)** a_det/a at 550 nm; **(e)** CDOM, a_cdom/a at 450 nm; **(f)** a_cdom/a at 550 nm; **(g)** total phytoplankton, a_phy/a at 450 nm; **(h)** a_phy/a at 550 nm. Dominant absorption constituent is shown in **(i)** for 450 nm and **(j)** for 550 nm: blue $= a_\mathrm{det}$; green $= a_\mathrm{phy}$; orange $= a_\mathrm{cdom}$; red $= a_\mathrm{w}$. In (**i** and **j**) the opacity is scaled by the log of the total PAR.

Figure 16. Model output along extended AMT-15 transect (annual mean) of **(a–f)** ratio of optical constituents contribution to total scattering: **(a)** water molecules, b_{w}/b at 450 nm; **(b)** b_{w}/b at 550 nm; **(c)** detrital matter, b_{det}/b at 450 nm; **(d)** b_{det}/b at 550 nm; **(e)** total phytoplankton, b_{phy}/b at 450 nm; **(f)** b_{phy}/b at 550 nm. Dominant scattering constituent is shown in **(g)** for 450 nm and **(h)** for 550 nm: blue $= b_{\mathrm{det}}$; green $= b_{\mathrm{phy}}$. In (**g** and **h**) opacity is scaled by the log of the total PAR.

Figure 17. Detritus sensitivity experiments. **(a)** Absorption by detritus (a_{det}, units m^{-1}) at 450 nm with 1 % total light contour (black line) and for 400, 450, 500, 550, 600 nm wavebands (purple, dark blue, light blue, green, red). **(b)** Total phytoplankton biomass (mg C m^{-3}). **(c)** Dominant phytoplankton type (red = diatom, orange = coccolithophores, blue = pico-eukaryotes, yellow = *Synechococcus*, green = *Prochlorococcus*; opacity represents the total biomass). **(d)** 450 nm remotely sensed reflectance (sr^{-1}). Black line in (**b** and **c**) indicated the 1 % total irradiance contour. Each row represents a different experiment. EXP0 is the default experiment showcased in the earlier text. EXP-D1 = no a_{det}; EXP-D3 = 4 · a_{det}; EXP-D3 = no b_{det}; EXP-D4 = 4 · b_{det}; EXP-D5 = a_{det} parameterized as function of POC concentration.

Figure 18. CDOM sensitivity experiments. **(a)** Absorption by CDOM (a_{cdom}, units $1 \, \text{m}^{-1}$) at 450 nm with 1 % total irradiance contour (black line) and for 400, 450, 500, 550, 600 nm wavebands (purple, dark blue, light blue, green, red). **(b)** Total ~~Ttotal~~ phytoplankton biomass (mg C m^{-3}). **(c)** Dominant phytoplankton type (red = diatom, orange = coccolithophores, blue = pico-eukaryotes, yellow = *Synechococcus*, green = *Prochlorococcus*; opacity represents the total biomass). **(d)** 450 nm remotely sensed reflectance (sr^{-1}). Black line in (**b** and **c**) indicated the 1 % total irradiance contour. Each row represents a different experiment. EXP0 is the default experiment showcased in the earlier text. EXP-C1 = no a_{cdom}; EXP-C2 = $4 \cdot a_{\text{cdom}}$; EXP-C3 = a_{cdom} a function of Chl a; EXP-C4 = a_{cdom} a function of DOM; EXP-C5 = a_{cdom} uniform.

Figure 19. Phytoplankton sensitivity experiments. **(a)** Absorption by phytoplankton (a_{phy}, units m^{-1}) at 450 nm with 1 % total irradiance contour (black line) and for 400, 450, 500, 550, 600 nm wavebands (purple, dark blue, light blue, green, red). **(b)** Total phytoplankton biomass (mg C m^{-3}). **(c)** Dominant phytoplankton type (red = diatom, orange = coccolithophores, blue = pico-eukaryotes, yellow = *Synechococcus*, green = *Prochlorococcus*; opacity represents the total biomass). **(d)** 450 nm remotely sensed reflectance (sr^{-1}). Black line (**b** and **c**) indicated the 1 % total irradiance contour. Each row represents a different experiment. EXP0 is the default experiment showcased in the earlier text. EXP-P1 = no a_{phy}; EXP-P2 = 4·a_{phy}; EXP-P3 = no b_{phy}; EXP-P4 = a_{phy}^{chl} spectrum mean for all phytoplankton; EXP-P5 = b_{phy}^{C} spectrum mean for all phytoplankton.